ADVANCED CONTROL STRATEGIES FOR RENEWABLE ENERGY INTEGRATION FOR SYSTEM SUPPORT

LI YUJUN

Ph.D

The Hong Kong Polytechnic University

2017

The Hong Kong Polytechnic University

Department of Electrical Engineering

ADVANCED CONTROL STRATEGIES FOR RENEWABLE ENERGY INTEGRATION FOR SYSTEM SUPPORT

LI YUJUN

A thesis submitted in partial fulfillment of the requirements

for the Degree of Doctor of Philosophy

May 2017

CERTIFICATE OF ORIGINALITY

I hereby declare that this thesis is my own work and that, to the best of my knowledge and belief, it reproduces no material previously published or written nor material which has been accepted for the award of any other degree or diploma, except where due acknowledgement has been made in the text.

__ ___(Signed)

_____LI Yujun_____(Name of student)

Abstract

This thesis mainly focuses on the power system inertia less problem with the high penetration of renewables and accordingly proposes several concerned system support strategies. The typical variable speed wind turbines (VSWT) employing power electronic grid interface are gradually replaced with similar sized conventional thermal/hydro generation machines, which leads to the considerably lowered inertia available for the power grid. Further, the main function of these power converters is to realize the maximum power point tracking (MPPT) for maximally harvesting renewable energy and controlling the power transmission to the grid. It effectively decouples the rotation of the wind turbine (WT) and network frequency. As a result, the contribution of WTs to the system inertia support is also reduced. Accordingly, it has become mandatory that WTs are required to equip with frequency regulation control according to the grid codes in many countries.

In this thesis, two novel control strategies that enable system inertia supports by permanent magnetic synchronous generator (PMSG) wind turbines during transient events are investigated. The first strategy seeks to provide inertia support to the system through simultaneous utilization of DC-link capacitor energy, and WT rotor kinetic energy (KE). The second strategy supports system inertia through orderly exerting DC-link capacitor energy of WT and then WT rotor KE via a cascading control scheme. Both strategies can effectively provide system inertia support by fully utilizing WT's own potentials, while the second strategy distinguishes itself by minimizing its impacts on wind energy harvesting. Case studies of one synchronous generator (SG) connected with a PMSG-based

WT considering sudden load variations have been studied to validate and compare the two proposed strategies on providing rapid inertia response for the system.

In recent years, wind power capacity has grown steadily, which raises concerns about the secure and reliable operation of the power system. Particularly, the popular MPPT algorithm adopted by VSWTs may cause supply-demand imbalance of the power system when wind power is more than system needs. Accordingly, the traditional SGs are required to operate at part-load levels or even shut down for some time to realize power balance in the system, which results in a reduced life cycle and the increased costs. To minimize such impacts, some countries have required WTs mandatorily to fulfil the dispatch demand set by system operator based on their grid codes.

To effective dispatch wind power according to e.g. operator command or market schedule, a variable utilization level (UL) scheme is proposed for a wind power plant (WPP) to fulfil the dispatch order while reducing the loss of total energy production in this thesis. Considering different wind conditions, the proposed scheme directs the power output for each WT according to a specific UL, which is adaptively adjusted according to WT rotor speed so that the less reduction of energy production can be ensured. Meanwhile, more rotational KE can be stored in WPP, which can be later released for system support when needed. The proposed variable UL scheme is fully investigated in a doubly fed induction generator (DFIG)-based WPP and the results clearly indicate the proposed scheme can harvest more energy than the conventional same UL one while fulfilling the dispatch demand.

When wind power penetration is high, particularly in the context of a microgrid, the wind generation according to the maximum power tracking control may significantly disturb the supply-demand balance. To counterbalance the impacts, an optimal power sharing control scheme that seeks to cope with the power dispatching demand by system operator while harvesting as much wind energy as possible is proposed for DFIG wind turbines. The control scheme can fulfill the dispatching command via maximizing the rotational kinetic energy stored in DFIGs, which can be later released for system support when needed. The proposed method has proved to be effective through a case study in a microgrid, which indicates the high potential for industrial applications.

Traditionally, wind and photovoltaic (PV) generation is non-dispatchable and subject to Maximum Power Point Tracking (MPPT) control, which can be of highly disturbance to system dispatch in particularly context of microgrid. To effectively fulfil dispatch command or market schedule, a novel cascading power sharing control (PSC) scheme is proposed to coordinate wind and PV productions in microgrid while minimizing the possible reduction of renewable energy production involved. Considering different properties of wind and PV systems, the discrepancies between dispatch command (market schedule) and the actual renewable generation is counterbalanced by firstly adjusting wind output via temperately storing or releasing kinetic energy of turbine rotors. Only when the total production still prevails, should PVs deload their generation. The proposed PSC scheme is fully tested in a microgrid with wind and PV and the simulation results clearly indicate more wind energy can be captured in the proposed scheme compared to the traditional dispatch method while fulfilling the dispatch demand.

Acknowledgement

First and foremost, I want to express my sincere gratitude to my chief supervisor, Dr. Zhao Xu, for his continuous support and encouragement throughout my PhD study and research. His knowledge, experience and intelligence always impress me and enlighten me. He helped me solve all kinds of academic problems so patiently. I will not forget he revised my paper in the many dark nights. His optimistic attitude to life encourages me to keep going every time I fail. To me, Dr. Xu is not only my supervisor but also my trusted and respected friend. It is my honor and fortune to study under his guidance.

I also would like to give special thanks to my good friend Dr. Jianliang Zhang, for the stimulating discussions we had, for all help he gave to me, and for the day and night we worked together. I learnt a lot of important things from him, not only the research skills and experiences but also the can-do attitude and hardworking spirit. I will always remember the past one year with him. My sincere thanks also go to my paper reviewers and thesis examiners for their constructive comments to this research.

Moreover, I would like to thank my dear parents Jianbao Li and Honghua Yu for their selfless and unconditional love, support, and encouragement ever since I was born. I also owe many thanks to my wife Junying Yan for her thoughtfulness to let me concentrate on my study and consolation to dissolve my frustration.

Without all these people backing me up, I would never have been able to complete my PhD study.

Last but not least, I would like to acknowledge the support from my Ph.D. studentship awarded by The Hong Kong Polytechnic University.

Table of Contents

Lists of Figures, Tables and Abbreviations

List of Figures

List of Tables

List of Abbreviations

APC	Active Power Control
DFIG	Doubly fed Induction Generator
DG	Distributed Generators
ESS	Energy Storage System
GSC	Grid-Side Converter
KE	Kinetic Energy
MPPT	Maximum Power Point Tracking
ROCOF	Rate of Change of Frequency
PSC	Power Sharing Control
PMSG	Permanent Magnetic Synchronous Generator
PV	Photovoltaic
RSC	Rotor-Side Converter
SG	Synchronous Generator
UL	Utilization Level
VSWT	Variable Speed Wind Turbine
WECS	Wind Energy Conversion System
WPP	Wind Power Plant
WT	Wind Turbine
WG	Wind Generator

Chapter I

Introduction

1.1 Background and Literature Review

Environmental concerns and global energy crisis lead to a rapid proliferation of wind energy worldwide. In 2015, increase in wind generation was equal to the almost half of global electricity growth according to the global wind report [1], which results in wind energy as the most prosperous kind of renewable that can be deployed. However, the most important properties of wind generation are intermittent, variable and uncertain. Accordingly, variable power with uncertain nature may cause severe consequences in power system such as the decrease of the available system inertia, increase in voltage and frequency fluctuations, the rising need for system reserve, and the impaired effects on power quality and economics.

1.1.1 Reduced System Inertia with High Penetration of Wind Power

With high penetration of wind energy integration into power grid, variable speed wind turbines (VSWT) employing power electronic grid interface are gradually replacing similar sized conventional thermal or hydro generation machines, which leads to the considerably lowered inertia available for the power grid [2]. Further, the main function of these power converters is to realize the maximum power point tracking (MPPT) [3] for maximally harvesting renewable energy and controlling the power transmission to the grid. It effectively decouples the rotation of the wind turbine (WT) and the network frequency. As a result, the contribution of WTs to the system inertia support is also reduced. It is an established fact that more generators participating into system frequency regulation may result in less frequency excursions after system disturbance. Accordingly, it has become mandatory that WTs are required to equip with frequency regulation control according to the grid codes in many countries [4-6]. In Hydro Quebec, it is required that, in the case of severe frequency excursion, wind turbines must provide an active power response equivalent to that of a SG with an inertia constant of 3.5s for a period of 10 s [4]. In the Ireland and Northern Ireland system, the transmission system operators (TSOs), have proposed to the energy regulator new fast frequency responses services, in which WT should participate [5-6].

Frequency Support Mechanism of Conventional Synchronous Generators

Whenever there is supply/demand power imbalance, synchronous generators (SGs) in a power system respond in three stages to bring the system frequency back to the normal value. The initial stage is called “system inertia response”, which is characterized by the releasing or absorbing of rotational kinetic energy of the rotating mass of the SG. This is a physical and inherent property of SGs. For instance, if there is a sudden increase in system load, the electrical torque of the SG will increase in response to the sudden load increase change, which the mechanical toque of the SG governor turbine remains as constant. Hence, the SG rotor decelerates, given by $J(d\omega/dt)=T_m - T_e$, and the kinetic energy stored in the SG is release to support the load change. When the frequency excursion exceeds the certain limits, the governor control of SG will be activated to change the power input to the prime mover. The rotor speed acceleration will become zero and the system frequency reaches a new steady state. This is referred to as “primary frequency control”. The specific SG will accordingly change the power set points to remove the steady error, and the network frequency is brought back to the nominal value, which is called “secondary frequency control”. These three steps take place in succession in power systems to restore the system frequency back to the normal operating equilibrium [7-10].

WTs will normally be operated to maximize their output under all possible wind conditions. Accordingly, they are not allowed or available to provide a sustained increase or decrease in output generation, which cannot participate in the “secondary frequency control” [11-13] as several conventional plants usually do. However, they can provide the two critical components of inertial and primary response for supporting the system frequency in a short-time period.

1.1.2 Method to enable Variable Speed Wind Turbine Inertia and Primary Response

To equip WTs with the capability to regulate the system frequency, many experts and scholars have been doing a large number of researches. Generally, there are three main methods to enable VSWTs to participate effectively in system frequency regulation. The first one is the emulated inertia control scheme [14-24], the second one is the power reserve control scheme [25-35], and the third one is to utilize DC link capacitors [36-42] in the converters of WT.

Emulated Inertia Control for Short-term Frequency Support (Inertia Response)

The prominent advantage of the power electronics interfaced with wind conversion system is that they can regulate the active or reactive power transmitted to the power grid independently and rapidly [43-45]. This property can be exploited to render system inertia or frequency support. In general, a supplementary loop is added into the classical active control loop. This control loop is activated when detecting system frequency deviation. For instance, when there is a reduction in the system frequency, the active power controls increase the power setting of the WT, which injects the stored kinetic energy from the rotating mass for the power grid. This is called “emulated inertia control” of WT [14-24].

Emulated inertia control of WT can be broadly classified into three categories. The first scheme gives the WT a response to the frequency derivations, which is mimicking the inherent behavior of a SG. The supplementary frequency loop (the additional amount of power supplied) is proportional to the system frequency derivation, which is normally called virtual inertia control. Derivation controller may emulate a synchronous inertia-like response well, but it may lead to system instability due to the noise in the frequency measurement [15-17]. The second one is similar to the primary frequency control that is deployed by conventional SG. The additional amount of the power supplied is proportional to the network system deviation, which is generally called “droop control” [18-20]. In [21], the authors combine the two control schemes to provide inertia response for the WTs. The supplementary power loops that are proportional to the frequency deviation and derivation are together utilized in order to exert more frequency support when severe system frequency excursions happen. The impacts of implementing droop control in DFIG-based wind turbines on microgrid are fully investigated in [19]. It is reported that torque- and power- droop implementations in DFIG-based units can provide short-time frequency support to the power grid. However, it may induce wear and tear and increase the maintenance cost for wind turbines with high droop parameters [22]. In [16], droop control can be considered as an alternative inertia response strategy for WT. The steady error induced by the droop control can be effectively eliminated by adding a high-pass filter. The third emulated inertia response is obtained from the fixed trajectory response. Any deviation in system frequency beyond a certain threshold, a fixed response shape can be triggered [24].

Variable droop gain based frequency control schemes were proposed for better system support. In [46, 47], the primary frequency response is significantly improved by continuously adjusting the droop of the wind turbine generator (WTG) in response to wind velocities. In [48, 49], the releasable kinetic energy of WT can be fully utilized to raise frequency nadir by adjusting frequency loop gain in a WT controller. This is based on the fact that higher rotor speed WT can release more kinetic energy and contribute more to the system frequency.

Power Reserve Control for Long-term Frequency Support (Primary Response)

Primary regulation of traditional SG is normally triggered by the governor-turbine to make up the imbalanced between demand and generation. A primary frequency regulation consists of a linear variation of the generated power with the grid frequency. Accordingly, if the grid frequency increases, the generated power should decrease and vice versa. Consequently, in order to be able to implement primary regulation in both directions, a power reserve is needed.

For maximization of revenue and resource utilization, variable speed wind turbines are normally controlled to capture as much power as possible from the wind. Hence, they are not available to provide a sustained increase in power output and therefore participate in secondary response services which conventional plants are able to do. The kinetic energy stored in their inertia gives the turbines the possibility to support primary frequency control for a short period. Therefore, in order to perform permanent active power control, it is generally necessary to force the wind turbine to operate in a non-optimal power point, this non-optimal operation of the wind turbine is called deloaded operation [25-28].

There are two alternatives to deload wind turbine for long-term system frequency support. One possible way is to utilize pitch angle control [29,30] to decrease the wind turbine output power. The other way is to over-speed wind turbine rotors [31-35] to realize the active power control of wind turbine.

Normally, partial wind energy will be reserved by pitch angle control of wind turbine. When there is over-generation in the power system, pitch angle will be increased by turbine blading to further decrease the generation of wind turbine [29]. In contrast, when there is over-consumption in the system, the power reserved by pitching can be somewhat released by decreasing the pitch angle for system support, and the wind turbine can extract more mechanical power from wind energy. In [29, 30], the author utilizes the reserved power by pitching to support the system frequency in the system. However, this scheme forces wind turbine to deviate from MPPT operating point and significant annual wind energy loss is inevitable. In addition, the response speed of pitching is relatively slow [30] and frequent activation may increase mechanical stress and fatigue to wind turbine.

The other way to deload the wind turbine is to operate the wind turbine at the increased rotor speed [31-35]. It can withhold the wind turbine output power through accelerating the rotor speed in the deloading control and partially wind energy can be converted into the rotating kinetic energy of wind turbine. On the contrary, the stored kinetic energy can be released back for the system through the proper designed control scheme. Compared to the pitch angle control based deloading control, this scheme can certainly provide the system frequency support while harvesting much more energy.

DC-link Voltage Control for Fast Frequency Support

The last source to implement virtual inertia for variable speed wind turbine is DC-link capacitor energy in the power electronic converters. DC-link voltage can be temporarily changed so as to release or absorb DC capacitor partial energy for system support. [36] proposed a coordinated control of the DC-link voltage and pitch angle of the permanent magnetic synchronous generator (PMSG) for smoothing WT output power. [39] proposed a supplementary control that combines the pitch angle control and modification of WT output power reference for system frequency support. [37] indicated the WT rotating mass or DC-link capacitor of doubly fed induction generator (DFIG) can be utilized to implement the virtual inertia of DFIG. However, the energy stored in DC-link capacitor of DFIG is relatively small [40, 41] and super-capacitor should be installed for obtaining large WT virtual inertia constant.

In a DFIG-based WPP, the effective wind speed of a downstream WT is lower than that of an upstream WT due to the wake interaction between WTs.

The well-studied Park model is one of the most prevalent wake models in existing literature [50-55]. In [48, 49], the releasable kinetic energy of WT can be fully utilized to raise the frequency nadir by adaptively adjusting frequency loop gain of a WT controller under under-frequency events. This is based on the fact that WT with higher rotor speed can release more kinetic energy to contribute to system frequency support.

1.1.3 Supply-demand Imbalance with High Penetration of Wind Farm

In recent years, wind power capacity has grown steadily, which raises concerns about the secure and reliable operation of the power system. Particularly, the popular maximum power point tracking (MPPT) algorithm adopted by variable speed wind turbines (VSWTs) may cause supply-demand imbalance of the power system when wind power is more than system needed [56-60]. Accordingly, traditional synchronous generators (SGs) are required to operate at part-load levels or even shut down for some time to realize power balance in the system, which results in a reduced life cycle and the increased costs [61]. To minimize such impacts, some countries have required wind turbines (WTs) mandatorily to fulfill the dispatch demand set by system operator based on their grid codes [62-64].

Energy Storage System

One direct solution is to utilize energy storage system (ESS), such as flying wheel, compressed air, or super-capacitors, which can smooth the wind power generated according to the MPPT algorithm to fulfil the dispatch demand set by the system operator [65-72]. The obvious advantage of this method is ESS can absorb the surplus energy from wind farms and release the storage energy for the system when there is a power scarcity in the system while wind turbines always work in a MPPT status. However, there are significant concerns from both technical and economic perspectives that may prevent wide use of these technologies. Such technologies including e.g. flywheels and super-capacitors have very low energy capabilities and can have large difficulties in tracking dispatch commands of a system operator once there the system stays for a long time in a state of generation scarcity. Though batteries can have enough capacities, the instalment and maintenance cost can be very high. In addition, ESS technologies may not be economic considering charging and discharging losses, high installation investment, and relatively low life cycles.

WT Self-Potential Capability

Based on the limitations of utilizing the ESS for power balancing in the power system, therefore, it is necessary to investigate new control schemes that can fully utilize the self-potentials of wind turbines (WTs). Actually, with a proper load sharing control algorithm, the output power of a wind power plant (WPP) can be regulated in accordance with dispatch command to realize power balance among the system. Specifically, when there is over-generation in the system, wind turbines (WTs) can withhold partial output power through so-called deloading control strategy [73-80]. Similarly, the overloading control can be applied to wind turbines when there is over-consumption in the system [81-85].

There are two active power control schemes to enable deloading or overloading control by each wind turbine. The first one is to utilize the reserved power by pitching [75, 76] to realize the supply-demand balance in the system. However, this scheme forces wind turbine to deviate from MPPT operating point and significant annual wind energy loss is inevitable. In addition, the response speed of pitching is relatively slow and frequent activation may increase mechanical stress and fatigue to wind turbine. The second widely used alternative is to utilize the rotating kinetic energy (KE) of wind turbine [77-79]. It can withhold its output power through accelerating the rotor speed in the deloading control and partially wind energy is converted into rotating kinetic energy of wind turbine [83-85]. On the contrary, the stored kinetic energy can be released back in the overloading control through decelerating the rotor speed. This method certainly can enable wind turbines for load sharing while harvesting much more energy than pitch control based scheme. Because of such advantage, this thesis further develops the kinetic energy based control scheme for load sharing control scheme to enable a WPP to fulfill power dispatch command while reducing the loss of wind energy production.

In [86, 87], an effective two-level control scheme for load sharing control for a WPP is proposed. This control scheme consists of a supervisory control level and a machine control level. The former one decides the power setting of each wind turbine from different optimization objections such as optimal power flow among a WPP [88-90] or minimization power loss in a WPP [90-93]. The latter one can be realized through deloading or overloading control scheme as above. The data of current wind speeds, rotor speeds of wind turbine, and configuration of WPP is required for this method, which is high-computational cost and not suitable for online application. In addition, the coordination of each wind turbine to fulfill the dispatch order and the dynamics of wind turbine are not considered as well. Another possible solution is make some wind turbines work at MPPT model and the rest of them can evenly share the remaining demand. However, this type of solution is susceptible to the inaccuracy in available wind power prediction and the rest of DFIGs should undertake all the power imbalance, which may make wind turbine easily trip off. In [94, 95], a simple and direct approach is proposed for load sharing by controlling the utilization level (UL) of each wind turbine, and maintaining it at a same value.

1.2 Primary Contributions

1. Most existing literatures focus on providing system inertia support via two virtual inertia sources, namely rotating mass or DC-link capacitor separately and how to cooperate them to contribute to system inertia support is not well discussed and designed. Focusing on the inertia support from PMSG, this thesis proposes two control strategies in order to fully utilize the WT own potentials to contribute to system inertia support. The first strategy seeks to provide system inertia support through utilization of DC-link capacitor and WT rotor KE simultaneously, which enables WT a larger virtual inertia constant than only WT rotating mass participating system support via conventional droop control. One drawback of the first proposed strategy is that it requires WT constantly deviating from the MPPT status whenever frequency disturbances occur, which may not be a cost-effective strategy for commercial wind farms. Therefore, the second strategy adopts a cascade structure to firstly exert DC-link capacitor energy and subsequently WT rotor KE to provide system frequency support, which stands itself out by minimizing the control impacts on wind energy harvesting. The inertia contributions of WT for the two strategies have been analytically derived.

2. Wind turbines in a WPP may deviate from MPPT status while fulfilling the dispatch demand and certainly wind energy production will be compromised. Because of the wake interactions among wind turbines, the energy compromised by each wind turbine in a WPP may not be equal. Therefore, using the same UL scheme certainly may not be an optimal option in terms of reducing the loss of total energy production in a WPP. This thesis firstly illustrates that under the conventional same utilization scheme, the overall energy reduction in a WPP may be high since the wind turbines at higher wind speeds may suffer more compromised energy production than those at lower wind speeds. In view of this, this thesis proposes a variable UL scheme for a DFIG-based WPP that

coordinates each DFIG to fulfill the dispatch order while reducing the total energy loss. The utilization level of each wind turbine in a WPP is adaptively adjusted based on different wind turbines' rotor speeds so that more rotational kinetic energy (KE) can be stored in wind turbines, which can be later released back to the system. The wake effect model is applied in calculating the wind speed at each DFIG in a WPP. The performance of the proposed scheme is validated effectively in *DIgSILENT/PowerFactory* and the results clearly indicate the proposed scheme can harvest more wind energy than the conventional same utilization level one while fulfilling the dispatch demand.

3. Wind generation can significantly disturb the power balance within particularly a weak power grid such as stand-alone microgrids. To counterbalance the impacts, an optimal power sharing control scheme that seeks to cope with the power dispatching demand by system operator while harvesting as much wind energy as possible is proposed for DFIG wind turbines. The control scheme can fulfill the dispatching command via maximizing the rotational kinetic energy stored in DFIGs, which can be later released for system support when needed. The proposed method has proved to be effective through a case study using a microgrid, indicating high potential for industrial applications.

4. Traditional dispatch methods may involve either optimal power flow or the same utilization level (UL) based scheme to adjust renewable generation output to ensure dispatch command alignment within a microgrid. Considering DGs like wind and PV can operate at different MPPT points because of different locations, the same UL based scheme may not provide optimal adjustments in terms of impacts caused to energy harvest. Meanwhile, wind generators (WGs) have the advantages of varying generation output at limited impacts to energy harvest and therefore should be highly prioritized for set point adjustment. Thus, this thesis proposes a novel cascading power sharing control (PSC) scheme for a microgrid to firstly adjust wind generators (WGs) and then PVs to optimally meet the dispatch command while minimizing the reduction of total energy

production. The WGs rotors can be fully utilized for temperately storing or releasing excessive energy, and the PV generation can be deloaded only when needed. Compared to the traditional methods, the efficiency of system operation can be largely improved by significantly reducing the compromised energy harvest.

1.3 Thesis Layout

The rest of this thesis consists of five chapters. Chapter II presents two control strategies of PMSG-Based wind turbines for system inertia support. Chapter III proposes a variable utilization level scheme for load sharing control of wind farm. Chapter IV presents an optimal power sharing control of wind turbines to cope with the power dispatching demand by system operator. Chapter V investigates cascading power sharing control for microgrid operation with wind and solar generation. Finally, the conclusions of the thesis are drawn in Chapter VII.

1.4 List of Publications

Journal paper

1. Yujun Li, Zhao Xu, and Ke Meng, "Optimal Power Sharing Control of Wind Turbines," *IEEE Transactions on Power Systems*, vol. 32, no. 1, pp. 824-825, Jan. 2017. (published)

2. Yujun Li, Zhao Xu, and Kit Po Wong, " Advanced Control Strategies of PMSG-Based Wind Turbines for System Inertia Support," *IEEE Transactions on Power Systems*, vol. 32, no. 4, pp. 3027-3037, July 2017. (published)

3. Yujun Li, Zhao Xu, Jacob Østergaard and David John Hill, "Coordinated Control Strategies for Offshore Wind Farm Integration via VSC-HVDC for System Frequency Support," *IEEE Transactions on Energy Conversion*, vol. 32, no. 3, pp. 843-856, Sept. 2017. (published)

4. Yujun Li, Zhao Xu, Jiangliang Zhang, Ke Meng, "Variable Droop Voltage Control for Wind Farm", *IEEE Transaction on Sustainable Energy*, July, 2017. (accepted)

5. Yujun Li, Zeren Zhang, Yong Yang, Yingyi Li, Hairong Chen, and Zheng Xu, "Coordinated control of wind farm and VSC-HVDC system using capacitor energy and kinetic energy to improve inertia level of power systems," *International Journal of Electrical Power & Energy Systems*, vol. 59, pp. 79-92, Jul 2014. (published)

6. Yujun Li, Zhao Xu, Hon Wing Ngan, and Siu-Chung Wong, "A Novel Topology Design for Integration of Offshore Wind Farm via High-voltage DC Transmission," *Electric Power Components and Systems*, vol. 43, pp. 1100-1112, Jun 15 2015. (published)

7. Yujun Li, and Zhao Xu, "Coordinated Control of Wind Farms and MTDC Grids for System Frequency Support," *Electric Power Components and Systems*, vol. 45, pp. 1-14, Feb, 2017. (published)

8. Yujun Li, Zhao Xu, Ke Meng and Kit Po Wong, "Power Flow Features and Balancing in MTDC Integrated Offshore Wind Farms", *Electric Power Components and Systems*, 45(10):1068-1079, July, 2017. (published)

9. Yujun Li, Zhao Xu, "Coordinated Control Strategies of Super-Capacitor and Kinetic Energy of DFIG for System Inertia Support", *IET Electrical Power Application*, 2016. (in revision)

10. Yujun Li, Zhao Xu, Jianliang Zhang, and Kit Po Wong, "Variable Utilization Level Scheme for Load Sharing Control of Wind Farm," *IEEE Transactions on Energy Conversion*, June,2017. (in revision)

11. Yujun Li, Zhao Xu, Balarko Chaudhuri, and Kit Po Wong, "Advanced Power Sharing Control for Microgrid Operation with Wind and Solar Generation" *IEEE Transaction on Smart Grid*, 2017. (in revision)

Conference paper

12. Yujun Li, Zhao Xu, Kit Po Wong, and Loi Lei Lai. "A two-stage power dispatching algorithm for system support by droop-controlled DC grids." *In Power & Energy Society General Meeting*, 2015 *IEEE*, Denver, U.S.A. pp. 1-5., 2015.

13. Yujun Li, Zhao Xu, and Li Yang. "Coordinated Control to improve the fault ride-through capability for the offshore wind farm integration via VSC-HVDC transmission." *In Proceedings of ICEE*, Hong Kong, 2015.

14. Yujun Li, and Zhao Xu, "Power Smoothing Control of Wind Turbines Using Different Strategies" *IEEE International Conference on Smart Grid Communications*, November 2016, Sydney, Australia.

Chapter II

Advanced Control Strategies of PMSG-Based Wind Turbines for System Inertia Support

2.1 Introduction

With the increased wind power penetration in power grids, the reduced inertia response has drawn considerable attentions from power system operators. Unlike the conventional power plants, variable speed wind turbines (VSWTs) are interfaced with the power grid through power electronic converters, whose main function is to realize the maximum power point tracking (MPPT) algorithm for maximized harvesting wind energy and guarantee the power transmitted to the grid. Because of the decoupled control between mechanical and electrical system, it effectively prevents the WTs from responding to the system frequency changes. Thus, given the same disturbances, the rate of change of system frequency (ROCOF) during first few seconds grows rapidly with high penetration wind energy.

In a variable speed wind energy conversion system (WECS), three sources can be utilized for providing system inertia support. The first one is to utilize the WT reserved energy by pitching [29-31] to support the system frequency. However, this control will force WT to deviate from MPPT operating point and sacrifice much captured energy for system support. In addition, the response speed is rather slow due to the mechanical regulation of pitch angle. Meanwhile, frequent activation of blade pitching for system support will increase mechanical stress and fatigue of WT.

Another source widely used in WECS is the rotating kinetic energy (KE) of WT, which can participate in system frequency regulation through proper designed emulated inertia control [15-24]. Emulated inertia control of WT can be broadly classified into three categories. The first scheme gives the WT a response to the frequency derivations, which is mimicking the inherent behaviour of a SG. The supplementary frequency loop (the additional amount of power supplied) is proportional to the system frequency derivation, which is normally called virtual inertia control. Derivation controller may emulate a synchronous inertia-like response well, but it may lead to system instability due to the noise in the frequency measurement [15-17]. The second one is similar to the primary frequency control that is deployed by conventional SG. The additional amount of the power supplied is proportional to the network system deviation, which is generally called “droop control” [18-20]. In [21], the authors combine the two control schemes to provide inertia response for the WTs. The supplementary power loops that are proportional to the frequency deviation and derivation are together utilized in order to exert more frequency support when severe system frequency excursions happen. The impacts of implementing droop control in DFIG-based wind turbines on microgrid are fully investigated in [19]. It is reported that torque- and power- droop implementations in DFIG-based units can provide short-time frequency support to the power grid. However, it may induce wear and tear and increase the maintenance cost for wind turbines with high droop parameters [22]. In [16], droop control can be considered as an alternative inertia response strategy for WT. The steady error induced by the droop control can be effectively eliminated by adding a high-pass filter. The third emulated inertia response is obtained from the fixed trajectory response. Any deviation in system frequency beyond a certain threshold, a fixed response shape can be triggered [24].

The last source to implement virtual inertia for variable speed wind turbine is DC-link capacitor energy in the power electronic converters. DC-link voltage can be temporarily changed so as to release or absorb DC capacitor partial energy for system support. [36] proposed a coordinated control of the DC-link voltage and pitch angle of the permanent magnetic synchronous generator (PMSG) for smoothing WT output power. [39] proposed a supplementary control that combines the pitch angle control and modification of WT output power reference for system frequency support. [37] indicated the WT rotating mass or DC-link capacitor of doubly fed induction generator (DFIG) can be utilized to implement the virtual inertia of DFIG. However, the energy stored in DC-link capacitor of DFIG is relatively small [40, 41] and super-capacitor should be installed for obtaining large WT virtual inertia constant.

This Section investigates two novel control strategies that enable system inertia supports by PMSG wind turbines during transient events. The first strategy seeks to provide inertia support to the system through simultaneous utilization of DC-link capacitor energy, and wind turbine (WT) rotor kinetic energy (KE). The second strategy supports system inertia through orderly exerting DC-link capacitor energy of WT and then WT rotor KE via a cascading control scheme. Both strategies can effectively provide system inertia support by fully utilizing WT's own potentials, while the second strategy distinguishes itself by minimizing its impacts on wind energy harvesting. Case studies of one synchronous generator (SG) connected with a PMSG-based WT considering sudden load variations have been studied to validate and compare the two proposed strategies on providing rapid inertia response for the system.

2.2 The Conventional Control of PMSG

For one thing, the capacity of PMSG DC-link capacitor is larger than that of DFIG, thus PMSG-based WT can provide more inertia support through the proposed control strategies. For another thing, the popularity of PMSG-based WT for application in large wind farms, especially offshore wind farm is increasing. Therefore, the proposed control strategies are performed on PMSG-based WT. The dynamic model of the PMSG and associated converters can be found in [96-98].

2.2.1 Rotor-Side Converter Control

The active power of the generator can be controlled via either rotor-side converter (RSC) or the grid-side converter (GSC). In this thesis, the RSC controls the generated active power, while the GSC is utilized to maintain constant DC-link voltage, as seen in Fig. 2.1. In the normal operation, the active power generated by the WT is controlled through the Maximum Power Point Tracking (MPPT) algorithm and the pitch angle control. The MPPT algorithm is implemented to calculate and set the optimal active power reference according to the current rotor speed (ω_r).

When studying the dynamic stability of wind turbine, the two-mass model of the drive train is important and it will induce low-frequency oscillation during WT dynamics. However, this impact can be effectively reduced by control method, which is realized by turning the PI parameters of WT speed controller [99]. In addition, in terms of frequency or inertia support from wind turbines, the variation of rotor speed of PMSG will not vary too much during this process [100]. The impact of two-mass model is limited and one-mass model is adequate for the next deduction. The total mechanical inertia constant H_s is represented as H_s=H_t+H_g. where H_t and H_g (per unit) are the turbine and generator inertia constants, respectively. Subsequently, the rotor speed dynamics is governed by the rotor motion equation described in (2.1),

$$2H_s \cdot \omega_r \cdot \frac{d\omega_r}{dt} = P_{wind} - P_{WT} \tag{2.1}$$

where P_{wind} and P_{WT} are the captured power from the WT and the WT output power, respectively. Because of the fast response of power electronic devices, WT output power can be regarded as same as its power reference determined by MPPT algorithm P_{MPPT}, that is $P_{WT} = P_{MPPT}$. Pitch angle control will be activated to constrain the rotor speed within its limit by increasing the pitch angle once detected over-speed of WT rotor. The reactive power of the PMSG can be controlled to zero or be regulated to maintain stator voltage [101].

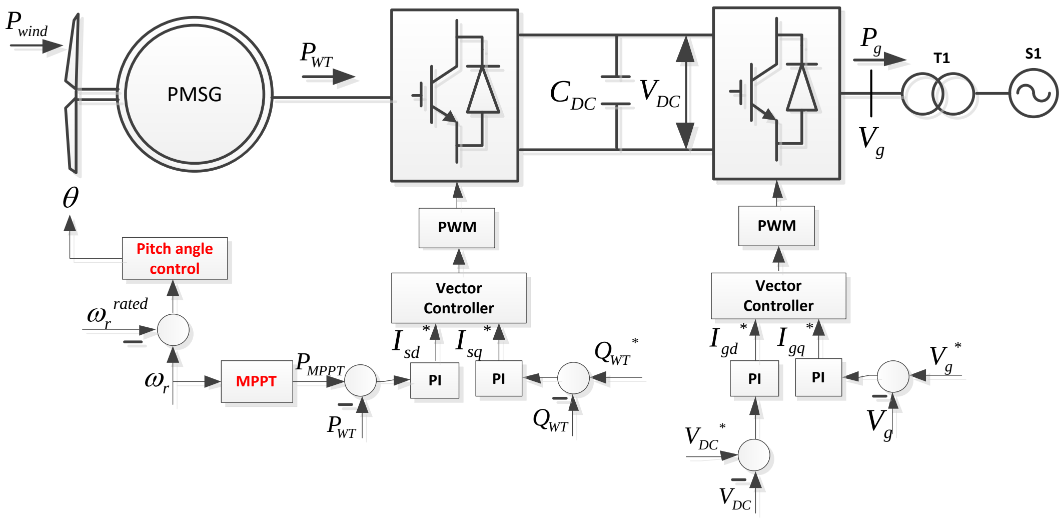

Fig. 2.1. Control diagram of a PMSG-based wind turbine

2.2.2 *Grid-Side Converter Control*

The grid-side converter aims at the control of DC-link voltage. The entire control scheme adopts the grid voltage reference frame where d-axis is chosen collinear to the grid voltage. The GSC controller is made up of two cascaded control loops. The outer loop controls the DC-link voltage VDC and the grid voltage V_g, which are associated with the d-axis current i_{gd} and the q-axis current i_{gq}, respectively. The reference V_{DC}^* is set as a constant value that guarantees the transmission of the captured wind energy to the grid side.

2.2.3 *Wind Turbine Model*

The mathematical expression of P_{wind} is as follows [101-104]:

$$P_{wind} = \frac{\rho}{2}\pi R^2 {v_w}^3 C_p(\lambda,\theta) \tag{2.2}$$

$$\lambda = \frac{\omega_t \cdot R}{v_w} = \frac{k \cdot \omega_r \cdot R}{v_w} \tag{2.3}$$

where ρ is the air density, R is the rotor blade radius, v_w is the wind speed, C_p is the power coefficient, λ is the tip speed ratio, k is the gear ratio of gearbox, ω_t is the wind turbine rotational speed and θ is the pitch angle. Normally, the pitch angle is kept zero when P_{wind} is below the rated power. Thus, C_p is the function of λ only and reaches the maximum C_{pmax} at certain λ. At this point; it obtains the optimal speed ω_r for a given v_w from (3), as shown in point A in Fig. 2.2. Any operation rotor speed deviation from optimal ω_r will result in the reduction of the captured wind power, as marked in point B and C in Fig. 2.2.

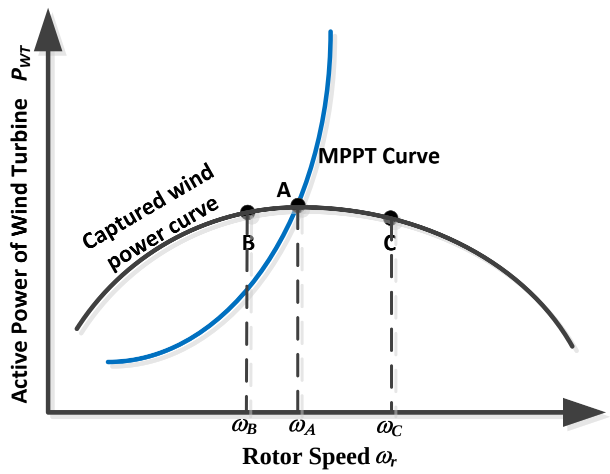

Fig. 2.2 Wind turbine operation characteristic

2.3 Strategy I: Simultaneous Control

Notably, wind turbine output power is traditionally controlled by the MPPT algorithm and insensitive to the system frequency due to the fast converter control. In addition, DC-link voltage is controlled as constant irrespective of grid frequency variations. Thus, conventional PMSG-based WT does not have frequency response during system disturbances.

2.3.1 Inertia Support from DC-link Capacitor

The DC-link capacitor voltage reflects the power balance of the power injected into RSC PWT and the power transmitted to the grid, P_g if ignoring the power losses among back-to-back converters. The dynamics of the DC-link voltage V_{DC} in per unit form can be written as follows:

$$C \cdot V_{DC} \cdot \frac{dV_{DC}}{dt} = P_{WT} - P_g \tag{2.4}$$

$$C = \frac{C_{DC} \cdot V_{DCn}{}^2}{S_B} \tag{2.5}$$

where S_B is the base value of the system. C_{DC}, C are the total capacitance and the equivalent capacitance in p.u., respectively. V_{DCn} is the nominal value of the DC-link voltage. In the following analysis, all the variables are in the per unit form.

It is well understood that any imbalance between the load and generation in the power system will lead to the alternation of the system frequency. A synchronous generator (SG) intrinsically uses its mechanical inertia to smooth the frequency deviation, which can be analyzed as follows:

$$2H \cdot f \cdot \frac{df}{dt} = \Delta P \tag{2.6}$$

where H is SG inertia constant, and f is the system frequency. ΔP is the deviation between the mechanical and the electrical power of the SG. It is noted that the value of H determines the ROCOF. Provided the same time frame, the higher H is, the smaller frequency variation will result.

In order to emulate the inertia in (2.6), P_{WT} and P_g in (2.4) can be roughly regarded as the mechanical and electrical power inputs to a SG, respectively. The DC-link voltage, to some extent, is analogous to the system frequency, thus

$$C \cdot V_{DC} \cdot \frac{dV_{DC}}{dt} = 2H_{DC} \cdot f \cdot \frac{df}{dt} \tag{2.7}$$

where H_{DC} is the equivalent virtual inertia constant provided by the DC-link capacitor. Integrating two sides of (2.7) over time,

$$\int_{V_{DC0}}^{V_{DC}} C \cdot V_{DC} \cdot dV_{DC} = \int_{f_0}^{f} 2H_{DC} \cdot f \cdot df \tag{2.8}$$

$$\frac{C \cdot (V_{DC}^{\ 2} - V_{DC0}^{\ 2})}{2} = H_{DC} \cdot (f^2 - f_0^2) \tag{2.9}$$

where V_{DC0} and f_0 are the nominal values of the DC-link voltage and the system frequency, respectively. Normally, they are set as 1 p.u. In practice, the DC-link voltage will vary within a small range in the normal operation. In this thesis, we set the DC-link voltage constraints as $\pm$0.1 p.u. The exact value depends on the insulation requirement and PWM pattern. Therefore, (2.9) can be linearized around its equilibrium point,

$$C \cdot V_{DC0} \cdot \Delta V_{DC} = 2H_{DC} \cdot f_0 \cdot \Delta f \tag{2.10}$$

Based on (2.10), the control process can be derived as follows:

$$V_{DC}^{\ *} = K_{DC} \cdot \Delta f + V_{DC0} \tag{2.11}$$

where K_{DC} is the control parameter and can be designed properly with respect to some technical requirements e.g. PWM frequency and the current rating of VSC etc. The control process above actually forms a DC-link voltage droop control scheme as illustrated in Fig. 2.3. From (2.10) and (2.11), the relationship between H_{DC} and K_{DC} can be written as follows:

$$H_{DC} = \frac{K_{DC} \cdot C \cdot V_{DC0}}{2 \cdot f_0} \tag{2.12}$$

2.3.2 Inertia Support from PMSG WT Rotor Kinetic Energy

In order to make the WT regulate its active power in response to system frequency alternation, the additional power deviation P_{ad}, which reflects the variation of system frequency should be added to P_{MPPT} determined by MPPT algorithm. A new reference active power for WT can be written as follows:

$$P_{WT}^{*} = P_{ad} + P_{MPPT} \tag{2.13}$$

where P_{WT}^{*} is the new reference active power for the PMSG-based WT. Two main controllers can be utilized to emulate P_{ad}. One is the derivative (D) controller, and the other is the proportional (P) controller. The D or P controller regulates P_{ad} through the differential and proportional operation of the system frequency deviation, respectively. In this thesis, P controller is utilized as an inertia response strategy for WT because of the possibility of instability caused by D controller due to the noises in frequency measurement [23].

Since active power of a PMSG can be regulated to a new value by its rotor side converter very quickly, replace P_{MPPT} in (2.1) with P_{WT}^{*} and $P_{WT}^{*} = P_{WT}$ and a modified rotor motion equation can then be derived in (2.14).

$$2H_s \cdot \omega_r \cdot \frac{d\omega_r}{dt} = P_{wind} - P_{WT} \tag{2.14}$$

With the similar transformation as in (2.6), (2.14) can be revised as follows:

$$2H_R \cdot f \cdot \frac{df}{dt} = P_{WT0} - P_{WT} \tag{2.15}$$

where H_R is the inertia constant, which is provided by the PMSG-based WT rotor kinetic energy (KE); P_{WT0} is the initial value of WT output power before system disturbance.

The tip speed ratio λ alters when the PMSG-based WT rotor speed changes during system disturbance, which leads to the captured wind power by WT P_{wind} decreases according to (2). Therefore, the relationship between initial WT output power P_{WT0} before system disturbance and the captured wind power P_{wind} during system disturbance results in,

$$P_{WT0} = P_{wind} + P_{loss} \tag{2.16}$$

The loss of captured wind power P_{loss} involved by the WT inertia control is relatively small based on the following two facts: Firstly, the slope of C_p curve is relatively small near the maximum point of C_p (C_{pmax}) as shown in Fig. 2.2, thus the variation of C_p around C_{pmax} is small. Secondly, the variation of ω_r is comparably small for the temporal system inertia support. Combine (14-16) gives (17) as follows,

$$2H_s \cdot \omega_r \cdot \frac{d\omega_r}{dt} + P_{loss} = 2H_R \cdot f \cdot \frac{df}{dt} \tag{2.17}$$

Integrate the two sides of (2.17) over time,

$$\int_{\omega_{r0}}^{\omega_r} 2H_s \cdot \omega_r \cdot d\omega_r + \int_{t_0}^{t} P_{loss} = \int_{f_0}^{f} 2H_R \cdot f \cdot df \tag{2.18}$$

$$H_s \cdot (\omega_r^{\ 2} - \omega_{r0}^{\ 2}) + E_{loss} = H_R \cdot (f^2 - f_0^{\ 2}) \tag{2.19}$$

where ω_{r0} is the initial WT rotor speed before the system disturbance and E_{loss} is the loss of captured wind energy involved by the PMSG-based WT inertia control. Assuming small changes of system states during system dynamics, linearize (2.19) at its initial operating point and transform into the following form:

$$H_s \cdot \omega_{r0} \cdot \Delta\omega_r + \frac{E_{loss}}{2} = H_R \cdot f_0 \cdot \Delta f \tag{2.20}$$

$$H_R = \frac{H_s \cdot \omega_{r0} \cdot \Delta\omega_r}{f_0 \cdot \Delta f} + \frac{E_{loss}}{2 \cdot f_0 \cdot \Delta f} \tag{2.21}$$

From (2.21), it is concluded that the inertia time constant H_R induced by WT inertia control consists of two parts: one is from rotor releasable or absorbable KE, the other is from the loss of captured wind energy E_{loss} due to the variation of WT rotor speed during system dynamics. For the first part, it highly depends on the change of WT rotor speed during the disturbance. The larger the deviation of the WT rotor speed, the more inertia the WT will provide. In addition, it is varied with the initial WT rotor speed. The higher the initial WT rotor speed, the more inertia the WT will render. For the second part, it relies on the direction of the system frequency deviation Δf. The inertia time constant H_R will increase if the system frequency deviation is positive, and the vise visa. Notably, the second part is relatively small due to the small value of E_{loss} during the system disturbances.

2.3.3 Further Discussion of Wind Turbine Inertia Support

It can be seen from (2.21) that the exact amount of the emulated inertia provided by the wind turbine is determined by the rotor speed variation if overlooking the small impact of E_{loss} on the emulated inertia H_R. However, the change of rotor speed depends on the control parameter K_B in the P controller and the MPPT curve adopted.

Replacing (2.13) in the (2.15), yields,

$$2H_R \cdot f \cdot \frac{df}{dt} = P_{WT0} - P_{ad} - P_{MPPT} \tag{2.22}$$

Integrate both side of (2.22) over time resulting in,

$$\int_{t_0}^{t} 2H_R \cdot f \cdot \frac{df}{dt} = \int_{t_0}^{t} P_{WT0}dt - \int_{t_0}^{t} P_{ad}dt - \int_{t_0}^{t} P_{MPPT}dt \tag{2.23}$$

$$2H_R \cdot f_0 \cdot \Delta f = P_{WT0} \cdot \Delta t - \int_{t_0}^{t} P_{ad}dt - \int_{t_0}^{t} P_{MPPT}dt \tag{2.24}$$

Accordingly, due to the droop control implemented to provide system inertia support, $P_{ad}=K_B\Delta f$, H_R can be expressed as,

$$H_R = \frac{P_{WT0} \cdot \Delta t - \int_{t_0}^{t} P_{MPPT}dt}{2 \cdot f_0 \cdot \Delta f} - \frac{\int_{t_0}^{t} K_B \cdot \Delta f dt}{2 \cdot f_0 \cdot \Delta f} = F_1 + F_2 \tag{2.25}$$

It is noted from (25) that the inertia provided by PMSG consists of two parts (F_1 and F_2). F_1 reflects the influence of the MPPT curve on H_R. F_2 represents the effect of droop control parameter K_B on H_R. With respect to the first part, MPPT controller may have impaired inertia response due to the interaction during rotor speed change [37]. For instance, if the system frequency drops, the droop control will try to reduce the rotor speed by increasing its active power output to release partial kinetic energy, which leads to the power reference from MPPT reducing as the rotor speed decreases. It indicates that the numerator of F_1 positive and F_1 is a negative value. The combined power for system inertia support is limited. However, considering small variation of PMSG rotor speed during system inertia support, the power reference from MPPT will not change too much during dynamics. In addition, P_{MPPT} will not alter when wind turbine operates at high wind speed, the influence of the MPPT curve on H_R (F_1 in (2.25)) may be somehow overlooked during system dynamics. Therefore, the emulated inertia provided by the wind turbine can be approximately as,

$$H_R \approx F_2 = -\frac{\int_{t_0}^{t} K_B \cdot \Delta f dt}{2 \cdot f_0 \cdot \Delta f} \tag{2.26}$$

It can be seen that in order to obtain a positive emulated inertia constant H_R, K_B should be negative. It is concluded that larger K_B will obtain higher H_R from (2.26).

Combine (2.4) and (2.15); (2.10) and (2.20), the total inertia constant H_{WT}, which is provided by the PMSG WT utilizing DC-link capacitor and WT rotor KE simultaneously can be calculated as follows:

$$C \cdot V_{DC0} \cdot \Delta V_{DC} + H_s \cdot \omega_{r0} \cdot \Delta\omega_r + \frac{E_{loss}}{2} = H_{WT} \cdot f_0 \cdot \Delta f \tag{2.27}$$

$$\begin{aligned} H_{WT} &= H_{DC} + H_R \\ &= \frac{C \cdot V_{DC0} \cdot \Delta V_{DC}}{2 \cdot f_0 \cdot \Delta f} + \frac{H_s \cdot \omega_{r0} \cdot \Delta\omega_r}{f_0 \cdot \Delta f} + \frac{E_{loss}}{2 f_0 \cdot \Delta f} \end{aligned} \tag{2.28}$$

Obviously, the proposed simultaneous control can provide more inertia support than single WT inertia control provided by WT rotor KE. In conclusion, the DC-link capacitor and the PMSG-based WT rotor KE together provide the inertia support by the proposed simultaneous control, as shown in Fig. 2.3. Taking the system frequency drop as an example, the GSC firstly lowers WT DC-link voltage reference in response to the decreasing system frequency and the stored DC-link capacitor energy is partially released to the system. Meanwhile, PWMG increases their active power reference through the P controller by detecting the decreasing system frequency and the rotor KE is released simultaneously for system support. Through a series of actions of the above controllers, the magnitude and the rate of the frequency change in the main grid are reduced. Accordingly, the overall stability of the power system is increased.

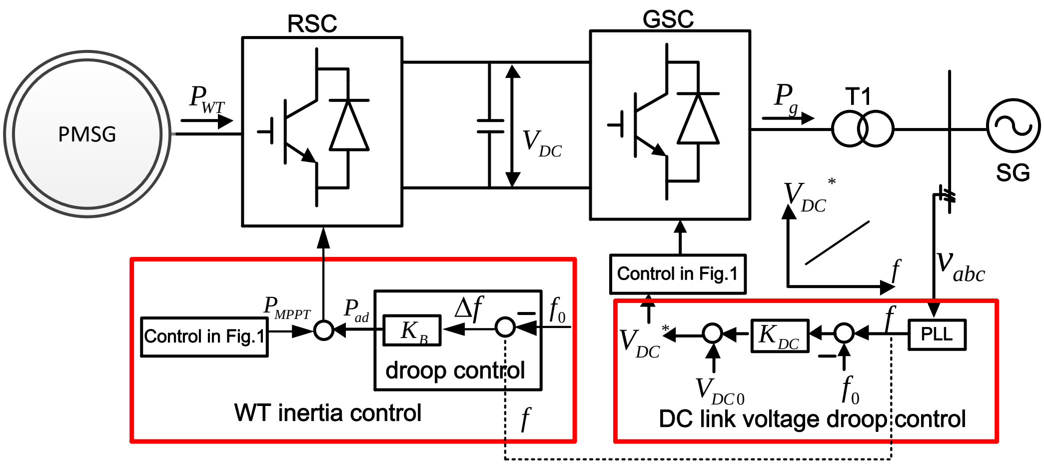

Fig. 2.3. Control scheme of the simultaneous control

2.4 Cascading Control

In the strategy I, WT rotor kinetic energy (KE) and DC-link capacitor simultaneously provide inertia support for the AC grid once disturbances occur. Even though this strategy can fully utilize the PMSG-based WT self-inertia to increase the system stability, it may require WT constantly deviating from the optimal reference points whenever frequency disturbances occur. As for DC-link voltage, it can vary in a small range from the nominal to provide system inertia support. However, using rotor KE to smooth the system frequency will inevitably lead to the rotor speed deviations from the optimal reference, which is determined by the MPPT algorithm. Put it differently, the strategy I may enable PMSG WT constantly deviating from its maximum power capture status in response to frequency disturbances, which may not be a cost-effective strategy for a commercial wind farm.

To avoid the aforementioned problem, a cascading control strategy that can sequentially activate the inertia supports from DC-link capacitor energy and then WT rotor KE automatically is proposed. The core of this strategy is that, within a certain energy tolerable limit, the energy stored in DC-link capacitor is always firstly utilized for system inertia support, while WT rotor KE is exerted only if the AC grid frequency deviation still exists. In the proposed cascading control, the stored energy in DC-link capacitor is maximally utilized to make sure less wind power is wasted due to the deviations from the MPPT operating points caused by WT inertia control while making the optimal use of available resources for system support. In the following, the detailed design of control strategies of GSC and RSC is presented for the cascading control scheme.

2.4.1 Cascading Control with DC-link Capacitor Activated Only

Under the cascading control, GSC still implements DC-link voltage droop control, which enables the coupling between DC-link voltage and system frequency. When the system frequency deviation is within a small range, DC-link capacitor will contribute alone for system inertia support, and WT inertia control will not be activated, minimizing the impacts to WT MPPT operation. Compared to the simultaneous control strategy, the proposed cascading control strategy can ensure better harvest of wind energy while supporting system frequency effectively, which is of economic significance in system daily operation where small frequency disturbances prevail.

2.4.2 Cascading Control with Both DC-link Capacitor and WT Rotor KE Activated

When DC-link voltage reaches its limitation in events of large system frequency disturbances, DC-link capacitor firstly uses up its stored energy. Consequently, WT rotor KE becomes the last resort for system inertia support. In order to activate WT inertia support illustrated in Section III.B, a proper designed dead band for AC system frequency is essential to sequentially cascade DC-link voltage droop control and WT inertia support control. In addition, frequent utilization of WT rotor KE is avoided through the designed dead band described as follows:

$$\Delta f_{WT} = \begin{cases} f - f^{'} - f_0 & when\ V_{DC} = 0.9\ or\ V_{DC} = 1.1 \\ 0 & when\ \ 0.9 < V_{DC} < 1.1 \end{cases} \tag{2.29}$$

where Δf_{WT} is the modified system frequency deviation for the RSC control of PMSG-based WT. $f^{'}$ is the cut-off frequency, whose value equals to the AC system frequency when DC-link voltage beyond its limitation, yielding:

$$f^{'} = \begin{cases} 0.1 / K_{DC} & when\ V_{DC} = 1.1 \\ -0.1 / K_{DC} & when\ V_{DC} = 0.9 \end{cases} \tag{2.30}$$

It is noted that when the AC system frequency deviation is within cut-off frequency determined in (2.30), only DC-link capacitor is activated to support system frequency. Once larger system frequency deviation occurs and exceeds the defined cut-off frequency, WT rotor KE is activated to provide fast inertia support. This cascading design well distributes the self-resources for system support and successfully resolves the paradox between harvesting wind energy and providing system inertia support. Similar to Equation (2.21), the virtual inertia constant H_R induced by WT inertia control is written as follows:

$$H_R = \frac{H_s \cdot \omega_{r0} \cdot \Delta\omega_r}{f_0 \cdot \Delta f_{WT}} + \frac{E_{loss}}{2 f_0 \cdot \Delta f_{WT}} \tag{2.31}$$

Fig.4 shows the overall control scheme of the cascading control, and correspondingly, the total virtual inertia constant H_{WT} provided by single PMSG-based WT is given below:

$$H_{WT} = \begin{cases} H_R & when\ \ V_{DC} = 0.9\ or\ V_{DC} = 1.1 \\ H_{DC} & when\ \ 0.9 < V_{DC} < 1.1 \end{cases} \tag{2.32}$$

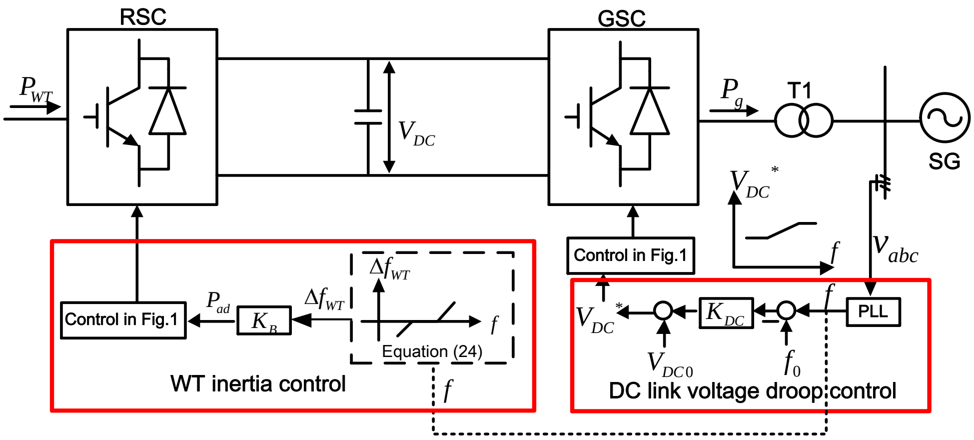

Fig. 2.4. Control scheme of the cascading control

2.4.3 Selection of Control Parameters

In order to fairly compare two control schemes, the control parameters of K_{DC} and K_B with cascading control should be tuned properly. K_{DC} of Strategy II is determined based on two following facts:

1. K_{DC} of Strategy II K_{DCII} should be larger than K_{DC} in Strategy I K_{DCI}

Compared (2.32) with (2.2), in order to fully utilize the inertia support capability of DC-link capacitor, K_{DC} in Strategy II K_{DCII} should be larger than K_{DC} in Strategy I K_{DCI}. If two K_{DC} in both control schemes are tuned the same, Strategy II may be more energy-saving than Strategy I but cannot provide as much inertia support as Strategy I, which may not take the advantage of the Strategy II.

2. K_{DC} in Strategy II K_{DCII} should be less than the maximum K_{DCmax}

WT inertia will be frequently utilized if K_{DC} is set too high, and this will sacrifice the advantage of harvesting as much wind energy as possible by the cascading control. Consequently, the selection of K_{DC} can be based on the specific grid code with respect to the minimum grid frequency deviation for WT inertia control beginning to be activated during system disturbances set by the system operator (the minimum cut-off frequency f'_{min} in (2.30)). Therefore, the K_{DCmax}=0.1/f'_{min}.

Therefore, the range of K_{DCII} is as follows,

$$K_{DCI} \leq K_{DCII} \leq K_{DC\max} \tag{2.33}$$

The selection criterion of K_B of Strategy II is achieving the similar frequency nadir or summit as with Strategy I under the same system disturbances. In the above parameter selection method, the energy saved by two control schemes can be fairly compared while providing similar frequency support via two strategies. Certainly, there are some alternative ways to set the parameters, but this is outside the scope of this thesis.

2.4.4 Further Discussion of Strategy I and II

Both proposed control strategies for PMSG based WT can provide system inertia support for the system during transient events. In the first strategy (simultaneous control scheme), it seeks to provide inertia support to the system through simultaneous utilization of DC-link capacitor energy and WT rotor kinetic energy (KE), which enables WT a larger virtual inertia constant than only WT inertia participating inertia support in the conventional control.

However, this strategy may cause WT constantly deviating from the MPPT point once there is system frequency disturbance, which may significantly affect the wind energy harvesting. In addition, extra wind energy will be sacrificed after system recovers from the disturbances because the droop frequency control implemented in the WT. Regarding this, we therefore further propose second strategy (cascading control scheme) which can orderly activate the inertia support form DC-link capacitors and WT inertia automatically. It has several innovative merits to enable both system support as well as maximally harvesting wind energy during system disturbances. Specifically, in the cascading control, the energy stored in the DC-link capacitor is always first utilized for system inertia support, while WT inertia is exerted only if the system frequency deviation still exists. It effectively avoids the frequency utilization of WT inertia and will be an energy saving strategy for commercial wind farm. In addition, steady error in the WT output power is eliminated due to the proper designed dead band for the system frequency. Therefore, WT can return back to its MPPT status after disturbances.

In sum, strategy II successfully resolves the paradox between harvesting wind energy and providing system inertia support, which is of economic significance in system daily operation where small frequency disturbances prevail and can potentially facilitate future penetration of wind energy into system.

2.5 Simulation Studies

In order to validate the proposed control strategies, a simple simulation system consisting of one synchronous generator (SG), a PMSG-based WT, and two local loads (L_1 and L_2) is described in Fig. 2.5. The SG is built by a seventh-order model [105] that simply represents the power grid. The rating of SG is 3MVAR, while the PMSG-based WT is rated at 2 MVAR, which gives a wind power capacity penetration of around 40% for the test system. L1 consists of a fixed load $P_{L1}+Q_{L1}$ as 3MW+0.3 MVAR, and the other dump load L2 $P_{L2}+Q_{L2}$ as 0.3MW+0.03MVAR. In the test system, SG regulates the frequency by its governor with permanent droop of 4%. The AC common coupling voltage is 6.6 kV and the PWM frequency for the PMSG converters is 10 kHz. More parameters of the test system can be referred to Appendix.

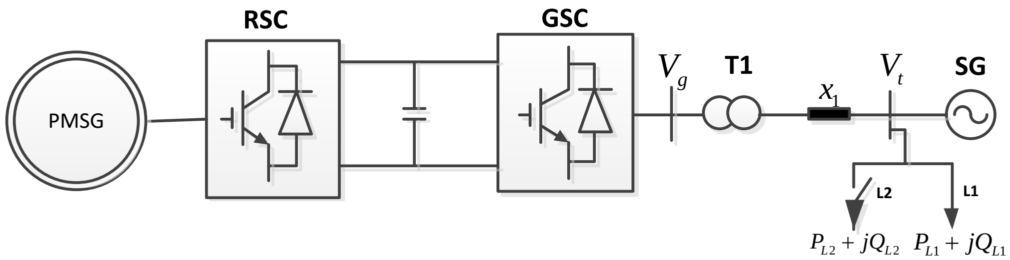

Fig. 2.5 The outline of the test system

2.5.1 Sudden load increase with same control parameters

Fig. 2.6 shows the sudden load increase event on the AC system, where the dump load $P_{L2}+Q_{L2}$ is switched on at t=10s. Four different situations namely without any additional control, with WT inertia control only, with proposed control strategy I and II are compared in Fig. 2.6. Droop control parameter K_B is set as -4 with WT inertia control only. Control parameters of DC-link voltage droop control and WT inertia control K_{DC}=2 and K_B=-4 are set the same in both proposed control schemes in this case. As shown in Fig. 2.6 (a), it is clearly seen that three control strategies take effect in fast system inertia support from PMSG-based WT. With simultaneous control, it provides most inertia support and the frequency nadir is the highest among three control schemes. This is because with Strategy I, the inertia support comes from both DC-link capacitor and WT rotor KE. However, with the cascading control, the inertia support is solely from DC-link capacitor if DC-link voltage is within its limitation. With traditional droop control, the inertia support comes only from WT rotor KE. Due to the limited capacitance of DC-link capacitor of PMSG based WT; the frequency quality with Strategy II is not largely improved. Similarly, the frequency profile with Strategy I is not largely improved compared with traditional droop control. However, the situation can be improved by installing larger DC-link capacitor or ESS between back-to-back converters of PMSG. Therefore, it is concluded that, given the same control parameters, Strategy I may provide more inertia support than Strategy II within DC-link voltage limitation. The mechanical power of SG begins to increase to compensate the load gap as shown in Fig. 2.6 (c). It indicates that the mechanical power of SG increases fastest without any control. With Strategy I, it increases more softly than with Strategy II because it provides more inertia support under same system disturbances. Correspondingly, more active power is transmitted to the AC grid from PMSG than that with cascading control, as shown in Fig. 2.6 (e). The DC-link voltages with the proposed control schemes as shown in Fig. 2.6 (d) show the same patterns as system frequency because of DC-link voltage droop control in both schemes. However, with WT inertia control only, DC-link voltage is kept as a constant during system transients, which cannot provide inertia support from DC-link capacitor during disturbances. DC-link voltages of both proposed strategies are within limitations due to a relatively small K_{DC} selected. Correspondingly, the cascading control does not activate WT inertia control and the rotor KE of WT is not released as shown in Fig. 2.6 (f) and (h). It is shown in Fig. 2.6 (h) that a slight oscillation appears in the generator speed of PMSG at the initial of system disturbances due to the two-mass model of PMSG. Fig. 2.6 (f) indicates that the RSC active power increases after system disturbance by Strategy I. Correspondingly, it leads to the PMSG rotor speed decreasing to compensate power gap between its mechanical and electrical power. Due to the rotor speed deviation from its optimal speed determined by MPPT algorithm, the captured wind power is lower than the maximum power point as shown in Fig. 2.6 (g). The difference of wind power harvesting by two schemes is roughly calculated as 0.1551 (shadow area marked in S), which indicates the loss of captured wind energy during system disturbances. It is therefore concluded that the cascading control can be more energy efficient while providing similar control functions, which can be beneficial for wind farm owners.

Both proposed control strategies for PMSG based WT can provide system inertia support by utilizing two virtual inertia source, namely WT rotor KE and DC-link capacitor, which enables WT a larger virtual inertia constant than only WT inertia participating system support via conventional control. However, since K_{DC} in both control schemes are tuned the same, Strategy II may be more energy-saving than Strategy I but cannot provide as much inertia support as Strategy I, which leads to WT inertia control being not activated and may not take advantage of the Strategy II. Different control parameters are adopted for the following cases to show the superiority of Strategy II.

2.5.2 Sudden load increase with different control parameters

Fig. 2.7 shows the simulation results for the same sudden load increase event on the AC system. DC voltage droop control parameter K_{DC} is set as 2 and 5 for the strategies I and II respectively. The selection of K_{DC} in Strategy II is based on the minimum cut-off frequency f'_{min}. In this thesis, f'_{min} is selected as 0.01 p.u. Correspondingly, K_{DCmax}=10. In order to better illustrate the difference between two control schemes, a larger K_{DC} for strategy II (K_{DCII}=5) is selected. In order to achieve similar frequency nadirs, K_B of the two strategies are set as -4 and -10, respectively.

It is shown from Fig. 2.7 (a) and (b) that, with the simultaneous control, the absolute ROCOF value in the inception of the event is slightly larger than that of cascading control. This is not unreasonable since Strategy II adopts a larger droop parameter, thus providing more inertia support. As shown in Fig. 2.7 (d), due to the larger K_{DC} in Strategy II, it enables DC-link voltage to reach its limitations faster, and once this occurs, DC-link capacitor cannot provide inertia support any more, which explains the unsmoothed profile of PMSG active power as shown in Fig. 2.7 (e) in Strategy II. Sequentially, cascading control will then activate WT inertia control. Fig. 2.7 (f) shows clearly that the active power output from RSC increases after system disturbance, which is achieved by WT rotor speed reduction to release KE as shown in Fig. 2.7 (h). It is shown in Fig. 2.7 (h) that there is generation rotor oscillation at the initial of system disturbances due to the two-mass model of PMSG. However, this oscillation is too slight to influence the performance of the proposed two control schemes, which validates one-mass model can be adequate to analyze the inertia support from WT. It is noted in Fig. 2.7 (g) that the cascading control causes less loss of wind energy production compared to the simultaneous control during the disturbance. The actual wind energy losses are 0.1551 per unit (marked as S1) and 0.0561 (marked as S2) for Strategy I and II respectively, which again validates the energy efficient advantage of the latter.

2.5.3 Sudden load increase with different control parameters

Fig. 2.8 shows the sudden load decrease event on the AC system, where dump load is suddenly switched out at t=10s. It is clearly seen that, with two proposed schemes, the frequency peaks during the disturbance are lower than that without any additional control. In order to compare the impact on the energy harvesting ability by two proposed schemes, the control parameters of two proposed control schemes are set the same in Case B. The cascading control enables a quicker rise of DC-link voltage towards the limitation as shown in Fig. 2.8 (d) due to the larger voltage droop control parameter K_{DC}. Notably, DC-link capacitor uses up its energy once DC-link voltage reaches the limitation, which explains the much unsmoothed profile of PMSG active power by the Strategy II observed in Fig. 2.8 (e).

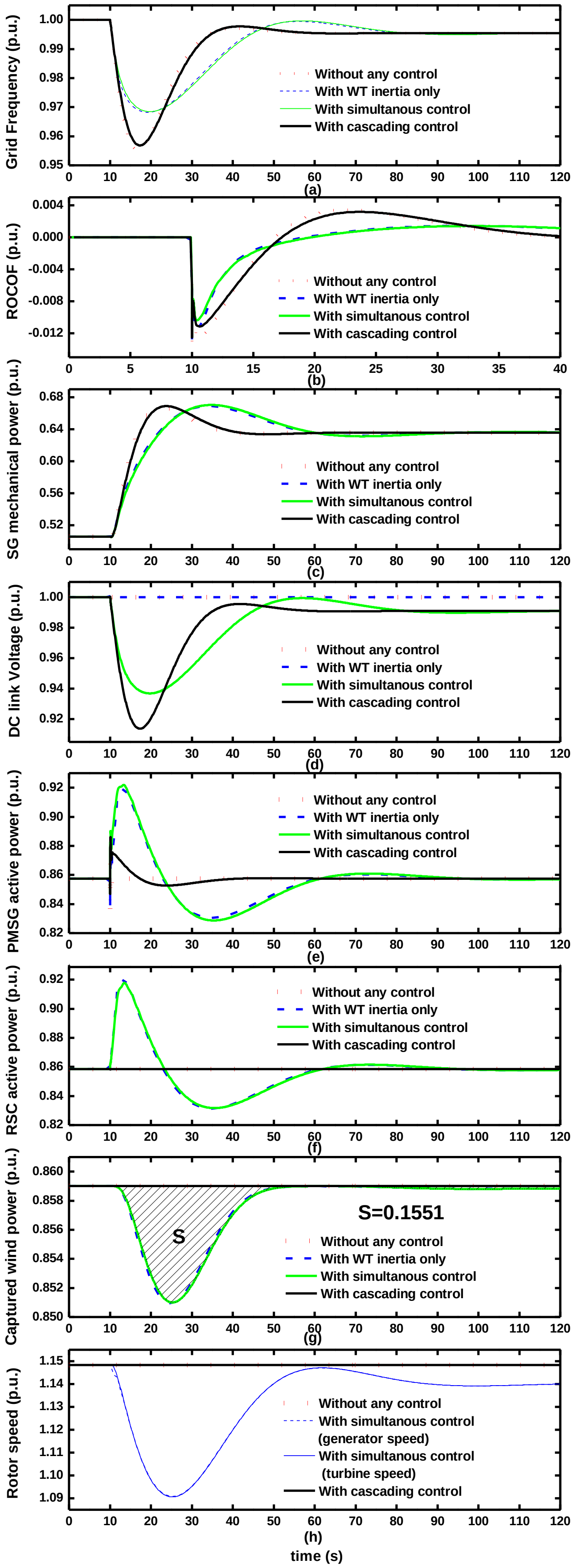

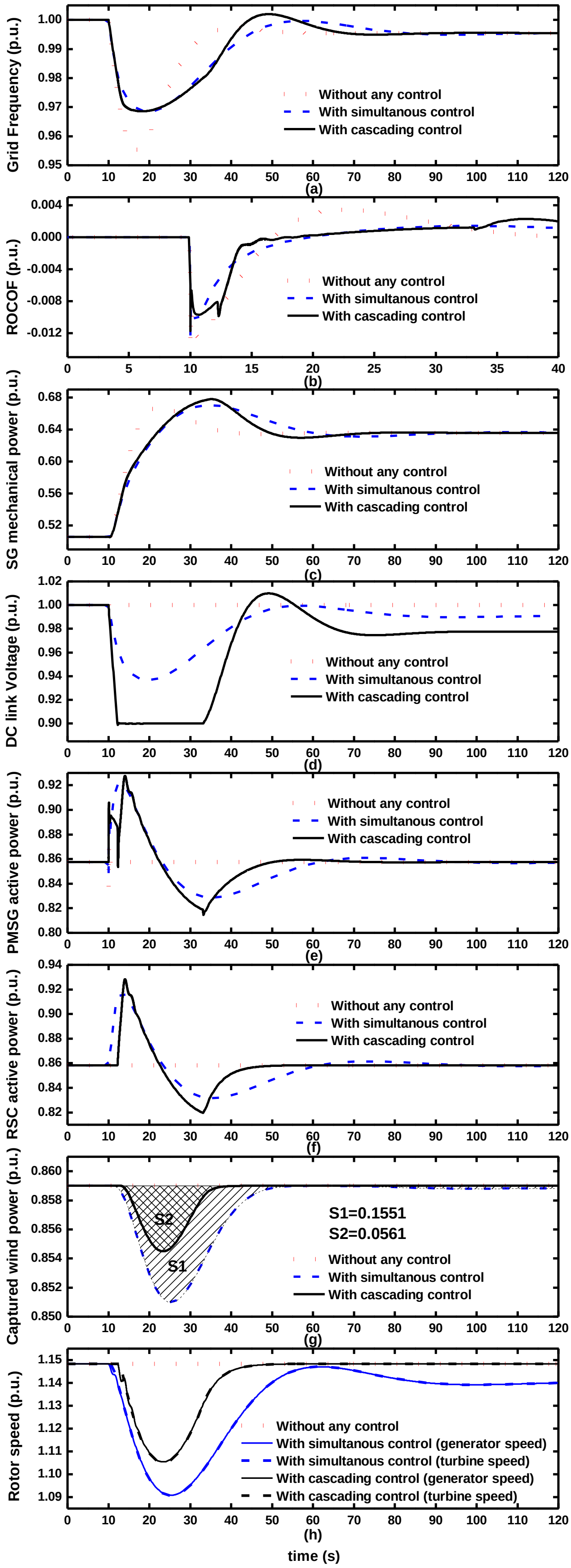

Fig. 2.6 Results for sudden load increase with same control parameters
Fig. 2.7 Results for sudden load increase with different control parameters

Since the Strategy II only activates WT inertia control support when DC-link voltage reaches the limitation, it results in a faster recovery of RSC power output after the disturbance in Fig. 2.8 (f). It is clearly seen from Fig. 2.8 (g) and (h), the cascading control also leads to smaller deviation from the optimal rotor speed determined by MPPT algorithm in this case study. Consequently, the cascading control observes a less loss of wind energy harvest (S2=0.0246) than that with the simultaneous control (S1=0.0821). Therefore, from the Case B and C, it can be concluded that the cascading control can actually harvest more wind power than the simultaneous one while providing similar frequency support.

2.6 Summary

This chapter proposes and analyzes two novel control strategies for PMSG-based wind turbine to provide fast system inertia support. The first simultaneous control seeks to utilize the DC-link capacitor energy and WT rotor kinetic energy simultaneously for AC grid support. In contrast, the proposed cascading control can sequentially exert DC-link capacitor energy and then WT rotor KE to provide fast system support. Detailed design and case studies of two proposed control schemes have been conducted. Given the same disturbance event, both control strategies can provide similar performance in stabilizing system frequency if the control parameters are set properly in advance. In addition, the proposed cascading strategy distinguishes itself by enabling better energy harvest during disturbances. It is believed that the two proposed novel strategies can provide additional benefit for system stability and are well suited for wind power application.

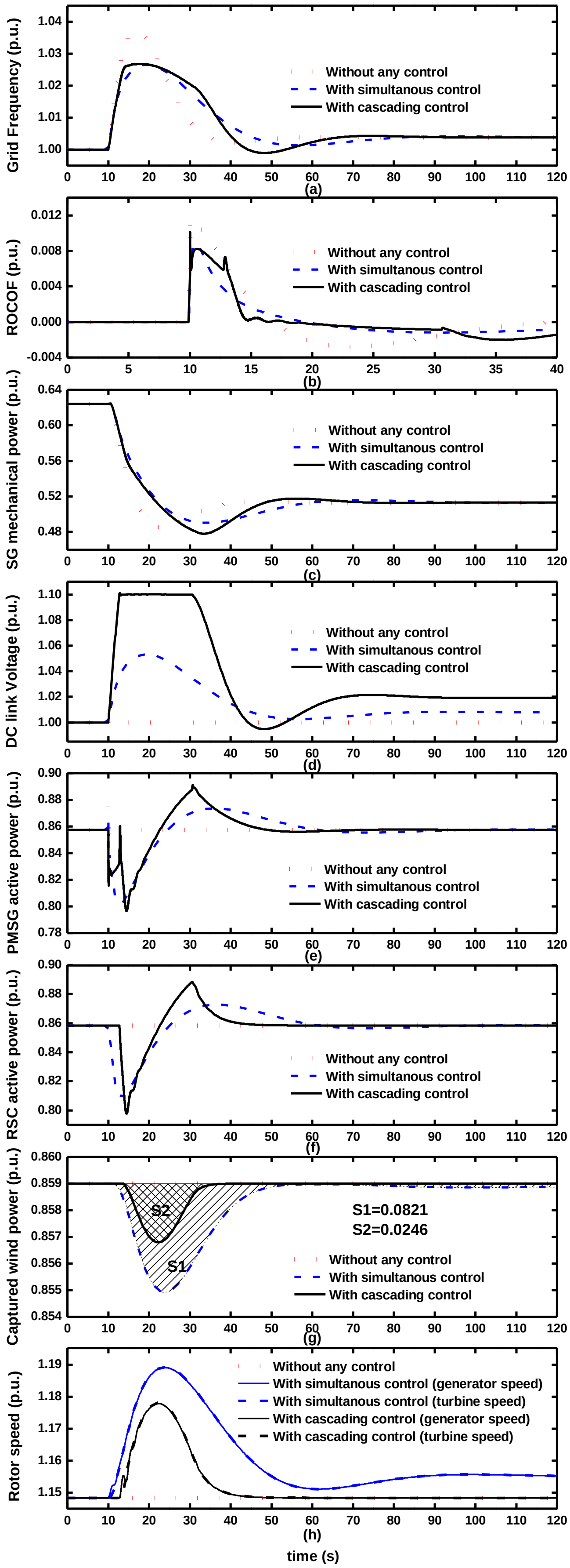

Fig. 2.8. Results for sudden load decrease with different control parameters

Chapter III

Variable Utilization Level Scheme for Load Sharing Control of Wind Farm

3.1 Introduction

Under Maximum Power Point Tracking (MPPT) control, wind power is not dispatchable and can be highly disturbing to the supply-demand balance control in particularly context of microgrid. To effective dispatch wind power according to e.g. operator command or market schedule, In [94], a simple and direct approach is proposed for load sharing by controlling the utilization level (UL) of each wind turbine, and maintaining it at a same value.

Wind turbines in a WPP may deviate from MPPT status while fulfilling the dispatch demand and certainly wind energy production will be compromised. Because of the wake interactions among wind turbines, the energy compromised by each wind turbine in a WPP may not be equal. Therefore, using the same UL scheme certainly may not be an optimal option in terms of reducing the loss of total energy production in a WPP.

This section firstly illustrates that under the conventional same utilization scheme, the overall energy reduction in a WPP may be high since the wind turbines at higher wind speeds may suffer more compromised energy production than those at lower wind speeds. In view of this, this thesis proposes a variable UL scheme for a DFIG-based WPP that coordinates each DFIG to fulfill the dispatch order while reducing the total energy loss. The utilization level of each wind turbine in a WPP is adaptively adjusted based on different wind turbines' rotor speeds so that more rotational kinetic energy (KE) can be stored in wind turbines, which can be later released back. The wake effect model is applied in calculating the wind speed at each DFIG in a WPP. The performance of the proposed scheme is validated effectively in *DIgSILENT/PowerFactory* and the results clearly indicate the proposed scheme can harvest more wind energy than the conventional same utilization level scheme while fulfilling the dispatch demand.

3.2 Wind Turbine Model and Conventional Load Sharing Control Scheme

Some preliminary knowledge is introduced herein. First, wind turbine (WT) model and classical maximum power point tracking (MPPT) algorithm for WT are briefly presented. Then, the wake interaction model among wind turbines is introduced. Lastly, the conventional same utilization level (UL) scheme for load sharing is described.

3.2.1 Wind Turbine Model

The mechanical power extracted from the wind P_{wind}, is defined by

$$P_{wind} = \frac{\rho}{2}\pi R^2 {v_w}^3 C_p(\lambda, \beta) \tag{3.1}$$

where ρ is the air density (kg/m^3), R is the rotor blade radius (m), v_w is the wind speed (m/s), λ is the tip speed ratio, β is the pitch angle (deg), and C_p is the power coefficient. As in [103], the expression of C_p in this thesis, as

$$C_p = 0.22(\frac{116}{\lambda_i} - 0.4\beta - 5)e^{-12.5/\lambda_i} \tag{3.2}$$

$$\lambda_i = \frac{1}{\frac{1}{(\lambda + 0.08\beta)} - \frac{0.035}{(\beta^3 + 1)}} \tag{3.3}$$

where the blade tip speed ratio λ,

$$\lambda = \frac{\omega_t \cdot R}{v_w} = \frac{k_g \cdot \omega_D \cdot R}{v_w} \tag{3.4}$$

where k_g is the gear ratio of gearbox, ω_t and ω_D is the wind turbine and DFIG generator rotational speed in per unit, respectively. Normally, the pitch angle will be controlled to zero when P_{wind} is below the rated power. Thus, C_p is the function of λ only and has a maximum value C_{pmax} at a certain λ, where the wind turbine obtains the maximum power and the optimal rotor speed ω_D for a given v_w from (3.4). Substituting (3.4) into (3.1), yields:

$$P_{MPPT} = \frac{\rho\pi R^5 k_g{}^3 C_{p\max}}{2\lambda^3} \cdot \omega_D{}^3 = C_M \cdot \omega_D{}^3 \tag{3.5}$$

where P_{MPPT} is the power output order determined by maximum power point tracking (MPPT) algorithm. Equation (3.5) is the expression of MPPT curve when ω_D operates in a range of 0.7-1.2 p.u. (B-C segment in Fig. 3.1). When ω_D is below 0.7 p.u. (A-B segment in Fig. 3.1), P_{MPPT} dramatically drops to zero. However, P_{MPPT} linearly increases to the rated power with ω_D in a range of 1.2-1.22 p.u. (C-D segment in Fig. 3.1) and finally be limited to the rated power by the pitch angle control (D-E segment in Fig. 3.1).

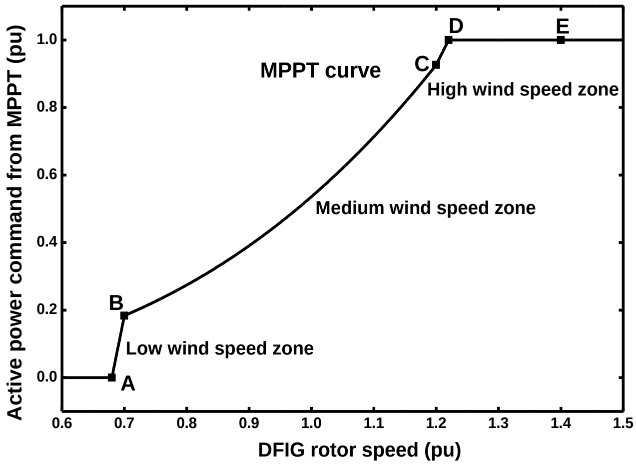

Fig. 3.1. Maximum power point tracking curve of DFIG

3.2.2 Wake Interaction Model

In a wind power plant (WPP) consisting of multiple DFIGs, the effective wind speed of a downstream wind turbine is lower than that of an upstream one due to the wake interaction between wind turbines. The well-studied Park model is one of the mainstream wake models in the existing literature [50-55]. It assumes that the wake wind speed is linearly expanded, as shown in Fig. 3.2. For any wind turbine $i \in n$ (assuming there are totally n wind turbines in WPP), the wind velocity is given by,

$$V_i = V_\infty (1 - \delta V_i) \tag{3.6}$$

where V_∞ is the free wind speed. The velocity deficit δV_i seen by turbine i is

$$\delta V_i = 2\sqrt{\sum_{j \in N: x_j < x_i} \left(a_j \left(\frac{D_j}{D_j + 2k(x_i - x_j)} \right)^2 \frac{A_{j \to i}^{overlap}}{A_i} \right)^2} \tag{3.7}$$

where D_j is the diameter of the turbine j blades. A_i is the rotor-swept area of a turbine i in m^2. $A_{j \to i}^{overlap} / A_i$ is the ratio between the overlapping area and swept area of the turbine i. a_j is the axial induction factor of turbine j. x_i is the radial distance of turbine i. k is a roughness coefficient. It has been found empirically for different environments, e.g., k=0.075 for farmlands and k=0.04 for offshore locations [51].

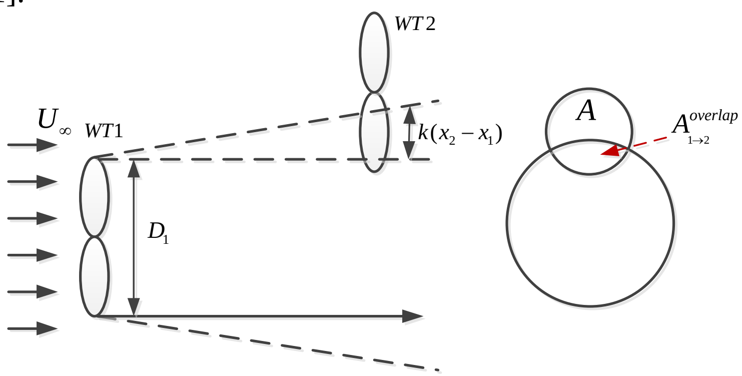

Fig.3.2. Wake interaction model between two wind turbines.

3.2.3 *Same Utilization Level Scheme for Load Sharing*

Fig. 3.3 shows a simple microgrid with a WPP of multiple DFIGs, a synchronous generator (SG), and several local loads. The SG provides reactive power for maintaining voltage and generates additional active power during low wind conditions. The total active power demand (P_d) for the WPP can be represented as follows,

$$P_d = \sum_{i=1}^{m} P_{Li} - P_G + P_{Loss} \tag{3.8}$$

where m is the number of the local loads in the microgrid. P_G is the active power from SG, P_{Li} is the ith local demand calculated based on local load. P_{Loss} is the active power loss among microgrid and can be regarded as a small percentage of P_d.

If the power loss among a WPP is neglected, the total available power generation from the WPP (P_{wm}) can be calculated as follows,

$$P_{wm} = \sum_{i=1}^{n} P_{mi} \tag{3.9}$$

where n is the number of DFIGs in a WPP, P_{mi} denotes the predicted maximum wind power generation of ith DFIG, which depends on the current wind speeds. Suppose P_d is the dispatch demand set by system operator, and if P_d is larger than P_{wm}, all DFIGs should be operated at MPPT status. If P_d is less than P_{wm}, a suitable deloading strategy is required to share the load among DFIGs. This is achieved by controlling the utilization levels (K_u) of DFIGs, maintaining them at a same value [94],

$$\begin{aligned} K_u &= \min\left\{\frac{P_d}{P_{wm}}, 1\right\} \\ P_{wti} &= K_u \cdot P_{mi} \end{aligned} \tag{3.10}$$

where P_{wti} is the active power generation set of the ith DFIG. The above same utilization level scheme can guarantee the supply-demand balance in a stand-alone microgrid. The actual wind power generation of WPP (P_{wpp}) can be expressed,

$$P_{wpp} = \sum_{i=1}^{n} K_u \cdot P_{mi} = \frac{P_d}{P_{wm}} \cdot \sum_{i=1}^{n} P_{mi} = P_d \tag{3.11}$$

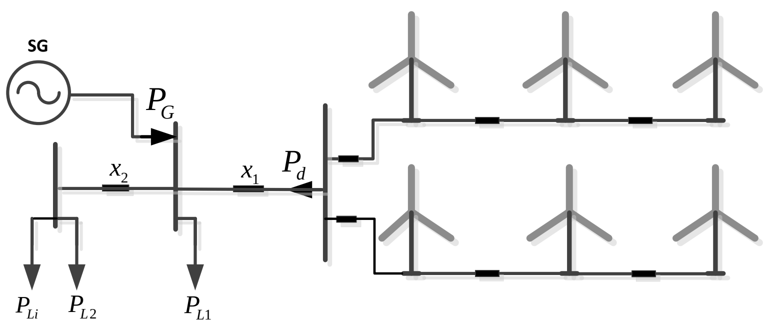

Fig. 3.3 Configuration of a simple stand-alone microgrid

3.3 Wind Energy Production Analysis for Different Deloading Strategies of DFIGs

When the available wind generation exceeds the system demand, a proper deloading strategy should be utilized instead of traditional MPPT algorithm to cope with the supply-demand imbalance. DFIG in a WPP may be controlled to temporally reduce its output by regulating its utilization level, while this may require DFIG to deviate from the optimal reference point and consequently, partial energy harvest is compromised during this process. Meanwhile, pitch angle based deloading control for load sharing is activated for front row DFIG in a WPP facing with high wind speed. However, kinetic energy (KE) based deloading control via accelerating wind turbine rotor is utilized to fulfill the power demand for back row DFIG with low wind speed. Therefore, DFIG energy production reduction or loss due to different deloading controls adopted for load sharing is analyzed in the section. It is assumed that all wind turbines are in MPPT operation prior to the system demand change. Therefore, wind speed is coupled with rotor speed of wind turbine according to (3-4). In the following, all the variables are in the per unit form.

The output power of each DFIG while adopting deloading control should be expressed as follows,

$$P_{wti} = K_i \cdot P_{mi} = K_i \cdot C_M \cdot \omega_{Di}^{3} \tag{3.12}$$

where K_i is the utilization level of the *ith* DFIG. Due to the fast active power regulation of rotor side converter in DFIG, the active power of a DFIG based wind turbine can be regulated to a new value very quickly. The power imbalance between captured wind power and electrical power of DFIG is imposed on the machine rotor. In addition, power loss of converters and wind turbines can be neglected in the dynamic analysis of wind turbine. Accordingly, rotor motion equation of DFIG can be written as (3.13),

$$2H_D \cdot \omega_{Di} \cdot \frac{d\omega_{Di}}{dt} = P_{wi} - P_{wti} \tag{3.13}$$

where H_D is the total inertia constant of the DFIG. In this theis, one-mass model of DFIG is utilized for simplification, since load sharing control among DFIGs is concerned. Furthermore, dynamic oscillations of DFIG can be effectively reduced during first few seconds of a transient event and it has little impact on active power control of each DFIG. P_{wi} and P_{wti} are the captured wind power and output active power of *ith* DFIG respectively. Integrate both sides of (3.13) over time yields the total captured wind energy (E_{Di}) by single DFIG under deloading control,

$$E_{Di} = \int_{t_0}^{t} P_{wi} dt = \int_{t_0}^{t} P_{wti} dt + \int_{t_0}^{t} 2H_D \cdot \frac{d\omega_{Di}{}^2}{dt} dt \tag{3.14}$$

Define E_{Di0} as the total captured wind energy by *ith* DFIG with no load sharing control involved. Since a relatively small power system is studied in this thesis, and the customer load is variable, the dispatch order will be short in few minutes. For simplification, it is assumed that wind speed does not change dramatically in a short time dispatch order. E_{Di0} can be described as follows,

$$E_{Di0} = \int_{t_0}^{t} P_{mi} dt = P_{mi} \cdot (t - t_0) \tag{3.15}$$

Based on (3.12), (3.14) and (3.15), the compromised wind energy $E_{Dloss,i}$ of *ith* DFIG during transient process due to the deloading control can be expressed as,

$$\begin{aligned} E_{Dloss,i} &= E_{D0i} - E_{Di} \\ &= (1 - K_i) \cdot P_{mi} \cdot (t - t_0) - \int_{t_0}^{t} 2H_D \cdot \frac{d\omega_{Di}{}^2}{dt} dt \\ &= (1 - K_i) \cdot P_{mi} \cdot (t - t_0) - H_D \cdot (\omega_{Di}{}^2(t) - \omega_{Di}{}^2(t_0)) \end{aligned} \tag{3.16}$$

Obviously, Equation (3.16) can be divided into two separated parts (E_{1i} *and* E_{2i}) as follows,

$$\begin{aligned} E_{1i} &= (1 - K_i) \cdot P_{mi} \cdot (t - t_0) \\ E_{2i} &= -H_D \cdot (\omega_{Di}{}^2(t) - \omega_{Di}{}^2(t_0)) \end{aligned} \tag{3.17}$$

It is noted from (3.17) that the compromised wind energy $E_{Dloss,i}$ during deloading control of wind turbine consists of two parts. E_{1i} represents the influence of the dispatch demand set by system operator on the wind energy loss $E_{Dloss,i}$, while E_{2i} shows the effect of rotation mass inertia on $E_{Dloss,i}$ during the transient process. Accordingly, the total loss of wind energy production (E_{Dloss}) within a WPP can be expressed as follows:

$$
\begin{aligned}
&E_{Dloss} = E_1 + E_2 \\
&E_1 = (t - t_0)\cdot\sum_{i=1}^{n}(1-K_i)\cdot P_{mi} = (t-t_0)\cdot(\sum_{i=1}^{n}P_{mi} - \sum_{i=1}^{n}K_i\cdot P_{mi}) \\
&\quad = (t-t_0)\cdot(P_{wm} - P_d) \\
&E_2 = -\Delta E_k = -(E_{\kappa}^{t} - E_{\kappa}^{t_0}) = -\sum_{i=1}^{n}H_D\cdot(\omega_{Di}{}^2(t) - \omega_{Di}{}^2(t_0))
\end{aligned}
\tag{3.18}
$$

where ΔE_k is the total rotor kinetic energy alternation while all DFIGs adopting deloading control within a wind power plant (WPP). E_k^t and E_t^{t0} are the total stored kinetic energy with in a WPP at time t and t_0 respectively. Similarly, the sacrificed wind energy due to load sharing control within a WPP E_{Dloss} consists of two separated parts: E_1 in (3.18) is a constant value, irrespective of DFIG utilization level K_i. It only reflects the imbalanced energy between the maximum energy a WPP can generate and the system demand during the deloading control. The expression of E_2 indicates some DFIGs may withhold partially kinetic energy with deloading control, which effectively harvest partially wind energy during load sharing control within a WPP. However, this value is determined based on different deloading controls of wind turbines adopted, and it influences the total stored kinetic energy within a WPP.

3.3.1 Overspeeding based Deloading Control

Fig. 3.4 shows the dynamic process of overspeeding based deloading control. Assume DFIG works at its optimal power point ***A*** under the wind speed of 12 m/s (*Segment A-C* in Fig. 3.1), When the available wind power exceeds the system needed, the wind turbine with lower wind speed (back row DFIG) decreases its output by reducing its utilization level. Due to the imbalanced power between the captured wind power and output power of wind turbine, DFIG begins to accelerate and finally reaches point ***B*** as a stable point. Assume DFIG operates at two different utilization levels (point ***B*** and ***C*** in Fig. 4).

Therefore, based on (3.17), the expression of E_{1i} and E_{2i} for two deloading points ***B*** and ***C*** can be calculated as follows,

$$\begin{cases} E_{1i} = (1-K_B)\cdot P_A \cdot \Delta t \\ E_{2i} = -H_D \cdot (\omega_{D,B}{}^2 - \omega_{D,\mathrm{A}}{}^2) \end{cases} (K_i = K_B)$$
$$\begin{cases} E_{1i} = (1-K_C)\cdot P_A \cdot \Delta t \\ E_{2i} = -H_D \cdot (\omega_{D,\mathrm{C}}{}^2 - \omega_{D,\mathrm{A}}{}^2) \end{cases} (K_i = K_C) \tag{3.19}$$

It can be obviously concluded that with the overspeeding based deloading control, the lower utilization level of each DFIG-based wind turbine is, the more rotor kinetic energy wind turbine can be stored.

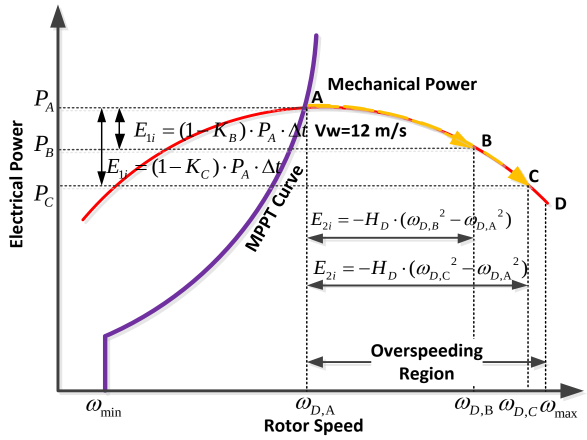

Fig. 3.4 Illustration of the overspeeding control strategy

3.3.2 Pitch Angle based Deloading Control

At high wind speed region (*Segment C-E* in Fig. 3.1), pitch angle control of front row DFIG will be activated to limit the output power of DFIG as the rated power and accordingly the DFIG rotor speed is constrained to the high-speed threshold set as 1.22 p.u. in this thesis. Assume that the DFIG operates at Point *E* at the wind speed of 15 m/s, which hits the upper boundary of rotor speed. Sequentially, wind turbine is required to operate under two deloading conditions with K_F and K_G, as shown in Fig. 5. Similarly, the expression of E_{1j} and E_{2j} with two different utilization levels based on (3.17) can be calculated as follows,

$$\begin{cases} E_{1j} = (1-K_E)\cdot P_A \cdot \Delta t \\ E_{2j} = 0 \end{cases} \quad (K_i = K_E)$$
$$\begin{cases} E_{1j} = (1-K_F)\cdot P_A \cdot \Delta t \\ E_{2j} = 0 \end{cases} \quad (K_i = K_F) \tag{3.20}$$

It can be obviously concluded from (3.20) that with the pitch angle based deloading control, partially wind energy will be curtailed and wasted. Moreover, the lower utilization level of each DFIG-based wind turbine is, the more wind energy will be sacrificed via blade pitching.

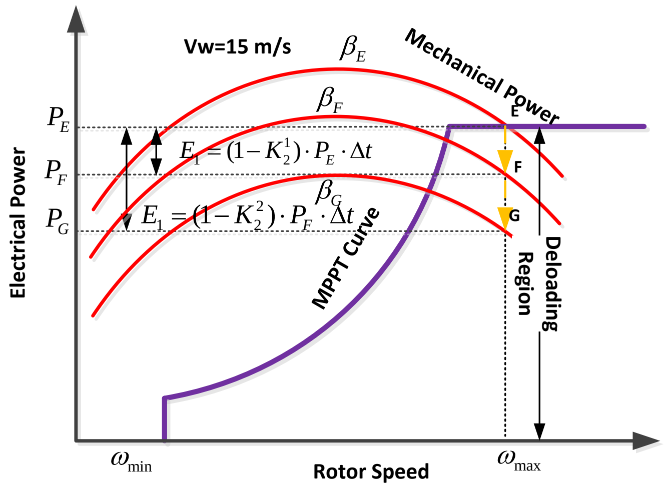

Fig. 3.5. Illustration of the pitch angle control strategy

3.3.3 Wind Energy Production Analysis within a WPP

Assume that the uniform utilization level is K_u for all wind turbines (WTs) in a WPP. Consider a WPP comprising of $n=N+M$ WTs, which are divided into two groups. Group one consists of low wind speed WTs whose rotor speeds are below the speed threshold ($i\in \mathrm{N}$). While, the rotational speeds of high wind speed WTs in Group two reach the speed threshold ($j\in \mathrm{M}$). Therefore, the output power of WPP can be expressed as,

$$P_d = P_{WPP} = K_u \cdot \sum_{i=1}^{N} P_{wmi} + K_u \cdot \sum_{j=1}^{M} P_{wmj} \tag{3.21}$$

where P_{WPP} is the wind power plant (WPP) output power and P_d is the system demand. P_{wmi} and P_{wmj} are the predicted maximum power by wind turbine i and j, respectively. It should be noted that pitch angle control will be activated while wind turbine rotor speed exceeds the predefined threshold speed. Accordingly, the harvested wind power will be directly curtailed / wasted by such control for high wind speed wind turbines (Group two). However, low wind speed turbines (Group one) can reduce their output power via overspeeding their rotors. In other words, Wind turbines of Group one can withhold partially wind energy by converting it into rotor kinetic energy of wind turbines through overspeeding based deloading control. Therefore, the energy reserved by Group one E_R through overspeeding based deloading control can be expressed as,

$$E_R = -\Delta E_k = -(E_\kappa^t - E_\kappa^{t_0}) = -\sum_{i=1}^{N} H_D \cdot (\omega_{Di}{}^2(t) - \omega_{Di}{}^2(t_0)) \qquad (3.22)$$

In comparison, in the proposed variable utilization level scheme, assume the utilization level is K_i and K_j for wind turbine i and j in a wind power plant (WPP). The following equation should be satisfied,

$$\begin{aligned} &P_d = P_{WPP} = \sum_{i=1}^{N} K_i \cdot P_{wmi} + \sum_{j=1}^{M} K_j \cdot P_{wmj} \\ &\sum_{i=1}^{N} K_i \cdot P_{wmi} < K_u \cdot \sum_{i=1}^{N} P_{wmi} \\ &\sum_{i=1}^{M} K_j \cdot P_{wmi} > K_u \cdot \sum_{j=1}^{M} P_{wmj} \end{aligned} \qquad (3.23)$$

In this thesis, to realize the relationship in (3.23), the deloading coefficient is adaptively adjusted according to wind turbine rotor speed. Consequently, high wind speed wind turbines adopt higher utilization level, which makes sure less wind energy will be sacrificed in a WPP. Moreover, more kinetic energy can be stored for low wind speed wind turbines with lower utilization level. The energy reserved $E_R{}'$ by the proposed variable utilization level scheme can be written as follows,

$$E_R{}' = -\Delta E_k{}' = -(E_\kappa^{t'} - E_\kappa^{t_0}) = -\sum_{i=1}^{N} H_D \cdot (\omega_{Di}{}'^2(t) - \omega_{Di}{}^2(t_0)) > E_R \qquad (3.24)$$

It should be noted that $\omega_{Di}{}'(t)$ in (3.24) should be larger than $\omega_{Di}(t)$ in (3.22) when a lower utilization level is adopted, which can be easily seen from Fig.4. Therefore, with the different utilization level scheme, the wind energy loss due to load sharing control in a WPP is reduced compared to the traditional same utilization level scheme given the same system dispatch command. In addition, the lower utilization level coefficient K_i for the back DFIG, the larger rotor speed variation of DFIG can be obtained and the more rotor kinetic energy of wind turbines will be stored within a WPP. In addition, utilizing overspeeding control for wind turbine deloading is more preferable than the pitch angle control with slow response due to the mechanical regulation involved. Furthermore, frequent activation of pitch angle may cause additional fatigue of wind turbine.

3.4 Proposed Variable Utilization Level Scheme for Load Sharing in a DFIG Based WPP

This thesis mainly focuses on load sharing control for a WPP of multiple DFIGs to cope with power mismatch between available wind generation (P_{wm}) and dispatch demand (P_d). Traditionally, the power mismatch can be shared by setting the same utilization level for all wind turbines available in WPP. However, this may not be an optimal option in terms of energy harvesting since the energy sacrificed via different deloading controls is not the same. Specifically, only back row DFIG at low wind speed can withhold partially wind energy through accelerating its rotor speed, which contributes to ΔE_k in (3.18). On the contrary, front row DFIG at high wind speed can reduce its output power via blade pitching, which has no contribution to ΔE_k in (3.18). Therefore, given the same dispatch command, in order to withhold as much wind energy as possible during load sharing control in a WPP, the back row DFIG should undertake more portion of supply-demand imbalance by converting more energy into rotor kinetic energy of wind turbine, and thus increasing ΔE_k in (3.18). Sequentially, the stored kinetic energy in a WPP in the deloading control can be later released back via proper designed overloading strategy.

A variable utilization level (UL) scheme for load sharing control in a WPP is proposed in this section. The proposed scheme differentiates the DFIGs depending on their current rotor speeds in the perspective of reducing the total loss of wind energy production while fulfilling the dispatch demand. The back row DFIG with lower rotor speed adopts lower utilization level, and the front DFIG with high rotor speed utilizes higher utilization level so that more kinetic energy can be stored in a WPP and less wind energy will be curtailed.

3.4.1 Deloading control of DFIGs for load sharing in a WPP

In order to achieve deloading control of wind turbines for load sharing while storing more kinetic energy in a WPP, one possible way for setting utilization levels of DFIGs can be as follows: define α_i as deloading coefficient for each DFIG in the deloading control, which is related to utilization level of K_i,

$$K_i = 1 - \alpha_i \tag{3.25}$$

The deloading coefficient α_i represents the deloading level of each DFIG. The larger of this value, the lower utilization level for each DFIG is. Actually, there are many ways to set deloading coefficient α_i of DFIG based on the different design purposes; Certainly, they can be set to be linear or square inversely proportional to the rotor speeds of WTs, which is out of scope in this thesis. However, in order to make the difference between each WT utilization level during deloading control large, one possible approach can be described as follows:

Define ω_{DH} as the highest rotor speed that all DFIGs in a WPP cannot exceed, and it is predefined as 1.25 p.u. in this thesis. Correspondingly, the difference between the current rotor speed of DFIG and the highest rotor speed can be expressed as follows:

$$\Delta\omega_{Di} = \omega_{DH} - \omega_{Di} \tag{3.26}$$

As a result, α_i is tuned so that the deloading coefficient of the *ith* DFIG is linearly proportional to the defined rotor speed difference $\Delta\omega_{Di}$ as follows,

$$\alpha_i \propto \Delta\omega_{Di} = \omega_{DH} - \omega_{Di} \tag{3.27}$$

Fig. 3.6 shows the proposed control scheme, where deloading coefficient α_i ($i \in n$) is adaptively adjusted based on the defined rotor speed difference $\Delta\omega_{Di}$. Consequently, the front DFIG at high wind speed adopts higher utilization level (lower deloading coefficient) for load sharing, which makes sure less wind energy will be sacrificed in a WPP. In order to realize the relationship described in (3.27), the following expression holds,

$$\frac{\alpha_i}{\omega_{DH}-\omega_{Di}}=\frac{\alpha_0}{\omega_{DH}-\omega_{D\max}} \tag{3.28}$$

where ω_{Dmax} is the maximum rotor speed of DFIG set as 1.22 p.u.. Particularly, α_0 is the deloading coefficient of DFIG while wind turbine operates at the maximum rotor speed. Accordingly, the selection of α_0 is based on the power balance equation described in (3.29),

$$\begin{aligned}\sum_{i=1}^{n}P_{wti} &= \sum_{i=1}^{n}K_i\cdot P_{mi}=\sum_{i=1}^{n}(1-\alpha_i)\cdot P_{mi}\\ &=\sum_{i=1}^{n}(1-\frac{\alpha_0}{\omega_{DH}-\omega_{D\max}}\cdot(\omega_{DH}-\omega_{Di}))\cdot P_{mi}=P_d\end{aligned} \tag{3.29}$$

Reorganizing (3.29), the deloading coefficient α_0 can be expressed as follows,

$$\alpha_0=\frac{(\sum_{i=1}^{n}P_{mi}-P_d)\cdot(\omega_{DH}-\omega_{D\max})}{\sum_{i=1}^{n}P_{mi}\cdot(\omega_{DH}-\omega_{Di})} \tag{3.30}$$

The corresponding deloading coefficient α_i and utilization level for each DFIG K_i while adopting the deloading control for load sharing in a WPP can be calculated based on (3.25) an (3.28),

$$\begin{aligned}\alpha_i &= \alpha_0\cdot\frac{(\omega_{DH}-\omega_{Di})}{\omega_{DH}-\omega_{D\max}}\\ K_i &= 1-\alpha_i\end{aligned} \tag{3.31}$$

It can be seen from (3.30) and (3.31) that the lower of the ω_{DH}, the smaller utilization level of back row DFIG will be and the more kinetic energy of DFIG based wind turbine can be stored in a wind power plant during deloading control.

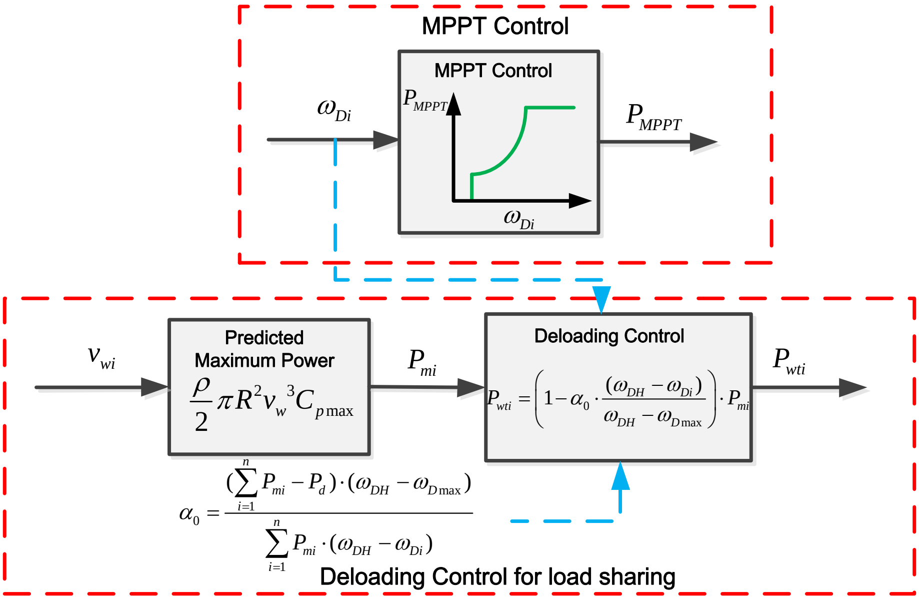

Fig 3.6 Proposed variable utilization level scheme for DFIG deloading control

3.4.2 Overloading control of DFIGs for load sharing in a WPP

When there is over-consumption in the system, the system required generation may be more than the maximum power a wind power plant (WPP) can produce. Accordingly, the stored kinetic energy via above deloading control can be released back via overloading scheme. One simple and direct way is to make the power difference between the system dispatch demand and the maximum power generation of wind turbines is evenly distributed to N low wind speed turbines (Group one). High wind speed turbines (Group two) return back to operate at the rated power. The power reference for each low wind speed turbine under overloading control can be expressed as,

$$P_{wti}{}^{ref} = P_{mi} + \left(P_d - \sum_{i=1}^{n} P_{mi}\right) / N \tag{3.32}$$

In order to make the stable operation of wind turbine in the overloading control, the wind turbine output power should be the minimal value of the MPPT value determined by the current rotor speed (blue line in Fig 3.7) and the wind turbine output power reference value for overloading control (green line in Fig 3.7), expressed as follows,

$$P_{wti} = \min\left\{P_{MPPT,i}, P_{mi} + \left(P_d - \sum_{i=1}^{n} P_{mi}\right)/N\right\} \tag{3.33}$$

This formula guarantees the wind turbine can return back to the MPPT status after releasing all the stored kinetic energy for system support. Otherwise, it can easily make wind turbine touch the minimal rotor speed limitations and finally trip off. Fig 3.7 shows the overall proposed control scheme. When there is over-generation in the system, wind turbine will deload from MPPT point ***A*** to point ***B*** based on (3.30) and (3.31), making sure more kinetic energy can be stored in a WPP. Sequentially, wind turbine overloads through the *Segment **B** to **A** via **C*** based on (3.32) and (3.33) when there is over-consumption by rereleasing the stored kinetic energy in the former step.

It should be noted that the overloading control in this thesis can be understood as a simple and effective way to release the stored kinetic energy of wind turbine back to the system, and an approach to verify the effectiveness of the proposed deloading strategy. There might have other strategies better than this one considering better system behavior such as system frequency profile in the disturbance, which however, is not the key focus of the work.

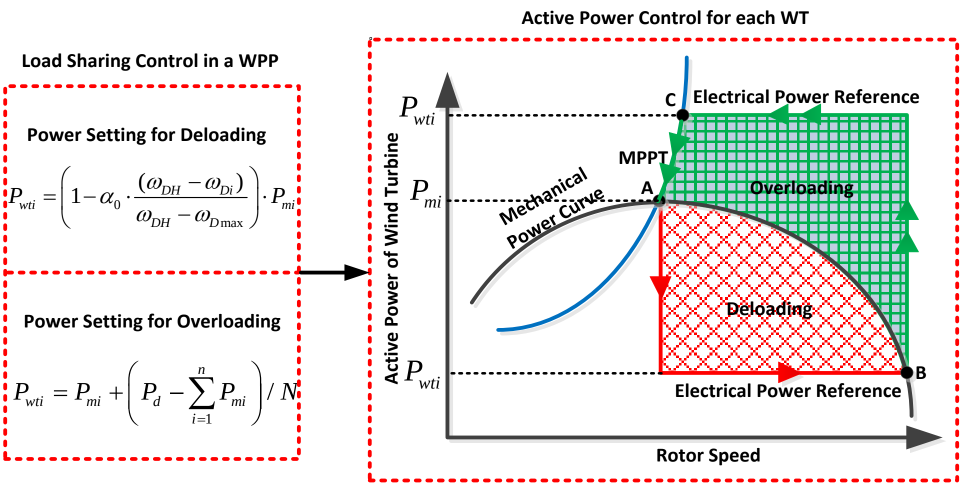

Fig 3.7 Proposed scheme for WT under deloading and overloading status

3.5 Case studies

To investigate the performance of the proposed control scheme, a model system was selected that contains one conventional SG, static loads, and a DFIG-based WPP, as shown in Fig 3.8. It was simulated using *DIgSILENT/ PowerFactory*. One SG of 30-MW built by a seventh-order model represents the power grid. The primary frequency control droop gain of the SG is set to 4%. A 24-MW WPP consists of 12 units of a 2-MW DFIG. Notably, the power rating of WPP is 40% of the overall generation capacity and it is mandatory to require the WPP to fulfill system dispatch demand via load sharing control. The DFIG model and the related control strategy can be referred to [27-29]. Four DFIGs are connected in each feeder, and three feeders are connected to the collector bus, which is connected to the power grid through transformers and cables. Considering wake interactive between WTs, the spacing of two adjacent DFIGs is *5D*, where *D* is the diameter of the DFIG blade (56 m). The length of the cables among the WPP as shown in Fig. 8 is *7D*, *5D*, *22D* respectively. Power grid contains two local loads (L1&L2). L1 consists of a fixed load $P_{L1}+jQ_{L1}$ as 26MW+4Mvar, and the other switching in/out load L2, marked as $P_{L2}+jQ_{L2}$. The dispatch order changes at every 100 seconds. More parameters of SG and DFIG are shown in Appendix.

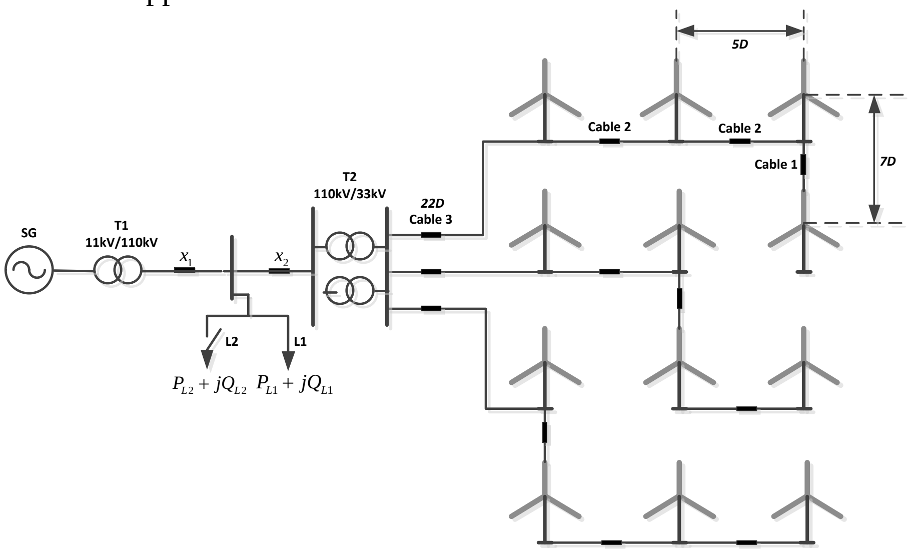

Fig 3.8 Test system configuration

3.5.1 Deloading control in a WPP with wind speed of 14m/s

As Table I shows, the effective wind speeds for wind turbines are calculated by the interactive model described in (3-6) and (3-7). Rotor speeds of DFIGs prior to the disturbances are determined by the MPPT algorithm indicated in (3-4) and (3-5). In the same utilization level (UL) scheme, K is calculated as 0.8652. In the proposed variable utilization level scheme, the initial variable utilization levels K_i calculated based on (3-27) and (3-28) are 0.957, 0.7922 and 0.7398 respectively. It is clearly seen that DFIGs at high wind speeds have higher utilization level compared with DFIGs at low wind speeds. The maximum power generation by the WPP is 14.98 MW (0.6243 p.u.).

The dump load $P_{L2}+jQ_{L2}$ as 2MW+0Mvar is switched off at t=10s. Due to the abundant wind resources available in light-load condition, the DFIGs begin deloading to 12.96 MW (0.5402 p.u.). Table II compares the results with the proposed variable utilization level strategy and the conventional control scheme. It shows from Table II that with the proposed variable utilization level control, the pitch angle of DFIG 1 is less than that with the conventional control. Therefore, the excessive energy is converted to the rotor kinetic energy (KE), making the overall rotor speeds higher than that with conventional control. As a result, the stored kinetic energy in a WPP by the proposed control is approximately calculated as 7.22 p.u. On the contrary, the stored kinetic energy with same utilization level scheme is nearly 6.81 p.u, and it effectively validates the cost-effective advantage of the former strategy.

Table 3.1

Wind, rotor speeds, predicted maximum power of DFIG, and concerned control gains for case study (high wind condition)

	Col.1	Col.2	Col.3
Wind speed	14m/s	11.34m/s	10.50m/s
Rotor speed	1.1911 p.u.	0.9656 p.u.	0.8939 p.u.
P_{mi}	0.9579 p.u.	0.5103 p.u.	0.4050 p.u.
P_{wm} / P_{d},	0.6243 p.u. / 0.5402 p.u.		
Same UL	0.8652	0.8652	0.8652
Initial variable UL	0.957	0.7922	0.7398

Table 3.2

Results with the proposed deloading strategy and conventional control strategy within a WPP (high wind condition)

	The proposed control			The conventional control		
	P_{Gi}	ω_{ti}	β	P_{Gi}	ω_{ti}	β
DFIG1	0.8674	1.2200	1.60	0.8288	1.22	2.34
DFIG2	0.4342	1.2026	0	0.4415	1.18	0
DFIG3	0.3191	1.1826	0	0.3504	1.098	0
Stored KE	7.22 p.u.			6.81 p.u.		

Three different situations namely without any additional control, with the traditional scheme and with proposed variable utilization level scheme are compared in Fig 3.9. It is clearly seen from Fig 3.9 (b) that with load sharing control, WPP decreases its output power to compensate the power mismatch between load and generation, which makes the system frequency stable during sudden load variation event as shown in Fig 3.9 (a). In contrast, with MPPT control of DFIGs, only SG undertakes the power mismatch of the system, and system frequency increases fast in the initial of the event. With proposed scheme, the utilization level of front row DFIG (DFIG 1) is higher than that of back row DFIG (DFIG 3) as shown in Fig 3.9 (e), which makes the rotor speed of DFIG 3 increase to a higher value during system dynamics, as illustrated in Fig 3.9 (d). Similarly, due to the higher utilization level of DFIG 1 in the proposed scheme, the rotor speed of DFIG 1 increases slower than that in the traditional scheme, which better explains the activation time of pitch angle control with proposed scheme lags off that with same utilization level scheme, as shown in Fig 3.9 (f). It is clearly seen from Fig 3.9 (d) that with the proposed scheme, the excessive energy can be temporally stored in the back row DFIGs, which can withhold as much wind energy as possible, and then release back when system needed.

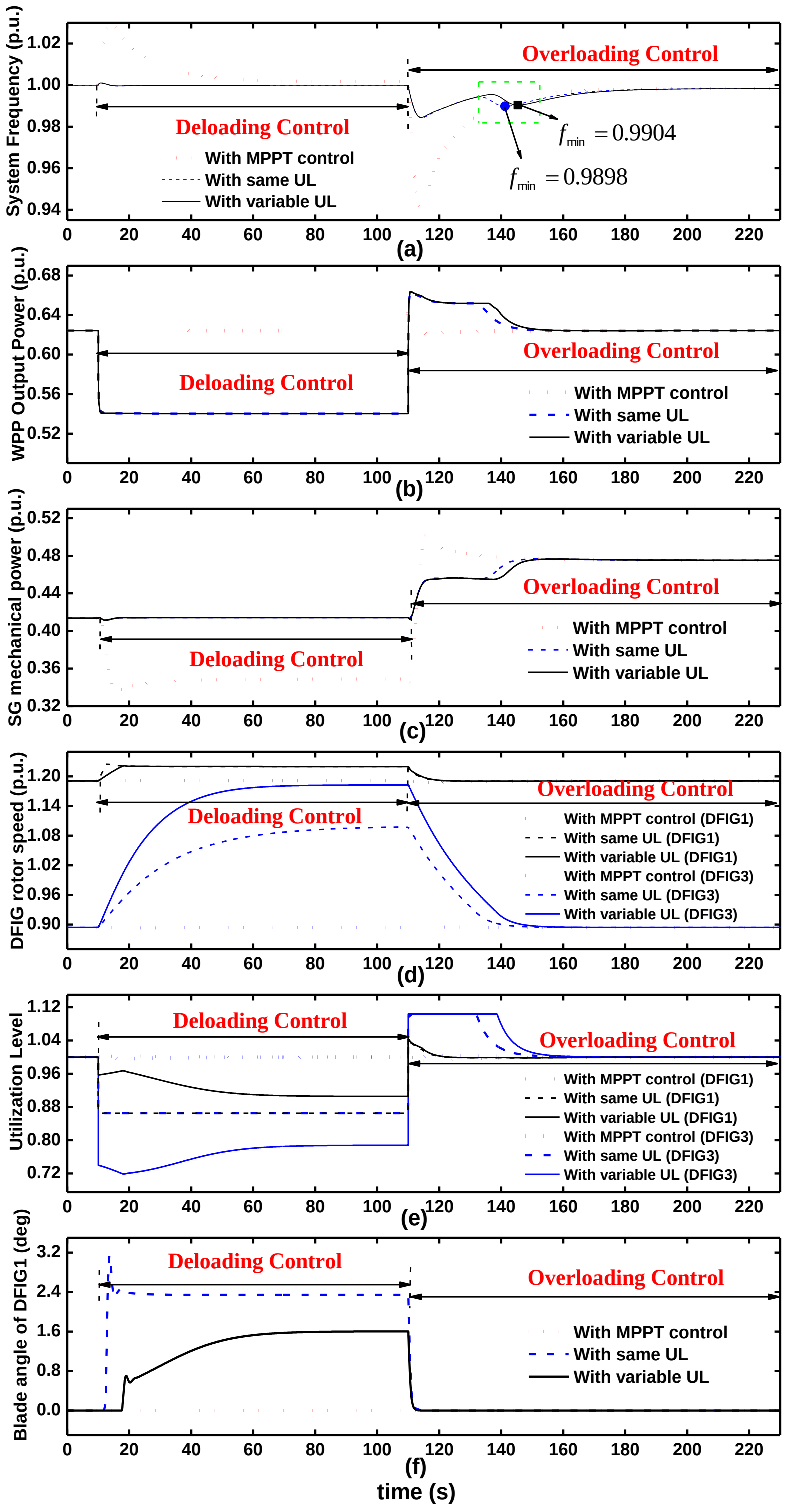

Fig. 3.9. Simulation results for Case Study. (a) System frequency, (b) WPP output power, (c) SG mechanical power, (d) DFIG rotor speed, (e) Utilization level of different control schemes, (f) Blade angle of DFIG 1

3.5.2 Overloading control in a WPP with wind speed of 14m/s

The dump load $P_{L2}+jQ_{L2}$ as 4MW+0Mvar is switched on at t=110s, and the DFIGs begin overloading to 15.88 MW (0.662 p.u.) afterwards. Fig. 3.9 shows the dynamic response of DFIGs and SG after sudden load changes. It is clearly seen from Fig. 3.9 (a) that with the proposed control, the second system frequency drop is 0.9904 p.u., which is larger than that of 0.9898 p.u. with traditional control scheme. This is not unreasonable because the overloading time of DFIGs with proposed control scheme is longer than that with traditional control scheme as shown in Fig. 3.9 (b). The slight improvement in the frequency drop is due to the relatively small amount of kinetic energy stored in wind turbines. Moreover, The SG mechanical power curve in Fig. 3.9 (c) indicates that in the proposed control scheme, the mechanical power from governor increases slower than that with same utilization level scheme. Because of the rotor speed of back row DFIG (DFIG 3) with proposed control scheme larger than that with conventional control in the deloading control, the time of releasing rotation kinetic energy stored in DFIG 3 in the overloading control scheme is longer than that with same utilization level scheme, as shown in Fig. 3.9 (d).

3.5.3 Impact of the parameter ω_{DH}

ω_{DH} is defined as the highest rotor speed that all DFIGs in a WPP cannot exceed. TABLE III shows the influence of the parameter ω_{DH} on the performance of the proposed control scheme. It is effectively validated that with lower ω_{DH}, larger initial utilization level deviation of each wind turbine will be with the proposed control scheme. As a result, the power reference for DFIG 3 in the deloading control with lower ω_{DH} is smaller than that with higher ω_{DH}, which makes the overall rotor speeds of wind turbines higher than that with higher value of ω_{DH}. Accordingly, the stored kinetic energy in a WPP with lower ω_{DH} is approximately calculated as 7.35 p.u. On the contrary, the stored kinetic energy with higher ω_{DH} is nearly 7.22 p.u, and it effectively validates the lower of the ω_{DH}, the smaller utilization level of back row DFIG will be and the more kinetic energy of DFIGs can be stored in a wind power plant (WPP). The system frequency drop is slightly improved as well since more kinetic energy of DFIGs can be released back for system support with lower ω_{DH}.

Table 3.3

Result with different ω_{DH} for the proposed control scheme

	ω_{DH}=1.23			ω_{DH}=1.25		
	DFIG1	DFIG2	DFIG3	DFIG1	DFIG2	DFIG3
Initial UL	0.9681	0.7835	0.7248	0.957	0.7922	0.7398
P_{Gi}	0.8776	0.4302	0.3128	0.8674	0.4342	0.3191
ω_{ti}	1.2200	1.2113	1.2029	1.2200	1.2026	1.1826
β	1.412	0	0	1.60	0	0
Stored KE	7.35 p.u.			7.22 p.u.		
f_{min}	0.9907 p.u.			0.9904 p.u.		

3.5.4 Power sharing control in a WPP with wind speed of 12m/s

The effective wind speed and optimal rotor speed for each row wind turbines under low wind condition are shown in Table IV, which are lower than those under high wind condition. Same sudden load decrease event happens at t=10s. The DFIGs deload to 7.6176 MW (0.3174 p.u.) afterwards. Since the maximum power generation by the WPP is 9.636 MW (0.4015 p.u.) under low wind condition, the utilization level for all wind turbines in the traditional scheme is calculated as 0.7905, which is smaller than that in the high wind condition. However, in the proposed variable utilization level scheme, the initial value of K_i for three column DFIGs are calculated as 0.8564, 0.741 and 0.7023 respectively. It is apparently shown that the higher rotor speeds of wind turbines are, the larger utilization levels of wind turbines are adopted. In addition, the power settings for back row wind turbines during deloading control with proposed scheme are lower than that with traditional one as shown in Table V. As a result, rotor speeds of back row wind turbines are higher and more kinetic energy can be stored in a WPP. Compared with the results from Table II, the total kinetic energy alternation under low wind condition is calculated as 0.91 p.u., which is higher than that under high wind condition as 0.41 p.u. This is not unreasonable that there is a larger over-speeding range under low wind speed condition and more available kinetic energy can be stored via overspeeding control in a WPP. It effectively validates that the proposed scheme is more energy-efficient since more wind energy can be harvested through storing in the form of rotor kinetic energy of wind turbines instead of directly curtailing.

It is clearly seen from Fig. 3.10 (b) and (c) that with MPPT control of DFIGs, only SG undertakes the power gap, and the system frequency drop is larger than that with load sharing control involved. However, WPP decreases its output power to compensate the power mismatch with load sharing control. With the proposed variable utilization level scheme, a lower utilization level is adopted for back row DFIG (DFIG 3) as shown in Fig. 3.10 (e), which makes the rotor speed of wind turbine increase to a higher value during system dynamics, as illustrated in Fig. 3.10 (d). On the contrary, the activation time of pitch angle control for front row DFIG (DFIG1) with the proposed scheme lags off that with traditional scheme, due to the higher utilization level for DFIG 1 as shown in Fig. 3.10 (f).

Same load increase event happens at t=110s, and the DFIGs begin to overload to 10.54 MW (0.439 p.u.) afterwards. The power imbalance between the dispatch order and the maximum power generation of wind turbines is evenly distributed to the wind turbines in the deloading scheme. It is clearly seen from Fig. 3.10 (a) that with the proposed control, the second system frequency drop is 0.9906 p.u., which is larger than that of 0.9886 p.u. with traditional control scheme. Compared with high wind condition, the frequency drop improvement is more obvious. This is because the stored kinetic energy in the proposed scheme is much larger than that with traditional one under low wind condition. Since more kinetic energy of wind turbines is stored in the proposed deloading scheme, the time of releasing kinetic energy in DFIG 3 in the overloading control is longer than that with traditional scheme, as shown in Fig. 3.10 (d). As a result, the frequency support time with proposed scheme is much longer than that with the traditional one, as shown in Fig. 3.10 (b) and accordingly, the mechanical power from SG governor increases much slower as shown in Fig. 3.10 (c).

Table 3.4

Wind, rotor speeds, predicted maximum power of DFIG, and concerned control gains for case study (low wind condition)

	Col.1	Col.2	Col.3
Wind speed	12m/s	9.85 m/s	9.13 m/s
Rotor speed	1.0218 p.u.	0.8384 p.u.	0.7768 p.u.
P_{mi}	0.6047 p.u.	0.3341 p.u.	0.2658 p.u.
P_{wm} / $P_{d,}$		0.4015 p.u. / 0.3174 p.u.	
Same UL	0.7905	0.7905	0.7905
Initial variable UL	0.8564	0.741	0.7023

Table 3.5

Results with the proposed deloading strategy and conventional control strategy within a WPP (low wind condition)

	The proposed control			The conventional control		
	P_{Gi}	ω_{ti}	β	P_{Gi}	ω_{ti}	β
DFIG1	0.5266	1.220	1.60	0.4779	1.22	3.34
DFIG2	0.2427	1.187	0	0.2641	1.10	0
DFIG3	0.1826	1.177	0	0.2101	1.02	0
Stored KE	7.14 p.u.			6.23 p.u.		

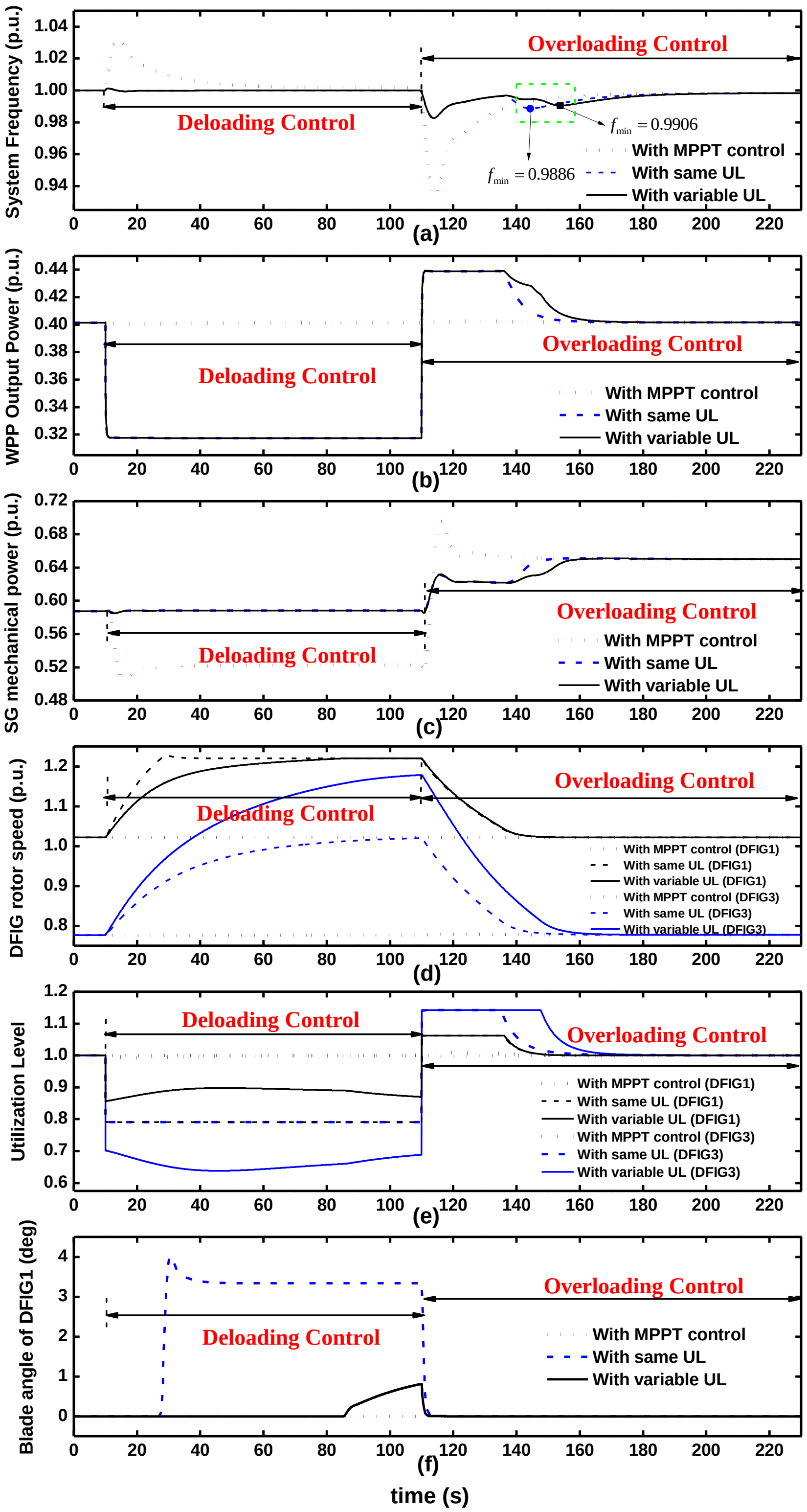

Fig. 3.10. Simulation results for Case Study. (a) System frequency, (b) WPP output power, (c) SG mechanical power, (d) DFIG rotor speed, (e) Utilization level of different control schemes, (f) Blade angle of DFIG 1

3.6 Summary

In this chapter, it has been analyzed that when fulfilling system dispatch demand, the traditional same utilization level based scheme may lead to wind turbines at higher wind speeds compromising more wind energy than those at lower wind speeds. To improve this, a variable utilization level scheme for a DFIG-based WPP is proposed to effectively reduce DFIG's wind energy loss due to load sharing control. To fullfill the dispatch demand while harvesting as much energy as possible in a WPP, the proposed scheme adaptively adjusts the utilization level of each wind turbine depending on its rotor speed so that more kinetic energy can be stored in a WPP, which can be later released back to the system when needed. The simulation results indicate the proposed scheme can reduce the loss of total energy production compared to the conventional same UL scheme for load sharing in a WPP. With increased wind energy penetration in the future, the scheme can be highly valuable for industrial applications.

Chapter IV

Optimal Power Sharing Control of Wind Turbines

4.1 Introduction

When wind power penetration is high, particularly in the context of a microgrid, the wind generation according to the maximum power tracking control may significantly disturb the supply-demand balance. In fact, with a proper control design, the power output of a DFIG wind turbine (WT) can be regulated in accordance with the dispatch demand from system operator while harvesting and storing as much as wind energy as possible. Specifically, WT can withhold the output power through accelerating its rotor, when there is over-generation in the system. This is often referred to as the deloading control of WT [81, 82]. Similarly, the overloading control can be applied to WT through decelerating its rotor, when there is over-consumption in system [86]. To implement deloading or overloading control, a simple approach is to equally share power reference variation to each WT [94], which results in equally accelerating or decelerating all WTs of a wind farm. This is certainly not an optimal option since the deloading or overloading capability of each WT is not equal under different wind conditions. To best fulfill the dispatching command, the deloading and overloading capability of WTs should be fully and optimally utilized, which is the focus of this thesis. The optimal deloading control for WTs within a wind farm is of particular interest, since this enables WTs to withhold as much wind energy as possible that can be released back for e.g. system support. This thesis proposes a novel optimal deloading control strategy, where power reference of each DFIG WT is obtained through a tailor-made optimization, aiming at maximizing the rotor kinetic energy stored in all WTs within a farm.

4.2 Optimal Power Share of Wind Turbines

4.2.1 Wind Power Generation Analysis

The active power generation P_{wt} of each WT can be calculated as $P_{wt}=1/2C_p(\lambda, \beta)\rho A v_w^3$, where ρ is air density, A= πR^2 is the effective area swept by WT blades of radius R, v_w is the average wind speed, C_p is the power coefficient of WT which is a function of tip speed ratio λ and WT blade pitch angle β [103]. Normally, β is assumed to be a minimum value (zero) for extracting maximum power. In order to facilitate the analysis of the optimal loading control strategy, the high-degree nonlinear C_p expression in [103] is substituted approximately by a polynomial of degree N_p and coefficients a_j.

$$C_p = \sum_{j=0}^{N_p} a_j \lambda^j = \sum_{j=0}^{N_p} a_j \frac{(\omega_t R)^j}{{v_w}^j} \tag{4.1}$$

The power generated by each WT i can then be expressed as,

$$\begin{aligned} P_{wti} &= \frac{1}{2}\rho A {v_{wi}}^3 \sum_{j=0}^{N_p} a_j \frac{(\omega_{ti} R)^j}{{v_{wi}}^j} \\ &= \frac{1}{2}\rho A \sum_{j=0}^{N_p} a_j R^j {v_{wi}}^{3-j} {\omega_{ti}}^j = \sum_{j=0}^{N_p} k_{ij} {\omega_{ti}}^j \end{aligned} \tag{4.2}$$

where, ω_{ti} is the rotor speed of WT i and k_{ij} is the concerned coefficient for WT i under the specific wind speed v_{wi} at a polynomial degree j.

4.2.2 Optimal Deloading Strategy

In order to achieve deloading control while maximizing kinetic energy stored in a wind farm, the pitch control should not be activated until WT rotor speed exceed a predefined threshold ω_{tt}. The proposed strategy is summarized below:

Step 1: Consider a wind farm comprising of *m* WTs, which are divided into two groups. Group one consists of WTs whose rotational speed is below the speed threshold, marked as *1, 2,…n*. The rotational speed of another group of WTs reaches the speed threshold, marked as *n+1, n+2,…m.*

Step 2: For group two, in contrast to [94], where the pitch angle is automatically increased when WT deloading, WTs at high wind speed generate the nominal power, which does not participate in the WT deloading.

Step 3: For group one, if neglecting all power losses among wind farm, in order to maximize the stored rotor kinetic energy, the optimization problem can be formulated as follows:

$$\begin{aligned} &Max\ \ f(\mathbf{x}) = \sum_{i=1}^{n} \frac{1}{2} J_i \omega_{ti}^{\ 2} \\ &s.t.\quad \sum_{i=1}^{n} P_{Gi} = P_d\ ; P_{Gi} = \sum_{j=0}^{N_p} k_{ij} \omega_{ti}^{\ j} \\ &\quad \omega_{toi} \le \omega_{ti} \le \omega_{tt} \\ &\quad \mathbf{x} = \left[\omega_{t1}, \omega_{t2}, \cdots, \omega_{tn}\right] \end{aligned} \tag{4.3}$$

where, P_d and P_{Gi} denote the system required active power generation and power reference for WTs under low wind speed when deloading, J_i is the inertia constant of WT *i*, and ω_{toi} is the optimal rotor speed of WT *i* at MPPT status.

Step 4: If Eq. (3) is unsolvable, the rotor speeds of all WTs may reach the threshold ω_{tt} and meanwhile, system power balance may not be ensured. Pitch angle control should be activated to further decrease the power generation, and the power reference of each WT should be,

$$P_{Gi} = \begin{cases} \sum_{j=0}^{N_p} k_{ij} \omega_{tt}^{\ j} - \left(\sum_{i=1}^{n} \sum_{j=0}^{N_p} k_{ij} \omega_{tt}^{\ j} + \sum_{i=n+1}^{m} P_{ni} - P_d \right) / m\ \left(i = 1, 2, \cdots, n\right) \\ P_{ni} - \left(\sum_{i=1}^{n} \sum_{j=0}^{N_p} k_{ij} \omega_{tt}^{\ j} + \sum_{i=n+1}^{m} P_{ni} - P_d \right) / m\ \ \left(i = n+1, \cdots, m\right) \end{cases} \tag{4.4}$$

where P_{ni} is the nominal power of WT *i.* In this thesis, the power difference between the required power generation and the wind power generated with rotor speed of all WTs reaching the speed threshold is evenly distributed among all the *m* WT.

When the system required generation is more than the maximum power wind farm can produce, the stored energy via the proposed deloading strategy can be released back for system support through the overloading strategy described below:

Step 1: For the *m*-*n* WTs under high wind speeds, the power reference is modified as nominal power.

Step 2: For *n* WTs under low wind speeds, the power difference between the system required power generation and the maximum power captured of WT is evenly distributed to *n* WTs, and P_{mi} is the maximum power captured by WT *i* at specific wind speed v_w.

$$P_{Gi} = P_{mi} + \left(P_d - \sum_{i=1}^{n} P_{mi} - \sum_{i=n+1}^{m} P_{ni} \right) / n \tag{4.5}$$

The proposed overall WT loading control is shown in Fig. 4.1.

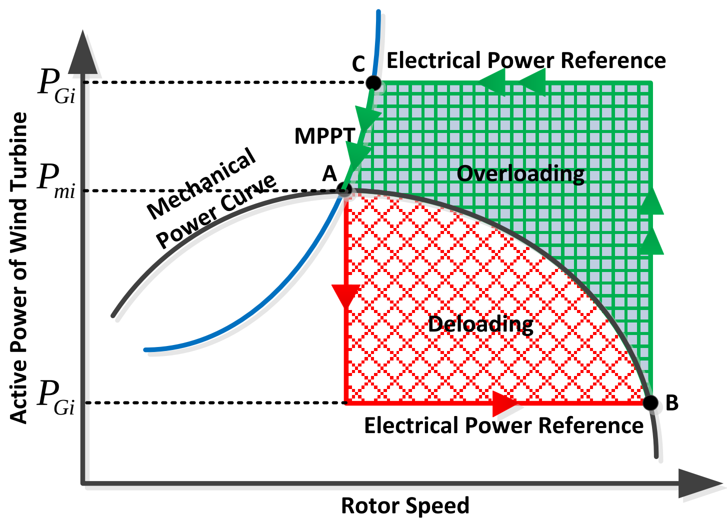

Fig. 4.1 Wind turbine under deloading and overloading status

4.3 Case Studies

The benchmark system is a typical stand-alone microgrid with a total load of 6 MW and 1 MVar, which is conducted in the DIgSILENT/PowerFactory. The constant power load model is used in the study. The wind speeds at four DFIGs are 14 m/s, 13 m/s, 12 m/s, and 11 m/s, respectively, which may generate as much as 5.6 MW (0.7 p.u.) of wind power. One local 5 MW synchronous generator (SG) is installed to supply the local load.

Table 4.1

Results with the propose optimal deloading strategy and conventional control strategy when DFIG deloading

	The proposed control			The conventional control		
	P_{Gi}	ω_{ti}	β	P_{Gi}	ω_{ti}	β
DFIG1	0.9520	1.2500	0	0.9049	1.2500	0.8267
DFIG2	0.7420	1.2158	0	0.7250	1.2500	0.0728
DFIG3	0.5830	1.1374	0	0.5705	1.1597	0
DFIG4	0.3630	1.2500	0	0.4396	1.0633	0

Due to the abundant wind resources available, the four DFIGs begin deloading to 5.28 MW (0.66 p.u.). Table I compares the results with the proposed optimal deloading strategy and conventional control strategy. It shows that with the optimal control, all WT pitch angles keep zero and all the excessive energy is converted to the rotor kinetic energy, making the overall rotor speeds higher than that with conventional control.

If the load suddenly rises to 7 MW at t=10s, and the DFIGs begin overloading to 6 MW (0.75 p.u.) afterwards. Fig 4.2 shows the dynamic response of DFIGs and SG after sudden load changes. It is clearly seen that with the proposed control, the overloading time of DFIG is longer. Moreover, the network frequency deviation is smaller and the system recovers faster with the proposed optimal control strategy.

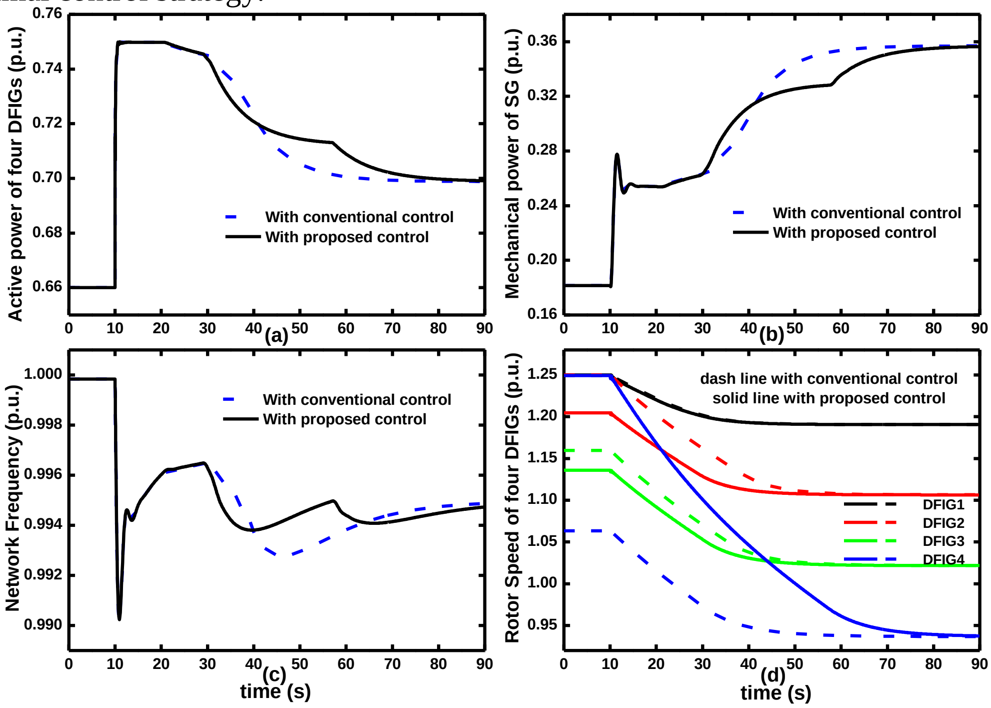

Fig. 4.2 Dynamic response of DFIGs and SG after sudden load changes

4.4 Summary

This chapter has proposed an optimal power sharing control strategy that can fulfill the power dispatching demand by system operator while harvesting as much wind energy as possible. The power reference of each DFIG is shared through maximizing the rotor kinetic energy stored in all WTs in a wind farm. Correspondingly, the stored energy can be later released back for system support through WT overloading control. The proposed control scheme that fully utilizes the loading capability of WTs has a high potential application in a weak grid with high wind power penetration.

Chapter V

Advanced Power Sharing Control for Microgrid Operation with Wind and Solar Generation

5.1 Introduction

In recent years, considerable attentions have been drawn on the secure and reliable operation of the power system due to the steadily growing penetration of renewables. Particularly, the popular maximum power point tracking (MPPT) algorithm adopted by distributed generations (DGs) such as wind and photovoltaic (PV) may cause supply-demand imbalance of the power system from time to time. Accordingly, traditional synchronous generators (SGs) are required to operate at part-load levels or even shut down for some time to realize power balance in the system, which results in a reduced life cycle and increased costs. To minimize such impacts, some countries have required DGs mandatorily to fulfill the dispatch demand set by system operator by their grid codes.

To resolve the discrepancy between dispatch command and renewable generation, one direct solution is to utilize energy storage system (ESS), such as pumped water and flying wheel, which can mitigate renewable output fluctuations to align with the dispatch demand [66-69]. Nevertheless, additional investments as well as some technical considerations may prevent wide use of storage systems. Thus, it is worthy of investigating alternative solutions based on the self-potentials of renewables.

Actually, with a proper control strategy, the output power of wind or PV generation can be regulated in accordance with dispatch command to realize power balance among the system, which is termed as power sharing control (PSC) herein. Specifically, some renewables like wind can withhold or release partially kinetic energy stored internally while having limited impacts on their energy harvesting process based on advanced control strategy [88-92]. For renewables with little internal energy like PV, deloading control can be applied to withhold partial generation output via regulating the terminal voltage of PV arrays [106,107]. The above controls may involve deviations from MPPT points to fulfill dispatch commands, but renewables can always return back to MPPT afterwards.

There are typically two possible ways to realize active power control by wind generators (WGs). The first one is to utilize the WG pitching control to reserve and release power in response to e.g. system frequency. Since this scheme forces WG to deviate from MPPT operating point and significant annual wind generation reduction is inevitable. In addition, the response speed of pitching can be somehow slow and frequent activation may also increase mechanical stress to WGs. The other alternative is to utilize the rotating kinetic energy (KE) of WG, with which WT can withhold or release additional kinetic energy through accelerating or decelerating the rotor speed. Compared to the pitch control, this method involves limited impacts to wind turbine energy harvest while manipulating generation output. Because of such advantage, this thesis further exploits the KE based active power control to enable WGs to fulfill system dispatch commands while minimizing the reduction of wind energy harvest.

In [91], a two-level control scheme for active power control for a microgrid is proposed. This scheme consists of a supervisory control level and a lower machine control level. The supervisory control level decides the power setting of each DG from different optimization objectives such as optimal power flow among a microgrid. The lower machine level can be realized through active power control schemes aforementioned. The data of current wind speeds, solar irradiation, and configuration of microgrid is required for this method, which makes it time-consuming and not suitable for online application. In addition, the coordination of each DG to fulfil the dispatch order and the dynamics of DG is not considered. In [94], a simple and direct approach of power sharing is proposed by equally adjusting the utilization level (UL) of each DG.

Traditional dispatch methods may involve either optimal power flow or the same UL based scheme to adjust renewable generation output to ensure dispatch command alignment within a microgrid. Considering DGs like wind and PV can operate at different MPPT points because of different locations, the same UL based scheme may not provide optimal adjustments in terms of impacts caused to energy harvest. Meanwhile, WGs have the advantages of varying generation output at limited impacts to energy harvest and therefore should be highly prioritized for set point adjustment. Thus, this thesis proposes a novel cascading PSC scheme for a microgrid to firstly adjust WGs generation and then PVs to optimally meet the dispatch command while minimizing the reduction of total energy production. The WGs rotors can be fully utilized for temperately storing or releasing excessive energy, and the PV generation can be deloaded only when needed. Compared to traditional methods, the efficiency of system operation can be largely improved by significantly reducing the compromised energy harvest.

5.2 Conventional Power Sharing Control for Microgrids

Some preliminary knowledge is included in this section. First, wind generation (WG) model including the wind turbine model and its Maximum Power Point Tracking (MPPT) control are briefly introduced. Then, the ideal circuit photovoltaic (PV) model are described. Lastly, the same utilization level based power sharing control (PSC) for AC microgrid is presented.

5.2.1 MPPT Control of Wind Generation (WG)

The mechanical power from the wind P_{mec}, is defined by

$$P_{mec} = \frac{\rho}{2}\pi R^2 {v_w}^3 C_p(\lambda, \beta) \tag{5.1}$$

where ρ is the air density, R is the rotor blade radius, v_w is the wind speed, λ is the tip speed ratio, β is the pitch angle, and C_p is the power coefficient. The expression of C_p [103] is as follows,

$$C_p = 0.22(\frac{116}{\lambda_i} - 0.4\beta - 5)e^{-12.5/\lambda_i} \tag{5.2}$$

$$\lambda_i = \frac{1}{\frac{1}{(\lambda + 0.08\beta)} - \frac{0.035}{(\beta^3 + 1)}} \tag{5.3}$$

where the blade tip speed ratio λ,

$$\lambda = \frac{\omega_t \cdot R}{v_w} = \frac{k_g \cdot \omega_D \cdot R}{v_w} \tag{5.4}$$

where k_g is the gear ratio of gearbox, ω_t and ω_D is the wind turbine and DFIG generator rotational speed, respectively. Normally, the pitch angle will be controlled to zero when P_{mec} is below the rated power. Thus, C_p is the function of λ only and has a maximum value C_{pmax} at certain λ. At this point, the WT obtains the maximum power and the optimal rotor speed ω_{Dopt} for a given v_w from (5.4). Substituting (5.4) in (5.1), yields:

$$P_{MPPT}^{WG} = \frac{\rho\pi R^5 k_g{}^3 C_{p\max}}{2\lambda^3} \cdot \omega_D{}^3 = C_M \cdot \omega_D{}^3 \tag{5.5}$$

where $P^{WG}{}_{MPPT}$ is the power reference of wind generator (WG) determined by maximum power point tracking (MPPT) algorithm. The active power of a WG is regulated both by the MPPT algorithm and the pitch angle control as shown in Fig.1 (a) when below the rated power. The MPPT model is used to calculate the reference active power according to the current rotor speed (ω_D). Optimal rotor speed will be automatically reached based on the rotor motion equation:

$$2H_D \cdot \omega_D \cdot \frac{d\omega_D}{dt} = P_{mec} - P_{MPPT}^{WG} \tag{5.6}$$

where H_D is the inertia constant of the DFIG. Due to the fast response of power electronic devices, the active power from WG can be regarded as the same as its reference, that is P_{WG} = $P^{WG}{}_{MPPT}$. Pitch angle control will be activated to constrain the rotor speed within its limit by increasing the pitch angle once over-speed of WT rotor is detected.

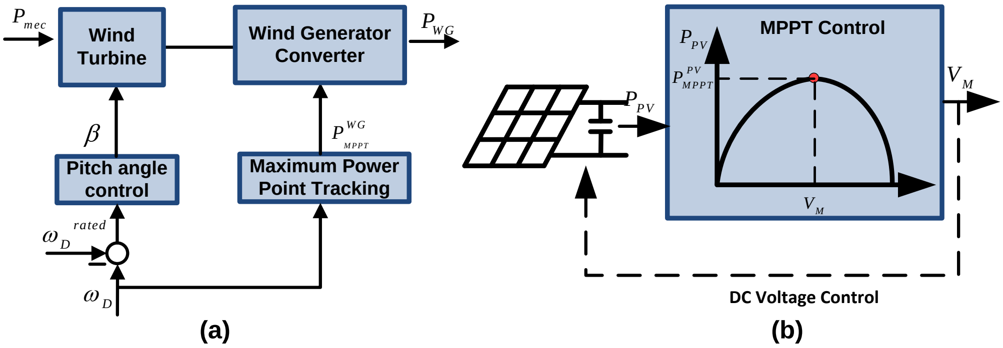

Fig. 5.1 Simplified active power control (APC) of WG (a) and PV generation (b).

5.2.2 *MPPT Control of Photovoltaic Generation*

In an ideal photovoltaic (PV) model, the equation that relates the output current I and terminal voltage V is expressed as,

$$I_{PV} = I_{Ph} - I_S\left[e^{qV/N_s KTA} - 1\right] \tag{5.7}$$

where q, K, T, and N_s are the electron charge, Boltzmann constant, module temperature, and number of series connected cells, respectively. The parameters I_{Ph}, I_s, and A are the photon current, saturation current, and the ideality factor of the diode, respectively. These three parameters can be determined relying only on the solar irradiance G, short circuit current I_{SC}, and open circuit voltage V_{oc}. Thus, for a given solar irradiance G and temperature T, the output current of PV is only related to the terminal voltage. The MPPT algorithm of PV is achieved by controlling the PV panel output voltage at optimal voltage V_{M}., as shown in Fig. 5.1 (b). The maximum output power of PV generation is reached as $P^{PV}{}_{MPPT}$, which yields as

$$P_{MPPT}^{PV} = P_{PV}(V_M) \tag{5.8}$$

5.2.3 *Same Utilization Level (UL) based Power Sharing Control (PSC) for AC Microgrid*

The supply-demand balance of e.g. a stand-alone microgrid must be always maintained. This requires the generation reference for each WT and PV generator should be properly set in accordance with the dispatch demand. A simple and traditional way to equally share power variation ratio according to each distributed generator (DG)' capability is introduced below. This is achieved by controlling the same utilization levels (ULs) of WG and PV generators.

Fig. 5.2 shows a simple AC microgrid with multiples of DGs including WG and PV generators, a synchronous generator (SG), and several local loads. The SG provides reactive power for maintaining voltage and generates additional active power during low outputs of DGs. The total active power demand (P_d) for DGs can be simply represented as follows,

$$P_d = \sum_{i=1}^{k} P_{Li} - P_G + P_{Loss} \tag{5.9}$$

where k is the number of the local loads in the microgrid. P_G is the active power from SG, P_{Li} is the *ith* local demand calculated based on local load. P_{Loss} is the active power loss among microgrid and can be regarded as a small percentage of P_d.

The total available power generation from the DGs (P_{DGm}) can be calculated as follows,

$$P_{DGm} = \sum_{i=1}^{n} P_{WGmi} + \sum_{j=1}^{m} P_{PVmj} \tag{5.10}$$

where n is the number of WGs in a microgrid, P_{WGmi} denotes the predicted maximum wind power generation of *ith* WG, which depends on the current wind speeds. m is the number of PV generators in a microgrid, P_{PVmj} denotes the maximum PV generation of *jth* PV panel based on the current irradiation and temperature. Suppose P_d is the dispatch demand set by system operator, and if P_d is larger than P_{DGm}, all DGs should be operated at MPPT status. If P_d is less than P_{DGm}, a suitable PSC is required to share the load demand among DGs. This is achieved by controlling the ULs (K_u) of DGs, maintaining them as a same value [94],

$$K_u = \min\{P_d / P_{DGm}, 1\}$$
$$P_{WGi} = K_u \cdot P_{WGmi} \quad (i = 1, 2, ...n) \qquad (5.11)$$
$$P_{PVj} = K_u \cdot P_{PVmj} \quad (j = 1, 2, ...m)$$

where P_{WGi} and P_{PVj} is the active power generation set of the *i*th WG and *j*th PV generator, respectively. The above same UL scheme can guarantee the supply-demand balance in a stand-alone microgrid. The actual power output of DGs (P_{DG}) can be expressed,

$$P_{DG} = \sum_{i=1}^{n} K_u \cdot P_{WGmi} + \sum_{j=1}^{m} K_u \cdot P_{PVmi}$$
$$= \frac{P_d}{P_{DGm}} \cdot (\sum_{i=1}^{n} P_{WGmi} + \sum_{j=1}^{m} P_{PVmi}) = P_d \qquad (5.12)$$

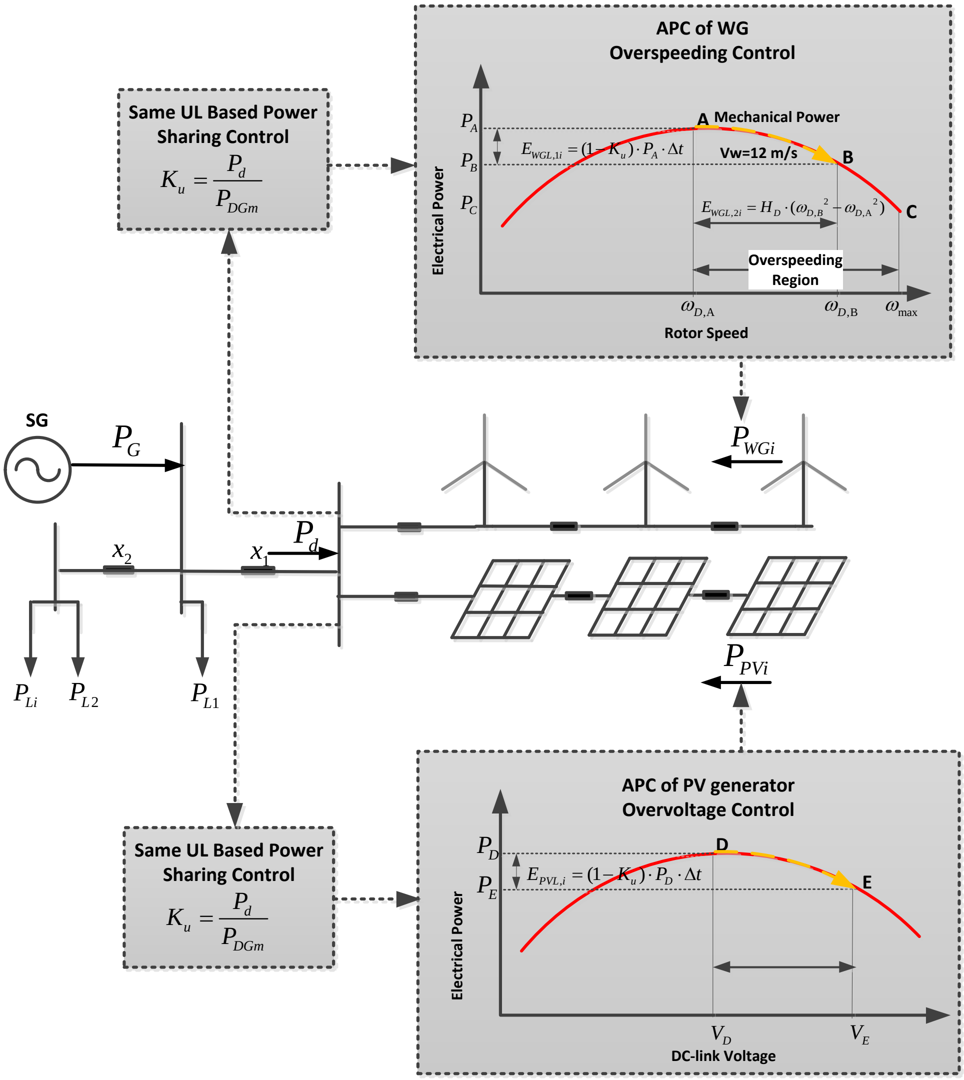

Fig. 5.2. Configuration of a simple stand-alone AC microgrid

5.3 Energy Production Analysis of WGs and PV Generators for PSC

When the available power generation from DGs exceeds the system demand, a proper PSC should be utilized instead of traditional MPPT algorithm to cope with the supply-demand imbalance in a microgrid. DGs in a microgrid may be controlled to temporally reduce their output by regulating their ULs, however energy reduction of DGs to compromise partial harvested energy during above process. WG may reduce its output power through overspeeding control, while PV generator deloads its generation by increasing the terminal voltage. Therefore, total energy production reduction due to different active power controls (APCs) for DGs with same UL scheme should be analyzed accordingly. It is assumed that all DGs are in MPPT operation prior to the system demand change. In the following, all the variables are in the per unit form.

5.3.1 Overspeeding Control for WG

The power of each WG when adopting active power control (APC) as shown in Fig. 5.2 should be expressed as follows,

$$P_{WGi} = K_u \cdot P_{WGmi} = K_u \cdot C_M \cdot \omega_{Di}{}^3 \tag{5.13}$$

where K_u is the universal utilization level (UL) for each WG and PV generator in a microgrid. Rewrite the rotor motion equation as (5.6),

$$2H_D \cdot \omega_{Di} \cdot \frac{d\omega_{Di}}{dt} = P_{meci} - P_{WGi} \tag{5.14}$$

where H_D is the inertia constant of the WG and assume all WGs have the same inertia constant for simplification. In this thesis, one-mass model of WG is utilized since the dynamic oscillation induced by two-mass model of WG is effectively damped during first few seconds, which has little impact on APC of WG. P_{meci} and P_{WGi} are the harvested wind power and active output of *ith* WG respectively. Integrate both sides of (5.14) over a time horizon yields the total captured wind energy (E_{WGi}) by single WT under APC,

$$E_{WGi} = \int_{t_0}^{t} P_{meci} dt = \int_{t_0}^{t} P_{WGi} dt + \int_{t_0}^{t} 2H_D \cdot \frac{d\omega_{Di}{}^2}{dt} dt \tag{5.15}$$

Define E_{WGi0} as the total captured wind energy by *ith* WG with no APC involved. Since a small microgrid is studied in this thesis, the dispatch order will be short in few minutes. For simplification, wind speed and solar irradiation do not change dramatically in a short time dispatch order,

$$E_{WGi0} = \int_{t_0}^{t} P_{WGmi}\, dt = P_{WGmi} \cdot (t - t_0) \tag{5.16}$$

Based on (5.13), (5.15) and (5.16), the energy loss $E_{WGL,i}$ of *ith* WG during transient involved by APC can be expressed in (5.17),

$$\begin{aligned} E_{WGL,i} &= E_{WGi} - E_{WGi0} \\ &= (1 - K_i) \cdot P_{WGmi} \cdot (t - t_0) - \int_{t_0}^{t} 2H_D \cdot \frac{d\omega_{Di}{}^2}{dt} dt \\ &= (1 - K_i) \cdot P_{WGmi} \cdot (t - t_0) - H_D \cdot (\omega_{Di}{}^2(t) - \omega_{Di}{}^2(t_0)) \end{aligned} \tag{5.17}$$

Obviously, Equation (5.17) can be divided into two separated parts ($E_{WGL,1i}$ *and* $E_{WGL,2i}$) as follows,

$$\begin{aligned} E_{WGL,i} &= E_{WGL,1i} + E_{WGL,2i} \\ E_{WGL,1i} &= (1 - K_i) \cdot P_{WGmi} \cdot (t - t_0) \\ E_{WGL,2i} &= -H_D \cdot (\omega_{Di}{}^2(t) - \omega_{Di}{}^2(t_0)) \end{aligned} \tag{5.18}$$

It is noted from (5.18) that the sacrificed wind energy $E_{WGL,i}$ during APC of each WG consists of two parts. $E_{WGL,1i}$ represents the influence of the dispatch demand set by system operator on the wind energy loss $E_{WGL,i}$, while $E_{WGL,2i}$ shows the effect of rotation mass inertia of WG on $E_{WGL,i}$ during above process. Accordingly, the total harvested wind energy production loss (E_{WGL}) by WGs within a microgrid can be expressed as follows:

$$\begin{aligned} & E_{WGL} = E_{WG1} + E_{WG2} \\ & E_{WG1} = (t - t_0) \cdot \sum_{i=1}^{n} (1 - K_u) \cdot P_{WGmi} = \\ & (t - t_0) \cdot (\sum_{i=1}^{n} P_{WGmi} - \sum_{i=1}^{n} K_u \cdot P_{WGmi}) = (t - t_0) \cdot (\sum_{i=1}^{n} P_{WGmi} - P_{WGd}) \\ & E_{WG2} = -\Delta E_k = -\sum_{i=1}^{n} H_D \cdot (\omega_{Di}{}^2(t) - \omega_{Di}{}^2(t_0)) \end{aligned} \tag{5.19}$$

where P_{WGd} is the power demand for WGs. ΔE_k is the total rotor kinetic energy (KE) alternation while all the WGs adopting APC within a microgrid. Similarly, the sacrificed wind energy during APC E_{WGL} composes of two separated parts.

E_{WG1} in (5.19) represents the imbalanced energy between the maximum energy WTs can generate and the system demand during transient process. The expression of E_{WG2} indicates WGs may withhold partial kinetic energy, which can save as much wind energy as possible during APC.

5.3.2 Overvoltage Control for PV Generator

Similarly, the power of each PV generator when adopting APC as shown in Fig. 2 should be expressed as follows,

$$P_{PVj} = K_u \cdot P_{PVmj} \tag{5.20}$$

where K_u is the utilization level (UL) for each PV generator within a microgrid. Because of the small capacitance of the terminal capacitor as shown in Fig. 5.1 (b), the dynamic process of DC-link capacitor can be negligible, and it is assumed that the captured solar energy by each PV panel equals to the output generation of PV generator. Therefore, the total solar energy captured by single PV generator (E_{PVj}) over a time horizon can be expressed in (5.21),

$$E_{PVj} = \int_{t_0}^{t} P_{PVj} dt = K_u \cdot \int_{t_0}^{t} P_{PVmj} dt \tag{5.21}$$

Similarly, define E_{PVj0} as the total harvested solar energy by *jth* PV generator with MPPT control,

$$E_{PVj0} = \int_{t_0}^{t} P_{PVmj}\, dt = P_{PVmj} \cdot (t - t_0) \tag{5.22}$$

Based on (5.20) ,(5.21) and (5.22), the sacrificed solar energy $E_{PVL,i}$ of *jth* PV generator during transient involved by APC can be expressed in (5.23),

$$E_{PVL,j} = E_{PVj} - E_{PVj0} = (1 - K_u) \cdot P_{PVmj} \cdot (t - t_0) \tag{5.23}$$

Accordingly, the total harvested solar energy production loss (E_{PVL}) by PV generators within a microgrid can be expressed as follows,

$$\begin{aligned} E_{PVL} &= (t - t_0) \cdot (\sum_{j=1}^{m} P_{PVmj} - \sum_{j=1}^{m} K_u \cdot P_{PVmj}) \\ &= (t - t_0) \cdot (\sum_{j=1}^{m} P_{PVmj} - P_{PVd}) \end{aligned} \tag{5.24}$$

where P_{PVd} is the power demand for PV generators within a mirogrid. Compared (5.19) and (5.24), the energy production reduction by PV generators during APCs only reflects the energy imbalance between the maximum solar energy PV panels can generator and system demand during above process. This is not unreasonable that PV generators have no inertia-like devices as rotating mass of WGs, which has no additional released or absorbed energy while adopting APC.

Based on (5.19) and (5.24), the overall energy reduction with in a microgrid (E_{MGL}) including PV generators and WGs can be expressed in (3.25),

$$
\begin{aligned}
E_{MGL} &= E_{WGL} + E_{PVL} \\
&= (t-t_0)\cdot\sum_{i=1}^{n}(1-K_u)\cdot P_{WGmi} + \sum_{j=1}^{m}(1-K_u)\cdot P_{PVmj} - E_{WG2} \\
&= (t-t_0)\cdot(\sum_{i=1}^{n}P_{WGmi} + \sum_{j=1}^{m}P_{PVmj} - P_{WGd} - P_{PVd}) - E_{WG2} \\
&= (t-t_0)\cdot(P_{DGm} - P_d) - \sum_{i=1}^{n}H_D\cdot(\omega_{Di}{}^2(t) - \omega_{Di}{}^2(t_0))
\end{aligned}
\tag{5.25}
$$

It can be concluded from (5.25) that, the energy production reduction with PSC scheme also consists of two parts. The first part reflects the difference between the maximum captured energy and the system demand, which is a constant value with the given power supply and dispatch demand. The second part is the rotor kinetic energy alternation for WGs. Therefore, it is more energy-efficient by using overspeeding control for WGs than overvoltage control for PV generators. This is because PV generators can only reduce their output power by increasing terminal voltage, and no additional energy can be reserved during this process. However, WGs can lower their output power by overspeeding their rotors, which can withhold partial wind energy by converting it into rotor kinetic enrgy of WGs through APC. Therefore, with same system dispatch demand, the more portion of power discrepancies for WGs (lower UL coefficients for WGs), the larger rotor speed variations of WGs will be obtained and the more rotor kinetic energy of WGs will be temporarily stored within a microgrid.

5.4 Proposed Cascading Power Sharing Control for A Microgrid With WG and PV Generator

This thesis mainly focuses on PSC scheme for renewables to copy with power mismatch between available wind or solar generation (P_{DGm}) and system demand (P_d) within a microgrid. Traditionally, the power mismatch can be shared by achieving same UL for all DGs available in a microgrid. However, this may not be an optimal option in terms of maximizing overall energy production in a microgrid since the overall energy loss by WGs and PV generators through different APCs is not the same. Specifically, WGs can withhold partial wind energy through accelerating their rotor speeds, which contributes to ΔE_{WG2} in (25). On the contrary, PV generators can reduce their output power via increasing terminal DC-link voltage, which cannot withhold partial energy during PSC as WGs. Therefore, the traditional same UL based PSC may not fully utilize the WGs' capabilities for load sharing in a microgrid.

To avoid the aforementioned problem, a cascading PSC scheme that can sequentially activate the overspeeding control of WGs and then overvoltage control of PV generators within a microgrid automatically is proposed. The core of this scheme is that, power discrepancies between the maximum active power DG can generate (P_{DGm}) and the system demand (P_d) is always first shared by WGs, while overvoltage control of PV generators is exerted only if all the rotor speeds of WGs reach the maximum limits. In the proposed cascading PSC, KE of all WGs are maximally utilized to temporally store excessive wind energy to make sure less harvested renewable energy is wasted due to the PSC. Sequentially, the stored KE in WGs in the PSC scheme can be later released back to the system. In the following, the detailed design of APCs for WGs and PV generators is presented for proposed PSC scheme.

5.4.1 Cascading PSC scheme with overspeeding control of WGs only

Under the cascading PSC scheme, WGs still reduce their output power through accelerating their rotor speeds, which withhold partial excessive wind energy into rotor KE. When the power mismatch between the maximum active power DGs can generate (P_{DGm}) and system demand (P_d) is within a small range, overspeeding control of WGs will contribute only for the power discrepancies sharing, and PV generators still work at their MPPT status, maximizing of utilizing the rotor KE to store excessive captured DG energy and minimizing the impacts to the overall energy production. Compared to the same UL based PSC scheme, the proposed PSC can ensure better harvest of renewable energy while fulfilling the system dispatch demand, which is of significantly economic in system daily operation.

5.4.2 Cascading PSC scheme with both overspeeding control of WGs and overvoltage control of PV generators only

When the power discrepancies in a microgrid is relatively large, all the rotor speeds of WGs reach their limitations. Therefore, rotor KE of WGs is maximized utilized to store the excessive DG energy, which yields as,

$$E_{WG2} = -\Delta E_{k\max} = -\sum_{i=1}^{n} H_D \cdot (\omega_{D\max}{}^2(t) - \omega_{Di}{}^2(t_0)) \tag{5.26}$$

where ΔE_{kmax} is the maximal total rotor kinetic energy (KE) alternation while all the WGs reach their speed limitations ω_{Dmax}. Meanwhile, the power demand P_d should satisfy,

$$P_d < P_{DGT} = \sum_{i=1}^{n} P_{WGi}(\omega_{D\max}) + \sum_{j=1}^{m} P_{PVmj} \tag{5.27}$$

where P_{WGi} (ω_{Dmax}) is the *i*th WG output power when its rotor speed reaches its limitation. P_{DGT} is the defined threshold of DG generations when all rotor speeds of WGs reach their limitations and all PVs operate at their MPPT status. When system power demand is less than defined P_{DGT}, WT rotor KE is maximally utilized. Consequently, there are two ways to share the remaining power mismatch between system demand and P_{DGT}. One is to use pitch angle control of

WG and the other is via overvoltage control of PV. However, utilizing overvoltage control of PV for load sharing is more preferable than the pitch angle control of WG with slow response due to the mechanical regulation involved. Furthermore, frequent activation of pitch angle may cause additional fatigue of WT. Therefore, the power difference between system required power P_d and the defined DG generation P_{DGT} is evenly disturbed among m PVs,

$$P_{PVj} = P_{PVmj} - \left(P_d - P_{DGT}\right)/m \tag{5.28}$$

In order to realize the above process, a PI controller is utilized to prevent the over-speeds of wind turbine rotors and reduce the output power of PV generators automatically when power mismatch in a microgrid is large, yields as,

$$\begin{gathered}\eta = \max(K_P \cdot (\omega_{Di} - \omega_{D\max}) + K_I \cdot \int (\omega_{Di} - \omega_{D\max}) \cdot dt\ ,\ 0) \\ \begin{cases} P_{WGi} = P_{WGmi} - \left(P_{DGm} - P_d\right)/n + \eta \\ P_{PVj} = P_{PVmj} - \eta \end{cases}\end{gathered} \tag{5.29}$$

where K_p, K_I are the concerned control parameters of PI controller. it should be noted that when the system demand is above the defined threshold DG generations P_{DGT}, and the rotor speeds of WGs do not reach their limitations, only WGs undertake the power mismatch between the maximum active power DGs can generate (P_{DGm}) and system demand (P_d). Once larger power mismatch occurs and all the rotors of wind turbines reach their limitations, overvoltage control of PVs in the microgrid is activated and reduction of PV generations is utilized for power sharing. This cascading control design well distributes self-resources for system supply-demand power balance and successfully resolves the paradox between energy harvesting of DGs and fulfilling the system dispatch demand. Each power generation of DG for power sharing with cascading control scheme should be as follows,

$$\begin{gathered}\begin{cases} P_{WGi} = P_{WGmi} - \left(P_{DGm} - P_d\right)/n \\ P_{PVj} = P_{PVmj} \end{cases} \quad when\ \ \omega_{D\max} > \omega_{Di} > \omega_{Diopt} \\ \begin{cases} P_{WGi} = P_{WGi}(\omega_{D\max}) \\ P_{PVj} = P_{PVmj} - \left(P_d - P_{DGT}\right)/m \end{cases} \quad when\ \ \omega_{Di} = \omega_{D\max}\end{gathered} \tag{5.30}$$

5.4.3 PSC scheme when there is over-consumption

When there is over-consumption in the microgrid, the system required generation (P_d) may be more than the maximum active power DGs can generate (P_{DGm}). Accordingly, the stored kinetic energy via proposed cascading control scheme can be released back to system through the following strategy as shown in Fig 5.4. One simple and direct way is to share the power discrepancies in a microgrid is evenly distributed to *n* WGs, meanwhile PVs are working at their MPPT status.

$$\begin{aligned} P_{WGi} &= P_{WGmi} + \left(P_d - P_{DGm}\right)/n \\ P_{PVj} &= P_{PVmj} \end{aligned} \tag{5.31}$$

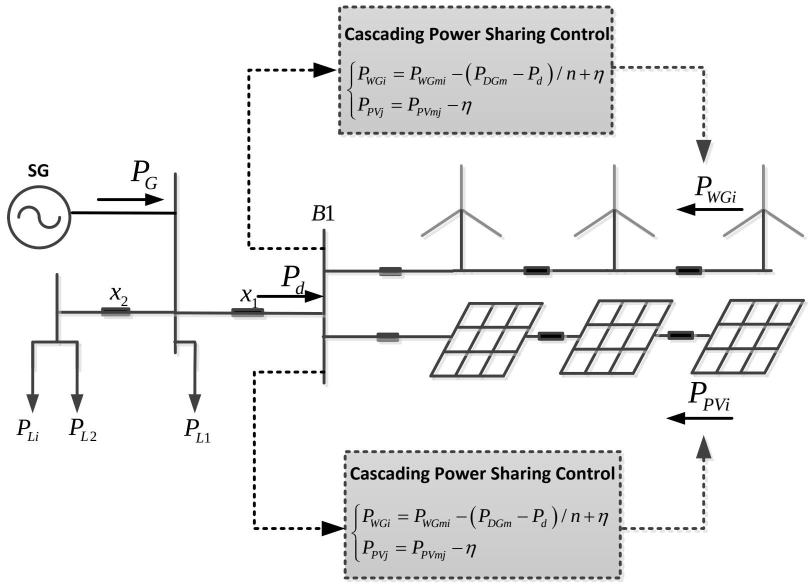

Fig. 5.3 Control scheme of the cascading control when over-generation

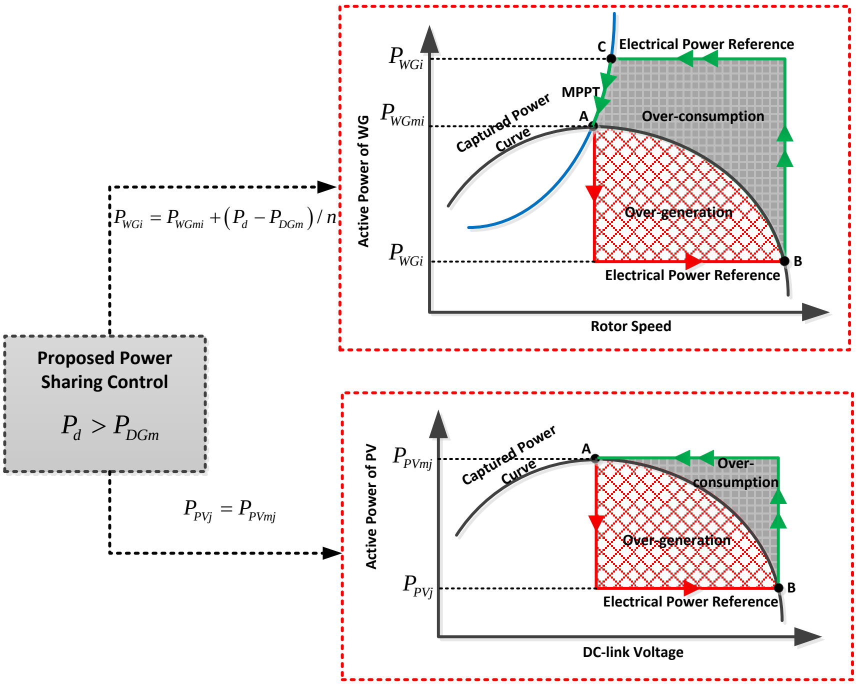

Fig. 5.4 PSC scheme for a microgrid when there is over-consumption

5.5 Case Studies

To validate the performance of proposed cascading control scheme, a small microgrid was selected that contains one conventional SG, variable loads, a PV-based solar farm and a DFIG-based wind farm, as shown in Fig 5.3. It was simulated in *DIgSILENT/ PowerFactory* [99]. One SG of 15-MW built by a seventh-order model [105] represents the power grid. A 6-MW wind farm consists of 3 units of a 2-MW DFIG. Similarly, a 6-MW solar farm is connected to the bus **B1** in parallel. Notably, the power rating of DGs is 40% of the overall generation capacity and it is mandatory to require the DGs to fulfill system demand via power sharing control. The DFIG model, solar model and the related control strategy can be referred to [27-29]. Since a relatively small microgrid is studied in this thesis, the dispatch order will be short in few minutes, and the dispatch order changes at every 150 seconds in case study. More parameters of SG, PV and DFIG are shown in Appendix.

5.5.1 Variable System Demand with Constant Wind Speed

As Table I shows, the maximum power generation by the wind farm and solar farm are 3.8118 MW (0.6353 p.u.) and 3.2778 MW (0.5463 p.u.) under specific wind speeds and solar radiations respectively. Accordingly, the total available power from DGs is 7.0896 MW (0.5908 p.u.). As shown in Fig. 5 (a), during the first dispatch order cycle (over-generation I), due to the abundant DG resources available in light-load, the power demand for DGs become 6.786 MW (0.5655 p.u.) based on (9). In the same utilization level (UL) scheme, K_u is calculated as 0.9572 based on (11). Accordingly, the generations from wind and solar farm decrease to 3.6486 MW (0.6081 p.u.) and 3.1374 MW (0.5229 p.u), respectively, as shown in Table II. As clearly shown in Fig. 5 (b), the wind and solar farm decrease their output with same utilization ratio based on their maximum generation. However, in the proposed cascading control scheme, the power discrepancies between the maximum power generations from DGs and the system demand in small system disturbance is entirely shared by wind farm as seen in Fig. 5 (b) in the black solid line. As a result, the generation from wind farm reduces to 3.5082 MW (0.5847 p.u.), while solar farm still works at its MPPT status. Because of the small disturbance in the system, the rotor speed of each WG increases to 1.2109 p.u. (less than the speed limitation set as 1.28 p.u. in this thesis), which is larger than the WG rotor speed of 1.158 p.u. via overspeeding control of WG in the same UL scheme, as shown in Table II and Fig. 5 (e). Correspondingly, the stored kinetic energy in a wind farm by the proposed control is approximately calculated as 5.132 p.u. On the contrary, the stored KE with same utilization level scheme is nearly 4.693 p.u., and it effectively validates the cost-effective advantage of the former strategy.

Table 5.1

Maximum generation of DGs, system demand and concerned control parameters for case A

Quantity	Values
Wind speed	12.2 m/s
Solar radiation	450 W/m^2
Maximum wind power	0.6353 p.u.
Maximum solar power	0.5463 p.u.
Maximum DG power	0.5908 p.u.

Table 5.2

Results with the proposed control and conventional control for load sharing for over-generation I and over-consumption I

	Proposed Control	Conventional Control
System dispatch demand	0.5655 p.u.	0.5655 p.u.
Solar farm output	0.5463 p.u.	0.5229 p.u. /K_u=0.9572
Wind farm output	0.5847 p.u.	0.6081 p.u. /K_u=0.9572
Rotor Speed of WG	1.2109 p.u.	1.1580 p.u.
Stored KE	5.132 p.u.	4.693 p.u.
Over-production energy	0.5626 p.u.	0.4418 p.u.
Over-production time	37.08 s	32.74 s

System demand changes to 7.446 MW (0.6205 p.u.) at t=180s due to the sudden load increase (over-consumption I) as shown in Fig 5.5 (a). Correspondingly, the wind farm begins to increase its output to 4.1682 MW (0.6947 p.u.) afterwards and the solar farm returns back to its MPPT status by both same utilization level and proposed cascading schemes, as shown in Fig 5.5 (b) and (c). It can be clearly seen from Fig 5.5 (d) that when there is over-consumption, with the proposed control, the over-production wind energy injected into power grid (marked as red shadow in **S2** in Fig 5.5 (d)) via releasing wind turbine rotor kinetic energy is proximately calculated as 0.5626 p.u. However, with the same utilization level scheme, the surplus energy production for wind farm during over-consumption is nearly calculated as 0.4418 p.u. marked as **S1** in blue in Fig 5.5 (d). It is verified the energy-effective merit of the proposed scheme. The slight improvement in the wind energy production when wind farm filling the system dispatch demand is due to the relatively small amount of kinetic energy stored in wind rotors. In addition, the over-production time for wind farm with proposed control is 37.08s, which is longer than that with traditional control scheme (32.74s) as shown in TABLE II and Fig 5.5 (d). Since the stored energy by wind farm when system in the over-generation by the proposed control scheme is larger than that with same UL based one, the time of releasing stored rotation kinetic energy in WG with proposed control is longer than that with same UL scheme, as shown in Fig 5.5 (e).

Sequentially, system demand changes to 6.4836 MW (0.5403 p.u.) in next dispatch order cycle (over-generation II).

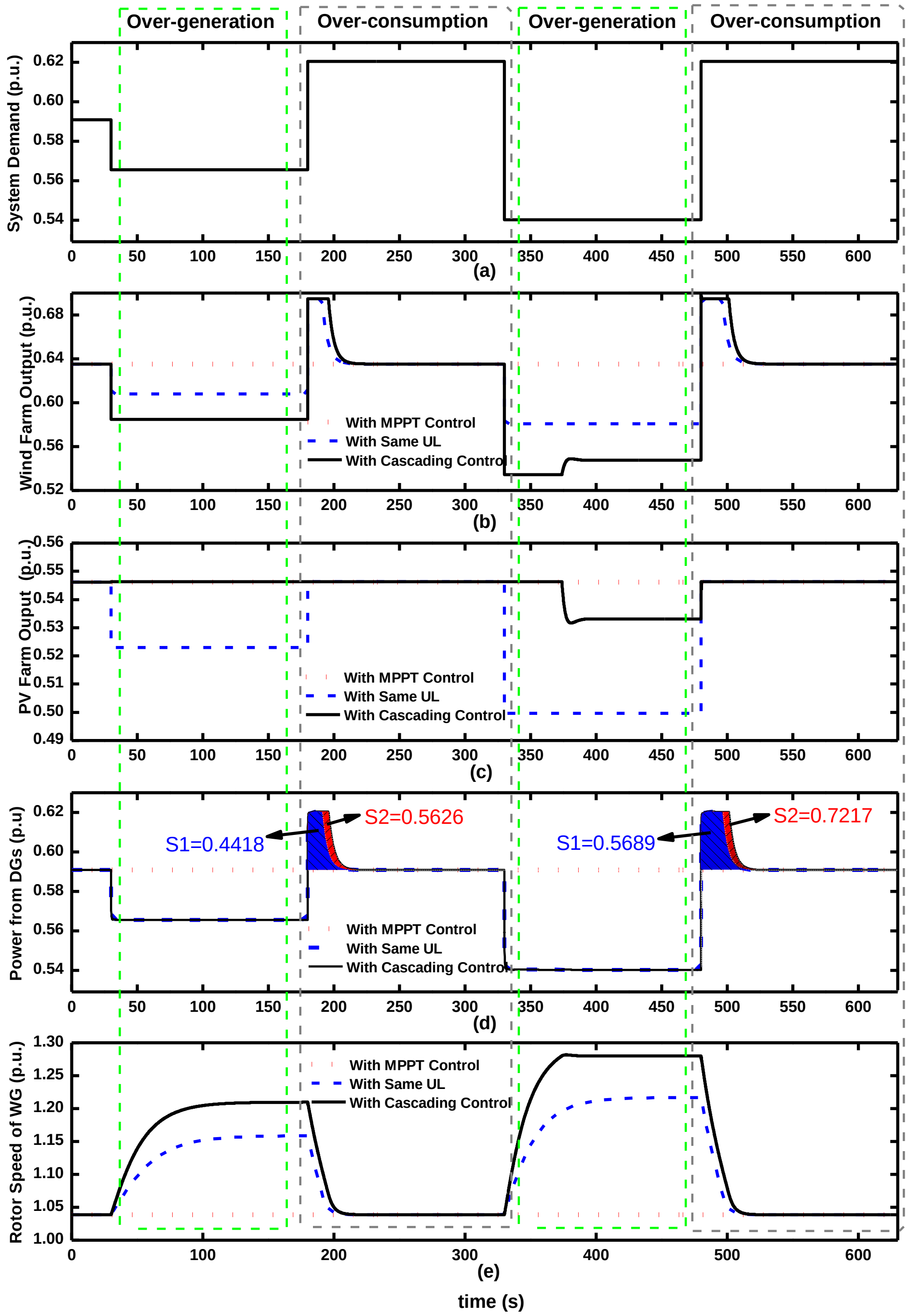

Fig. 5.5 Simulation results for Case A.

Due to large load shedding disturbance in the microgrid at *t=330s*.In the same utilization level scheme, K_u is calculated as 0.9145 based on (11). Similarly, the generation from wind and solar farm decreases to 3.4858 MW (0.5810 p.u.) and 2.9977 MW (0.4996 p.u) as shown in Table III and Fig. 5.5 (b) and (d). However, in the proposed cascading control scheme, the power discrepancies between system demand and the maximum DG generation is first shared by wind farm. Once all the rotor speeds of all WGs reach their limitations as shown in Fig. 5.5 (e), the designed PI controller in (30) is orderly activated to prevent the further increase of wind turbine rotors. At *t=386s*, the wind and solar farm output decreases to 3.2868 MW (0.5478 p.u.) and 3.1968 MW (0.5328 p.u.), respectively in the proposed scheme as shown in Fig. 5.5 (b) and (c). Similarly, the stored kinetic energy in the wind farm during system dynamics by two schemes are calculated as 5.734 p.u. and 5.184 p.u. respectively. It is again verified that the proposed cascading power sharing control is more energy-harvesting than the traditional one. In the next dispatch cycle, system demand returns to 7.446 MW (0.6205 p.u.) again at *t*=480s (over-consumption II) as shown in Fig. 5.5 (a). In the cascading control, the power difference is first shared by WGs until all rotor speeds of WGs reach their limits as shown in Fig. 5.5 (e), then by PVs. This cascading control design structure fully utilizes the rotational KE of WGs to absorb excessive energy while fulfilling system dispatch demand, which is more cost-effective than the traditional one.

Table 5.3

Results with the proposed cascading control and conventional control for load sharing for over-generation II and over-consumption II

	Proposed Control	Conventional Control
System dispatch demand	0.5403 p.u.	0.5403 p.u.
Solar farm output	0.5328 p.u.	0.499 p.u. (K_u=0.9145)
Wind farm output	0.5478 p.u.	0.581 p.u. (K_u=0.9145)
Rotor speed of WG	1.28 p.u.	1.217 p.u.
Stored KE	5.734 p.u.	5.184 p.u.
Over-production energy	0.7217 p.u.	0.5689 p.u.
Over-production time	47.73s	42.82s

5.5.2 Variable Wind Speed with Constant System Demand

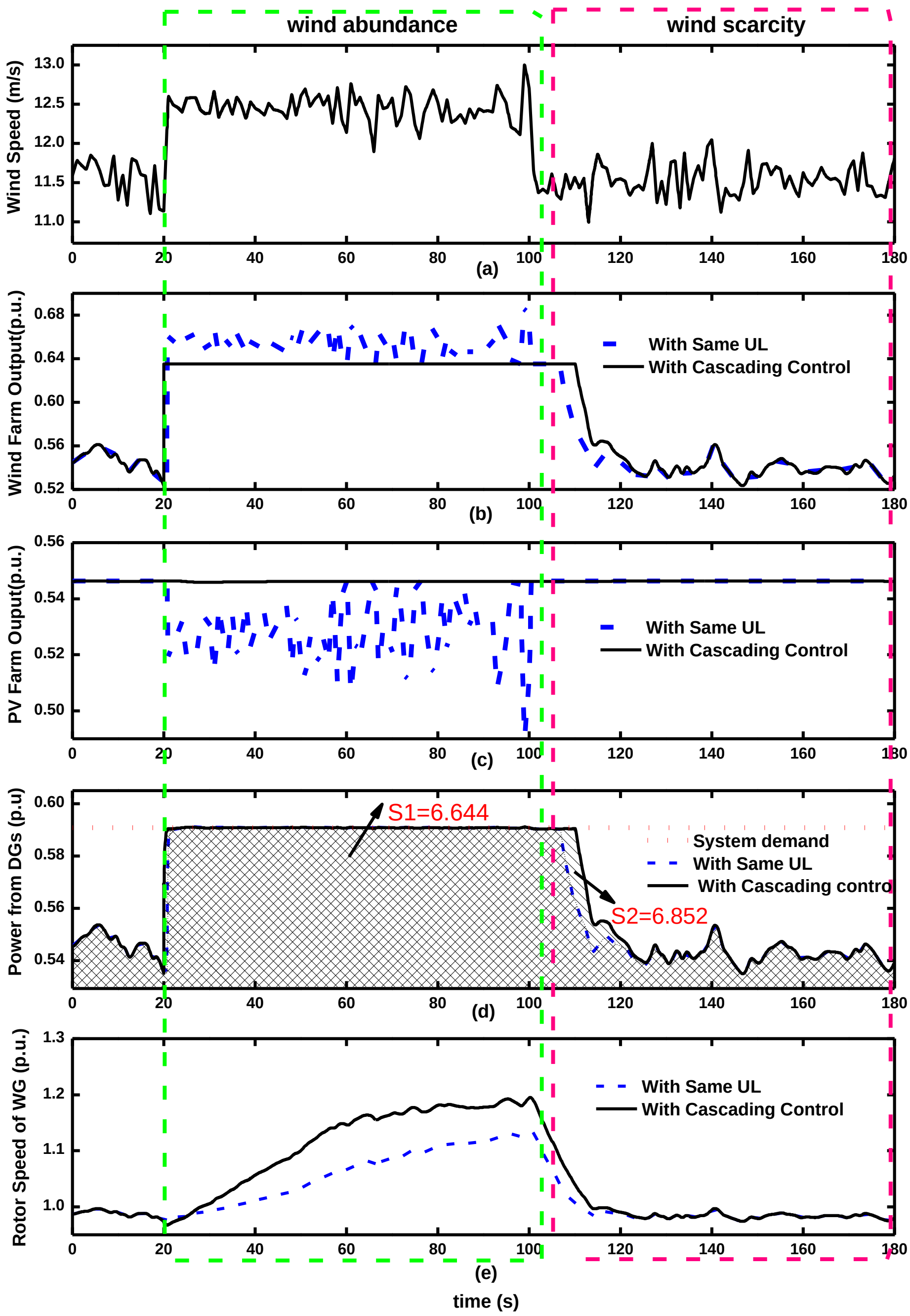

Fig. 5.6. Simulation results for Case B.

Fig. 5.6 shows the dynamic process of the microgrid when wind speed varies with constant power dispatch demand. At *t=20s*, the wind speeds suddenly change to the relatively high values with the average of the wind speeds as 12.5

m/s and the deviation as 0.4 m/s. During wind abundant period, both conventional same utilization level scheme and proposed cascading control scheme can track the power dispatch demand of P_d = 0.5908 p.u. well as shown in Fig. 5.6 (d). In the same utilization level scheme, the wind farm and solar farm decrease their output according to their maximum generation at each time, which is clearly seen from Fig. 5.6 (b) and (c). However, in the proposed scheme, all the power discrepancies between DG generation and the system dispatch demand is imposed on wind turbine rotors, which makes the output of wind farm constant as 0.6353 p.u. as shown in Fig. 5.6 (d). As a result, the rotor speeds of wind turbine are larger as shown in Fig. 5.6 (e) compared to the traditional scheme. Suddenly, At *t=100s*, the wind speeds changes to relatively low values with the average of the wind speeds as 11.5 m/s and the deviation as 0.4 m/s. In the wind scarcity period, wind and PV farm return back to their MPPT status in both schemes as shown in Fig. 5.6 (b) and (c). However, since more surplus wind energy is temporarily stored in the form of kinetic rotor energy via over-speeding rotors in the proposed cascading scheme and can be released back in the wind scarcity period, the DG energy production as shown in shadow area in **S2** in Fig. 5.6 (d) during this process is approximately calculated as 6.852 p.u. (based value is 0.53 p.u.) compared to 6.644 p.u. marked as **S1** in the traditional control scheme. It again effectively validates the cost-effective advantage of the proposed scheme under variable wind speeds.

5.6 Summary

In this chapter, it turns out that when fulfilling system dispatch demand, the traditional same UL scheme may lead to PV generators sacrificing more captured energy than WGs. To improve this, a cascading control scheme for a microgrid is proposed to effectively reduce total energy loss due to power sharing control. To guarantee the dispatch demand while saving as much energy as possible in a microgrid, the supply-demand imbalance is sequentially shared by WGs and then PVs via a cascading control design. The rotational mass of WG can be fully utilized for temporarily storing excessive energy and then the stored KE in WGs can be released back when needed. The simulation results indicate the proposed scheme can save more energy than the conventional same UL based scheme while fulfilling system dispatch demand. With increased renewable energy penetration in the future, the scheme can be highly valuable for industrial applications.

Chapter VI

Conclusions and Future Work

6.1 Conclusions

With high penetration of wind energy into power grids, the system inertia is gradually reduced since more conventional synchronous machines are replaced by the renewables. The power electronic devices in the variable speed wind turbines future decouples the rotation of the wind turbine and the network frequency. As a result, the contribution of WTs to the system inertia is also reduced. In this thesis, it mainly focuses on the power system inertia less problem with the high penetration of renewables and accordingly proposes several concerned system support strategies. Specifically, the primary conclusions and contributions of this research are summarized as follows:

i) A simple but effective control scheme of PMSG-based wind turbines for system inertia support

Two novel control strategies for PMSG-based wind turbine to provide fast system inertia support is proposed. The first simultaneous control seeks to utilize the DC-link capacitor energy and WT rotor kinetic energy simultaneously for AC grid support. In contrast, the proposed cascading control can sequentially exert DC-link capacitor energy and then WT rotor KE to provide fast system support. Detailed design and case studies of two proposed control schemes have been conducted. Given the same disturbance event, both control strategies can provide similar performance in stabilizing system frequency if the control parameters are set properly in advance. In addition, the proposed cascading strategy distinguishes itself by enabling better energy harvest during disturbances. It is believed that the two proposed novel strategies can provide additional benefit for system stability and are well suited for wind power application.

ii) A variable utilization level scheme for load sharing control of wind farm

It turns out that when fulfilling system dispatch demand, the traditional same utilization level based scheme may lead to wind turbines at higher wind speeds compromising more wind energy than those at lower wind speeds. To improve this, a variable utilization level scheme for a DFIG-based WPP is proposed to effectively reduce DFIG's wind energy loss due to load sharing control. To guarantee the dispatch demand while harvesting as much energy as possible in a WPP, the proposed scheme adaptively adjusts the utilization level of each wind turbine depending on its rotor speed so that more kinetic energy can be stored in a WPP, which can be later released back when system needed. The simulation results indicate the proposed scheme can reduce the loss of total energy production compared to the conventional same UL scheme for load sharing in a WPP. With increased wind energy penetration in the future, the scheme can be highly valuable for industrial applications.

iii) An optimal power sharing control strategy for fulfilling power dispatch demand while harvesting as much as wind energy as possible

An optimal power sharing control strategy that can fulfill the power dispatching demand by system operator while harvesting as much wind energy as possible is proposed. The power reference of each DFIG is shared through maximizing the rotor kinetic energy stored in all WTs in a wind farm. Correspondingly, the stored energy can be later released back for system support through WT overloading control. The proposed control scheme that fully utilizes the loading capability of WTs has a high potential application in a weak grid with high wind power penetration.

iv) A novel cascading power sharing control scheme that can coordinate wind and PV productions in microgrids while minimizing possible reduction of renewable energy production involved

It turns out that when fulfilling system dispatch demand, the traditional same UL scheme may lead to PV generators sacrificing more captured energy than WGs. To improve this, a cascading control scheme for a microgrid is proposed to effectively reduce total energy loss due to power sharing control. To guarantee the dispatch demand while saving as much energy as possible in a microgrid, the supply-demand imbalance is sequentially shared by WGs and then PVs via a cascading control design. The rotational mass of WG can be fully utilized for temperately storing excessive energy and then the stored KE in WGs can be released back when needed. The simulation results indicate the proposed scheme can save more energy than the conventional same UL based scheme while fulfilling system dispatch demand. With increased renewable energy penetration in the future, the scheme can be highly valuable for industrial applications.

6.2 Future Work

This thesis has proposed several novel control schemes for wind turbines or wind farm for system support. To make the current work more comprehensive, additional research topics can be investigated in the future including:

(1) With respect to the contribution *i*, wind turbines will deviate the maximum power tracking point while providing system frequency or inertia support. Traditional droop control based frequency regulation loop will be activated once there is frequency disturbance, which compromises large amount of wind power. One possible solution might be setting the dead band of the droop based frequency regulation loop. Accordingly, frequency control will not be activated in the dead band of frequency regulation loop. When the system frequency deviation touches

the bound limits, frequency droop control will be activated for providing better system support, which might partially save wind energy. Therefore, how to set the dead band of the frequency control may need further investigation.

(2) With respect to the contribution *i* and *iii,* main focuses have been drawn on how to provide system support by single wind turbine. However, considering one wind farm, how to optimize the droop constants of each single wind turbine to provide system support while saving as much wind energy as possible needs further research.

(3) As for the contribution *i,* the frequency control droop coefficient of the wind turbine is set as constant irrespective of large or small system frequency deviation. However, the possibility of large system disturbance might be small in the daily operation. Therefore, in a large frequency deviation, a relatively large droop constant may be implemented for system support, while a smaller frequency droop constant is applied for small frequency deviation. This variable droop control scheme might be more energy-harvesting while providing similar frequency support based on little chance of large frequency deviation happens in the daily system operation.

Appendices

A. Parameters of the SG in the thesis

Table A.1 Parameters of the SG in Chapter 2

Symbol	Item	Value
S_g	Rated MVA	3MVA
U_g	Terminal Voltage	6.6kV
H_g	Inertia Time constant	4s
x_{d}, x_d', x_d''	d-axis synchronous reactance	2.642, 0.377, 0.21
x_{q}, x_q'', x_l	q-axis synchronous reactance	2.346, 0.18, 0.18
T_d', T_d'', T_q''	SG Time constant	0.635, 0.015, 0.015
R_P	Turbine permanent droop	0.04
T_r	Governor time constant	8.408s
T_{servo}	Servo-motor time constant	0.5s
K_{gain}	Exciter regulator gain	400
T_e	Exciter time constant	0.01s

Table A.2 Parameters of the SG in Chapter 3 and 5

Symbol	Item	Value
S_g	Rated MVA	30 MVA
U_g	Terminal Voltage	11 kV
H_g	Inertia Time constant	4s
x_{d}, x_d', x_d''	d-axis synchronous reactance	2.642, 0.377, 0.21
x_{q}, x_q'', x_l	q-axis synchronous reactance	2.346, 0.18, 0.18
T_d', T_d'', T_q''	SG Time constant	0.635, 0.015, 0.015
R_P	Turbine permanent droop	0.04

T_r	Governor time constant	8.408s
T_{servo}	Servo-motor time constant	0.5s
K_{gain}	Exciter regulator gain	400
T_e	Exciter time constant	0.01s

Table A.3 Parameters of the SG in Chapter 4

Symbol	Item	Value
S_g	Rated MVA	5 MVA
U_g	Terminal Voltage	3.3 kV
H_g	Inertia Time constant	4s
x_d, x_d', x_d''	d-axis synchronous reactance	2.642, 0.377, 0.21
x_q, x_q'', x_l	q-axis synchronous reactance	2.346, 0.18, 0.18
T_d', T_d'', T_q''	SG Time constant	0.635, 0.015, 0.015
R_P	Turbine permanent droop	0.04
T_r	Governor time constant	8.408s
T_{servo}	Servo-motor time constant	0.5s
K_{gain}	Exciter regulator gain	400
T_e	Exciter time constant	0.01s

B. Parameters of the studied WG and PV

PMSG based wind turbine in chapter 2: cut in wind speed: 4m/s; lower limit of the wind speed: 7m/s; rated wind speed:14m/s; inertia constant: H_t=3.5s; damping coefficient: D_{sh}=0.01p.u.; shaft stiffness coefficient: K_{sh}=0.5p.u.; time constant of the pitch serve: T_β=0.25s.

PMSG: rated power: 2MW; rated voltage: 690V; rated rotor speed: 1.23p.u.; inertia constant: H_g=1.15s; stator resistance: R_a=50 μΩ; d axis inductance: L_d=0.0055H; q axis inductance: L_q=0.00375H; rotational damping D=0; number of pole paris: p=11.

Converters: resistance of grid side inductor: R_L=0.003 p.u.; inductance of grid side inductor: L=0.3 p.u.; DC-link capacitor: C_{DC} =90000μF; rated DC-link voltage V_{DCn}=2kV.

The parameters of studied DFIG wind turbine in chapter 3-5 are as follows:

Wind turbine: cut in wind speed: 4m/s; lower limit of the wind speed: 7m/s; rated wind speed:14m/s; damping coefficient: D_{sh}=0.01p.u.; shaft stiffness coefficient: K_{sh}=0.5p.u.; time constant of the pitch serve: T_β=0.25s.

Single-DFIG: rated power: 2MW; rated voltage: 690V; rated rotor speed: 1.23p.u.; total inertia constant: H_D=H_t+H_g=5.0s; friction coefficient: B=0.01p.u.; stator resistance: R_s=0.00706 p.u.; rotor resistance: R_r=0.0005 p.u.; stator leakage inductance: L_{ls}=0.171 p.u.; rotor leakage inductance: L_{1r}=0.156 p.u.; mutual inductance: L_m=3.5 p.u.

Converters: resistance of grid side inductor: R_L=0.003 p.u.; inductance of grid side inductor: L=0.3 p.u.; DC-link capacitor: C_{dc_dfig}=0.06F.

The parameters of studied PV in charpter 5 are as follows:

Open-circuit voltage: V_{OC}=43.8V; Short-circuit current: VSC=5A; MPPT voltage and current: V_M=35V, I_M=4.58A; Numbers of series and parallel modules: N=150, M=250.

Reference

[1] Global Wind Report. (2015). http://www.gwec.net/publications/global-wind-report-2/global-wind-report-2015-annual-market-update/.

[2] D. Gautam, L. Goel, R. Ayyanar, V. Vittal and T. Harbour, "Control Strategy to Mitigate the Impact of Reduced Inertia Due to Doubly Fed Induction Generators on Large Power Systems," *IEEE Transactions on Power Systems*, vol. 26, no. 1, pp. 214-224, Feb. 2011.

[3] L. Ruttledge and D. Flynn, "Emulated Inertial Response From Wind Turbines: Gain Scheduling and Resource Coordination," *IEEE Transactions on Power Systems*, vol. 31, no. 5, pp. 3747-3755, Sept. 2016.

[4] J. Brisbois and N. Aubut, "Wind farm inertia emulation to fulfil HydroQuebec's specific need," in *Proc. 2011 IEEE Power and Energy Soc.General Meeting*, 2011.

[5] ENTSO-E, "ENTSO-E Draft Requirements for Grid Connection Applicable to all Generators," ENTSO-E, Tech. Rep., 2011.

[6] EirGrid and SONI, "Ensuring a Secure, Reliable and Efficient Power System in a Changing Environment," Tech. Rep., 2011.

[7] L. Ruttledge, N. Miller, J. O'Sullivan, and D. Flynn, "Frequency response of power systems with variable speed wind turbines,"*IEEE Transactions on Sustainable Energy*, vol. 3, no. 4, pp. 683–691, Oct. 2012.

[8] I. Margaris, S. Papathanassiou, N. Hatziagyriou, A. Hansen, and P.Sørensen, "Frequency control in autonomous power systems with high

wind power penetration,” *IEEE Transactions on Sustainable Energy*, vol. 3, no. 2,pp. 189–199, Apr. 2012.

[9] L. Zeni, A. Rudolph, J. Münster-Swendsen, I. Margaris, A. Hansen, P. Sørensen, "Virtual inertia for variable speed wind turbines", *Wind Energy*, vol. 16, no. 8, pp. 1225-1239, 2013.

[10] W. Gao, Z. Wu, J. Wang, S. Gu, "A review of inertia and frequency control technologies for variable speed wind turbines", *Proc. Control and Decision Conf. (CCDC)*, 2013.

[11] X. Yingcheng, T. Nengling, "Review of contribution to frequency control through variable speed wind turbines", *Renewable Energy*, vol. 3, pp. 1671-1677, 2011.

[12] N. Jaleeli, L. S. VanSlyck, D. N. Ewart, L. H. Fink, and A. G. Hoffmann, "Understanding automatic generation control," *IEEE Transactions on Power Systems*, vol. 7, no. 3, pp. 1106-1122, Aug. 1992.

[13] B. H. Chowdhury and S. Rahman, "A review of recent advances in economic dispatch," *IEEE Transactions on Power Systems*, vol. 5, no. 4, pp. 1248-1259, Nov. 1990.

[14] J. M. Mauricio, A. Marano, A. Gomez-Exposito, and J. L. M. Ramos, "Frequency Regulation Contribution Through Variable-Speed Wind Energy Conversion Systems," *IEEE Transactions on Power Systems*, vol. 24, pp. 173-180, Feb 2009.

[15] Y. C. Xue and N. L. Tai, "System frequency regulation in doubly fed induction generators," *International Journal of Electrical Power & Energy Systems*, vol. 43, pp. 977-983, Dec 2012.

[16] F. Wilches-Bernal, J. H. Chow and J. J. Sanchez-Gasca, "A Fundamental Study of Applying Wind Turbines for Power System Frequency Control," *IEEE Transactions on Power Systems*, vol. 31, no. 2, pp. 1496-1505, March 2016.

[17] G. Lalor, A. Mullane, and M. O'Malley, "Frequency control and wind turbine technologies,"*IEEE Transactions on Power Systems*, vol. 20, pp. 1905-1913, Nov 2005.

[18] W. Yi, M. Jianhui, Z. Xiangyu, and X. Lie, "Control of PMSG-Based Wind Turbines for System Inertial Response and Power Oscillation Damping," *IEEE Transactions on Sustainable Energy*, vol. 6, pp. 565-574, 2015.

[19] M. Kayikci and J. V. Milanovic, "Dynamic Contribution of DFIG-Based Wind Plants to System Frequency Disturbances," in *IEEE Transactions on Power Systems*, vol. 24, pp. 859-867, May 2009.

[20] R. G. de Almeida and J. A. P. Lopes, "Participation of doubly fed induction wind generators in system frequency regulation," in *IEEE Transactions on Power Systems*, vol. 22, pp. 944-950, Aug 2007.

[21] W. He, X. Yuan and J. Hu, "Inertia Provision and Estimation of PLL-Based DFIG Wind Turbines," *IEEE Transactions on Power Systems*, vol. 32, no. 1, pp. 510-521, Jan. 2017.

[22] Y. Kim, M. Kang, E. Muljadi, J. W. Park and Y. C. Kang, "Power Smoothing of a Variable-Speed Wind Turbine Generator in Association With the Rotor-Speed-Dependent Gain," *IEEE Transactions on Sustainable Energy*, vol. 8, no. 3, pp. 990-999, July 2017.

[23] J. Tian, D. Zhou, C. Su, Z. Chen and F. Blaabjerg, "Reactive Power Dispatch Method in Wind Farms to Improve the Lifetime of Power

Converter Considering Wake Effect," *IEEE Transactions on Sustainable Energy*, vol. 8, no. 2, pp. 477-487, April 2017.

[24] L. R. Chang-Chien, W. T. Lin and Y. C. Yin, "Enhancing Frequency Response Control by DFIGs in the High Wind Penetrated Power Systems,"*IEEE Transactions on Power Systems*, vol. 26, no. 2, pp. 710-718, May 2011.

[25] H. Zhao, Q. Wu, Q. Guo, H. Sun, S. Huang and Y. Xue, "Coordinated Voltage Control of a Wind Farm Based on Model Predictive Control," *IEEE Transactions on Sustainable Energy*, vol. 7, no. 4, pp. 1440-1451, Oct. 2016.

[26] Y. Wang, H. Bayem, M. Giralt-Devant, V. Silva, X. Guillaud and B. Francois, "Methods for Assessing Available Wind Primary Power Reserve," *IEEE Transactions on Sustainable Energy*, vol. 6, no. 1, pp. 272-280, Jan. 2015.

[27] M. F. M. Arani and Y. A. R. I. Mohamed, "Analysis and Impacts of Implementing Droop Control in DFIG-Based Wind Turbines on Microgrid/Weak-Grid Stability," *IEEE Transactions on Power Systems*, vol. 30, no. 1, pp. 385-396, Jan. 2015.

[28] M. F. M. Arani and Y. A. R. I. Mohamed, "Analysis and Mitigation of Undesirable Impacts of Implementing Frequency Support Controllers in Wind Power Generation," *IEEE Transactions on Energy Conversion*, vol. 31, no. 1, pp. 174-186, March 2016.

[29] S. Wang, J. B. Hu, X. M. Yuan, and L. Sun, "On Inertial Dynamics of Virtual-Synchronous-Controlled DFIG-Based Wind Turbines," *IEEE Transactions on Energy Conversion*, vol. 30, pp. 1691-1702, Dec 2015

[30] L. Chiao-Ting, A. Changsun, P. Huei, and S. Jing, "Synergistic control of plug-in vehicle charging and wind power scheduling," *IEEE Transactions on Power Systems*, vol. 28, pp. 1113-1121, 2013.

[31] R. M. Kamel, A. Chaouachi, and K. Nagasaka, "Three Control Strategies to Improve the Microgrid Transient Dynamic Response During Isolated Mode: A Comparative Study," *IEEE Transactions on Industrial Electronics*, vol. 60, pp. 1314-1322, Apr 2013.

[32] C. Lin, C. Yao, L. Jin, and C. Singh, "Power System Reliability Assessment With Electric Vehicle Integration Using Battery Exchange Mode," *Sustainable Energy, IEEE Transactions on*, vol. 4, pp. 1034-1042, 2013.

[33] J. F. Conroy and R. Watson, "Frequency response capability of full converter wind turbine generators in comparison to conventional generation," *IEEE Transactions on Power Systems*, vol. 23, pp. 649-656, May 2008.

[34] G. Ramtharan, J. B. Ekanayake, and N. Jenkins, "Frequency support from doubly fed induction generator wind turbines," *IET Renewable Power Generation*, vol. 1, pp. 3-9, Mar 2007.

[35] L. H. Yang, Z. Xu, J. Ostergaard, Z. Y. Dong, and K. P. Wong, "Advanced Control Strategy of DFIG Wind Turbines for Power System Fault Ride Through," in *IEEE Transactions on Power Systems*, vol. 27, pp. 713-722, May 2012.

[36] A. Uehara, A. Pratap, T. Goya, T. Senjyu, A. Yona, N. Urasaki, et al., "A Coordinated Control Method to Smooth Wind Power Fluctuations of a

PMSG-Based WECS," *IEEE Transactions on Energy Conversion*, vol. 26, pp. 550-558, Jun 2011.

[37] M. F. M. Arani and E. F. El-Saadany, "Implementing Virtual Inertia in DFIG-Based Wind Power Generation," *IEEE Transactions on Power Systems*, vol. 28, pp. 1373-1384, 2013.

[38] D. Wang, Yunhe Hou and J. Hu, "Stability of DC-link voltage control for paralleled DFIG-based wind turbines connected to Weak AC grids," *2016 IEEE Power and Energy Society General Meeting (PESGM)*, Boston, MA, 2016, pp. 1-5.

[39] M. Davari and Y. A. R. I. Mohamed, "Robust DC-Link Voltage Control of a Full-Scale PMSG Wind Turbine for Effective Integration in DC Grids," *IEEE Transactions on Power Electronics*, vol. 32, no. 5, pp. 4021-4035, May 2017.

[40] J. Hu, Y. Huang, D. Wang, H. Yuan and X. Yuan, "Modeling of Grid-Connected DFIG-Based Wind Turbines for DC-Link Voltage Stability Analysis," *IEEE Transactions on Sustainable Energy*, vol. 6, no. 4, pp. 1325-1336, Oct. 2015.

[41] A. Zertek, G. Verbic and M. Pantos, "A Novel Strategy for Variable-Speed Wind Turbines' Participation in Primary Frequency Control," *IEEE Transactions on Sustainable Energy*, vol. 3, no. 4, pp. 791-799, Oct. 2012.

[42] A. Teninge, C. Jecu, D. Roye, S. Bacha, J. Duval and R. Belhomme, "Contribution to frequency control through wind turbine inertial energy storage," *IET Renewable Power Generation*, vol. 3, no. 3, pp. 358-370, Sept. 2009

[43] W. Qiao, "Dynamic modeling and control of doubly fed induction generators driven by wind turbines," *Power Systems Conference and Exposition, 2009. PSCE '09. IEEE/PES*, Seattle, WA, 2009, pp. 1-8.

[44] R. Pena, J. C. Clare and G. M. Asher, "Doubly fed induction generator using back-to-back PWM converters and its application to variable-speed wind-energy generation," *IEE Proceedings - Electric Power Applications*, vol. 143, no. 3, pp. 231-241, May 1996.

[45] J. F. Medina Padron and A. E. Feijoo Lorenzo, "Calculating Steady-State Operating Conditions for Doubly-Fed Induction Generator Wind Turbines," *IEEE Transactions on Power Systems*, vol. 25, no. 2, pp. 922-928, May 2010.

[46] K. V. Vidyanandan and N. Senroy, "Primary frequency regulation by deloaded wind turbines using variable droop," *IEEE Transactions on Power Systems*, vol. 28, no. 2, pp. 837-846, May 2013.

[47] P. Moutis, "Discussion on “Primary Frequency Regulation by Deloaded Wind Turbines Using Variable Droop”," *IEEE Transactions on Power Systems*, vol. 29, no. 1, pp. 414-414, Jan. 2014.

[48] J. Lee, E. Muljadi, P. Srensen, and Y. C. Kang, "Releasable Kinetic Energy-Based Inertial Control of a DFIG Wind Power Plant," *IEEE Transactions on Sustainable Energy*, vol. 7, pp. 279-288, 2016.

[49] J. Lee, G. Jang, E. Muljadi, F. Blaabjerg, Z. Chen and Y. Cheol Kang, "Stable Short-Term Frequency Support Using Adaptive Gains for a DFIG-Based Wind Power Plant," *IEEE Transactions on Energy Conversion*, vol. 31, no. 3, pp. 1068-1079, Sept. 2016.

[50] A. Scholbrock, “Optimizing wind farm control strategies to minimize wake loss effects,” M.S. thesis, Dept. Mech. Eng., Environ. Eng., Univ.Colorado Boulder, Boulder, CO, USA, Jul. 2011.

[51] I. Katic and N. O. Jensen, “A simple model for cluster efficiency", *Proceeding European Wind Energy Conference*. 1986, pp. 407–410.

[52] T. Sorensen, M. L. Thogersen, P. Nielsen, A. Grotzner, and S. Chun, “Adapting and calibration of existing wake models to meet the conditions inside offshore wind farms,” EMD Int. A/S, Aalborg, Denmark, Rep. 5899, 2008.

[53] J. R. Marden, S. D. Ruben, and L. Y. Pao, “A model-free approach to wind farm control using game theoretic methods,” *IEEE Transaction on Control System Technology*., vol. 21, no. 4, pp. 1207–1214, Jul. 2013.

[54] A. Feijóo and D. Villanueva, "Wind Farm Power Distribution Function Considering Wake Effects," *IEEE Transactions on Power Systems*, vol. 32, no. 4, pp. 3313-3314, July 2017.

[55] S. Poushpas and W. E. Leithead, "Wind farm simulation modelling and control for primary frequency support," *International Conference on Renewable Power Generation (RPG 2015)*, Beijing, 2015, pp. 1-6.

[56] Y. Li, Z. Xu, and K. Meng, "Optimal Power Sharing Control of Wind Turbines," *IEEE Transactions on Power Systems* , vol. 32, no. 1, pp. 824-825, Jan. 2017.

[57] Y. Li, Z. Xu, and K. P. Wong, "Advanced Control Strategies of PMSG-Based Wind Turbines for System Inertia Support," *IEEE Transactions on Power Systems* , vol. 32, no. 4, pp. 3027-3037, July 2017.

[58] Y. Ma, Y. Hao, S. Zhao and H. Bi, "Security constrained economic dispatch of wind-integrated power system considering optimal system state selection," *IET Generation, Transmission & Distribution*, vol. 11, no. 1, pp. 27-36, 1 5 2017.

[59] C. Shao, X. Wang, M. Shahidehpour, X. Wang and B. Wang, "Power System Economic Dispatch Considering Steady-State Secure Region for Wind Power," *IEEE Transactions on Sustainable Energy*, vol. 8, no. 1, pp. 268-278, Jan. 2017.

[60] S. Yang, D. Zeng, H. Ding, J. Yao, K. Wang and Y. Li, "Stochastic security-constrained economic dispatch for random responsive price-elastic load and wind power," *IET Renewable Power Generation*, vol. 10, no. 7, pp. 936-943, 7 2016.

[61] J. V. d. Vyver, J. D. M. D. Kooning, B. Meersman, L. Vandevelde, and T. L. Vandoorn, "Droop Control as an Alternative Inertial Response Strategy for the Synthetic Inertia on Wind Turbines," *IEEE Transactions on Power Systems*, vol. 31, pp. 1129-1138, 2016.

[62] D. L. Xie, Z. Xu, L. H. Yang, J. Ostergaard, Y. S. Xue, and K. P. Wong, "A Comprehensive LVRT Control Strategy for DFIG Wind Turbines With Enhanced Reactive Power Support," *IEEE Transactions on Power Systems*, vol. 28, pp. 3302-3310, Aug 2013.

[63] C. Wan, Z. Xu and P. Pinson, "Direct Interval Forecasting of Wind Power," *IEEE Transactions on Power Systems*, vol. 28, no. 4, pp. 4877-4878, Nov. 2013.

[64] L. Qu and W. Qiao, "Constant power control of DFIG wind turbines with supercapacitor energy storage", *IEEE Transactions on Industrial Application*, vol. 47, no. 1, pp. 359-367, 2011.

[65] J. Quanyuan, G. Yuzhong, and W. Haijiao, "A Battery Energy Storage System Dual-Layer Control Strategy for Mitigating Wind Farm Fluctuations," *IEEE Transactions on Power Systems,* vol. 28, pp. 3263-3273, 2013.

[66] K. W. Wee, S. S. Choi, and D. M. Vilathgamuwa, "Design of a Least-Cost Battery-Supercapacitor Energy Storage System for Realizing Dispatchable Wind Power," *IEEE Transactions on Sustainable Energy,* vol. 4, pp. 786-796, 2013.

[67] H. Daneshi and A. K. Srivastava, "Security-constrained unit commitment with wind generation and compressed air energy storage," *IET Generation, Transmission & Distribution,* vol. 6, pp. 167-175, 2012.

[68] M. I. Daoud, A. M. Massoud, A. S. Abdel-Khalik, A. Elserougi and S. Ahmed, "A Flywheel Energy Storage System for Fault Ride Through Support of Grid-Connected VSC HVDC-Based Offshore Wind Farms," *IEEE Transactions on Power Systems,* vol. 31, no. 3, pp. 1671-1680, May 2016.

[69] J. Quanyuan and W. Haijiao, "Two-Time-Scale Coordination Control for a Battery Energy Storage System to Mitigate Wind Power Fluctuations," *Energy Conversion, IEEE Transactions on,* vol. 28, pp. 52-61, 2013.

[70] F. Zhou, G. Joos, C. Abbey, L. Jiao, and B. T. Ooi, "Use of large capacity SMES to improve the power quality and stability of wind farms," in *Power*

Engineering Society General Meeting, 2004. IEEE, 2004, pp. 2025-2030 Vol.2.

[71] L. Shi, C. Wang, L. Yao, Y. Ni and M. Bazargan, "Optimal Power Flow Solution Incorporating Wind Power," *IEEE Systems Journal*, vol. 6, no. 2, pp. 233-241, June 2012.

[72] L. Jin, S. Yuanzhang, S. Yonghua, G. Wenzhong, and P. Sorensen, "Wind Power Fluctuation Smoothing Controller Based on Risk Assessment of Grid Frequency Deviation in an Isolated System," *Sustainable Energy, IEEE Transactions on,* vol. 4, pp. 379-392, 2013.

[73] Guoyi Xu, Dandan Ge and Tianzhi Cao, "Combined deload and kinetic energy control of variable speed wind turbines for frequency support," *2016 IEEE PES Asia-Pacific Power and Energy Engineering Conference (APPEEC)*, Xi'an, 2016, pp. 890-894.

[74] J. Tan and Y. Zhang, "Coordinated Control Strategy of a Battery Energy Storage System to Support a Wind Power Plant Providing Multi-Timescale Frequency Ancillary Services," *IEEE Transactions on Sustainable Energy*, vol. 8, no. 3, pp. 1140-1153, July 2017.

[75] P. Moutis , E. Loukarakis , S. Papathanasiou and N. D. Hatziargyriou, "Primary load-frequency control from pitch-controlled wind turbines", *Proc. 2009 IEEE Bucharest PowerTech*, pp. 1-7.

[76] H. Liu and Z. Chen, "Contribution of VSC-HVDC to Frequency Regulation of Power Systems with Offshore Wind Generation," *IEEE Transactions on Energy Conversion*, vol. 30, no. 3, pp. 918-926, Sept. 2015.

[77] D. Ochoa; S. Martinez, "Fast-Frequency Response provided by DFIG-Wind Turbines and its impact on the grid," *IEEE Transactions on Power Systems* , to be published.

[78] S. Ghosh, S. Kamalasadan, N. Senroy and J. Enslin, "Doubly Fed Induction Generator (DFIG)-Based Wind Farm Control Framework for Primary Frequency and Inertial Response Application," *IEEE Transactions on Power Systems,* vol. 31, no. 3, pp. 1861-1871, May 2016.

[79] H. Wang, Z. Chen and Q. Jiang, "Optimal control method for wind farm to support temporary primary frequency control with minimised wind energy cost," *IET Renewable Power Generation*, vol. 9, no. 4, pp. 350-359, 5 2015.

[80] A. Molina-García, I. Muñoz-Benavente, A. D. Hansen and E. Gómez-Lázaro, "Demand-Side Contribution to Primary Frequency Control With Wind Farm Auxiliary Control," *IEEE Transactions on Power Systems*, vol. 29, no. 5, pp. 2391-2399, Sept. 2014.

[81] N. R. Ullah, T. Thiringer and D. Karlsson, "Temporary Primary Frequency Control Support by Variable Speed Wind Turbines— Potential and Applications," *IEEE Transactions on Power Systems*, vol. 23, no. 2, pp. 601-612, May 2008.

[82] H. Geng; X. Xi; L. Liu; G. Yang; J. Ma, "Hybrid Modulated Active Damping Control for DFIG based Wind Farm Participating in Frequency Response," *IEEE Transactions on Energy Conversion* , to be published.

[83] Z. Wu, D. W. Gao, H. Zhang, S. Yan and X. Wang, "Coordinated Control Strategy of Battery Energy Storage System and PMSG-WTG to Enhance System Frequency Regulation Capability," *IEEE Transactions on Sustainable Energy*, vol. 8, no. 3, pp. 1330-1343, July 2017.

[84] R. Pearmine, Y. H. Song and A. Chebbo, "Influence of wind turbine behaviour on the primary frequency control of the British transmission grid," *IET Renewable Power Generation*, vol. 1, no. 2, pp. 142-150, June 2007.

[85] M. Wang-Hansen, R. Josefsson and H. Mehmedovic, "Frequency Controlling Wind Power Modeling of Control Strategies," *IEEE Transactions on Sustainable Energy*, vol. 4, no. 4, pp. 954-959, Oct. 2013

[86] R. G. de Almeida, E. D. Castronuovo and J. A. P. Lopes, "Optimum generation control in wind parks when carrying out system operator requests", *IEEE Transactions on Power Systems*, vol. 21, no. 2, pp. 718-725, 2006.

[87] S. Jung and G. Jang, "A Loss Minimization Method on a Reactive Power Supply Process for Wind Farm," *IEEE Transactions on Power Systems*, vol. 32, no. 4, pp. 3060-3068, July 2017.

[88] J. Cao, W. Du and H. F. Wang, "Weather-Based Optimal Power Flow With Wind Farms Integration," *IEEE Transactions on Power Systems*, vol. 31, no. 4, pp. 3073-3081, July 2016.

[89] J. Cao, W. Du, H. F. Wang and S. Q. Bu, "Minimization of Transmission Loss in Meshed AC/DC Grids With VSC-MTDC Networks," *IEEE Transactions on Power Systems*, vol. 28, no. 3, pp. 3047-3055, Aug. 2013..

[90] A. Rabiee and A. Soroudi, "Stochastic Multiperiod OPF Model of Power Systems With HVDC-Connected Intermittent Wind Power Generation," *IEEE Transactions on Power Delivery*, vol. 29, no. 1, pp. 336-344, Feb. 2014.

[91] B. Zhang, P. Hou, W. Hu, M. Soltani, C. Chen and Z. Chen, "A Reactive Power Dispatch Strategy With Loss Minimization for a DFIG-Based Wind Farm," *IEEE Transactions on Sustainable Energy*, vol. 7, no. 3, pp. 914-923, July 2016.

[92] B. Zhang, W. Hu, P. Hou and Z. Chen, "Reactive power dispatch for loss minimization of a Doubly fed induction generator based wind farm," *2014 17th International Conference on Electrical Machines and Systems (ICEMS)*, Hangzhou, 2014, pp. 1373-1378.

[93] E. Sáiz-Marín, E. Lobato, I. Egido and L. Rouco, "Power losses minimization within Spanish wind farms evacuation networks," *2013 IEEE Power & Energy Society General Meeting*, Vancouver, BC, 2013, pp. 1-5.

[94] W. Zhang, Y. L. Xu, W. X. Liu, F. Ferrese, and L. M. Liu, "Fully Distributed Coordination of Multiple DFIGs in a Microgrid for Load Sharing," *IEEE Transactions on Smart Grid*, vol. 4, pp. 806-815, Jun 2013.

[95] H. Xin, Z. Lu, Y. Liu and D. Gan, "A Center-Free Control Strategy for the Coordination of Multiple Photovoltaic Generators," *IEEE Transactions on Smart Grid*, vol. 5, no. 3, pp. 1262-1269, May 2014.

[96] Y. Li; Z. Xu; J. Ostergaard; D. J. Hill, "Coordinated Control Strategies for Offshore Wind Farm Integration via VSC-HVDC for System Frequency Support," *IEEE Transactions on Energy Conversion* , to be published.

[97] Li, Y., Zhang, Z., Yang, Y., Li, Y., Chen, H. and Xu, Z., 2014. Coordinated control of wind farm and VSC–HVDC system using capacitor energy and kinetic energy to improve inertia level of power systems. *International Journal of Electrical Power & Energy Systems*, *59*, pp.79-92.

[98] Li, Y. and Xu, Z., 2017. Coordinated Control of Wind Farms and MTDC Grids for System Frequency Support. *Electric Power Components and Systems*, *45*(4), pp.451-464.

[99] A.D. Hansen, F. Iov, P. Sørensen, N. Cutululis, C. Jauch, and F. Blaabjerg, "Dynamic wind turbine models in power system simulation tool", DIgSILENT Project Report Risø-R-1400(ed.2)(EN).

[100] J. Hu, L. Sun, X. Yuan, S. Wang and Y. Chi, "Modeling of Type 3 Wind Turbines With df/dt Inertia Control for System Frequency Response Study," *IEEE Transactions on Power Systems*, vol. 32, no. 4, pp. 2799-2809, July 2017

[101] J. Yao; L. Guo; T. Zhou; D. Xu; R. Liu, "Capacity Configuration and Coordinated Operation of A Hybrid Wind Farm With FSIG-Based and PMSG-Based Wind Farms During Grid Faults," *IEEE Transactions on Energy Conversion* , to be published.

[102] E. Rahmanian, H. Akbari and G. H. Sheisi, "Maximum Power Point Tracking in Grid Connected Wind Plant by Using Intelligent Controller and Switched Reluctance Generator," *IEEE Transactions on Sustainable Energy*, vol. 8, no. 3, pp. 1313-1320, July 2017.

[103] X. Luo; S. Niu, "A Novel Contra-Rotating Power Split Transmission System for Wind Power Generation and its Dual MPPT Control Strategy," *IEEE Transactions on Power Electronics* , vol. 32, no. 9, pp. 6924-6935, Sept. 2017.

[104] Z. Chen; M. Yin; Y. Zou; K. Meng; Z. Y. Dong, "Maximum Wind Energy Extraction for Variable Speed Wind Turbines with Slow Dynamic

Behavior," *IEEE Transactions on Power Systems* , vol. 32, no. 4, pp. 3321-3322, July 2017.

[105] P. Anderson and A. A. Fouad, Power System Control and Stability. Ames, IA: Iowa State Univ. Press, 1977.

[106] M.N. Kabir, Y. Mishra, G. Ledwich, Z. Xu, R.C. Bansal, “Improving voltage profile of residential distribution systems using rooftop PVs and Battery Energy Storage systems”, *Applied Energy* 134 (2014) 290 – 300.

[107] E. I. Batzelis, G. E. Kampitsis and S. A. Papathanassiou, "Power Reserves Control for PV Systems With Real-Time MPP Estimation via Curve Fitting," *IEEE Transactions on Sustainable Energy*, vol. 8, no. 3, pp. 1269-1280, July 2017.